mathematics

MDPI

Article

The Effect of Adhesion on Indentation Behavior of Various Smart Materials

Qinghui Luo [1], Yueting Zhou [1,*], Lihua Wang [1] and Shenghu Ding [2]

[1] School of Aerospace Engineering and Applied Mechanics, Tongji University, 100 Zhangwu Road, Shanghai 200092, China
[2] School of Mathematics and Statistics, Ningxia University, Yinchuan 750021, China
* Correspondence: zhouyt@tongji.edu.cn

Abstract: The nanoindentation technique plays a significant role in characterizing the mechanical properties of materials at nanoscale, where the adhesion effect becomes very prominent due to the high surface-to-volume ratio. For this paper, the classical adhesion theories were generalized to study the contact behaviors of various piezoelectric materials indented by conical punches with different electric properties. With the use of the Hankel integral transform, dual integral equations, and superposing principle, the closed-form solutions of the physical fields for the Johnson-Kendall-Roberts (JKR) and Maugis-Dugdale (M-D) models were obtained, respectively. The contribution of the electrical energy to the energy release rate under the conducting punch was taken into consideration. The relationships between the contact radius, the indentation load, and the indentation depth were set up using the total energy method for the JKR model and the Griffith energy balance for the M-D model, respectively. Numerical results indicate that increasing the half cone angle of the conical punch enhances the adhesion effect, which can significantly affect the accuracy of the results of characterization in nanoindentation tests. It was found that the effect of electric potential on adhesion behaviors is sensitive to different material properties, which are not revealed in the existing studies of axisymmetric adhesive contact of piezoelectric materials and multiferroic composite materials. The load-displacement curves under conical punches with different half cone angles have very different slopes. These results indicate that the half cone angle has a prominent effect on the characterization of mechanical properties of piezoelectric solids in nanoindentation tests.

Keywords: piezoelectric materials; conical punch; adhesive contact; analytical solution

MSC: 74E10; 74G05; 74G65; 74M15

Citation: Luo, Q.; Zhou, Y.; Wang, L.; Ding, S. The Effect of Adhesion on Indentation Behavior of Various Smart Materials. *Mathematics* **2022**, *10*, 4511. https://doi.org/10.3390/math10234511

Academic Editor: Denis N. Sidorov

Received: 19 October 2022
Accepted: 25 November 2022
Published: 29 November 2022

1. Introduction

As typical functional materials, piezoelectric materials have received increasingly wide applications in a variety of smart structures and devices, such as transducers [1], sensors [2], actuators [3], generators [4], energy harvest devices [5], and so on. It is essential for these various applications to accurately characterize the electric and mechanical properties of piezoelectric materials for realizing effective quality control and performance prediction [6,7]. In order to achieve these goals, many intelligent artificial algorithms, such as the genetic algorithm [7–10], and soft computing tools, such as neural networks [11,12], have been used. The nanoindentation technique, also known as instrumented indentation, has become one of the most widely used testing techniques for evaluating the mechanical properties of a variety of materials [13,14], including the traditional stiff piezoelectric ceramics, such as polycrystalline lead zirconate titanate (PZT), barium titanate ($BaTiO_3$), etc., and the new soft piezoelectric materials with low elastic modulus, such as polyvinylidene fluoride (PVDF). However, soft materials always display obvious and strong adhesion effects in nanoindentation experiments, which have significant influence on the results of characterization [15,16].

Adhesion is a phenomenon which describes the tendency of different surfaces or particles to cling to one another. The adhesion effect plays a significant role in micro/nanoscale contact behaviors owing to the high surface-to-volume ratio [17–19]. During the nanoindentation testing technique, the sample is pressed by a small indenter tip, and the force and displacement are continuously measured as a function of time with high accuracy and precision. The recorded indentation force-displacement curves are often viewed as the 'fingerprints' of the tested materials, which can be analyzed to evaluate their mechanical properties. However, there always exists an obvious adhesion effect between the nanoindenter tip and the soft sample, which can lead to inaccurate estimation of the mechanical properties, such as the elastic modulus and hardness values. For example, it has been verified by [20] that contact stiffness in the presence of adhesion effect is always smaller than the counterpart value in the absence of the adhesion effect at the same indentation depth, while for the same indentation force, the results are the opposite. Therefore, the adhesion effect should be considered to avoid obtaining incorrect results during the nanoindentation testing of soft materials.

Contact problems are not only very common in nature but also a key issue in practical engineering. Whether discussing traditional indentation or nanoindentation technique, their theoretical foundations are both in contact mechanics [13]. During the past few years, the contact mechanics of piezoelectric materials have received comprehensive and rapid development through theoretical deductions, numerical simulations, and experimental observations. Various contact problems have received considerable attention and been widely studied by many investigators, including the indentation problems under some typical indenter profiles [21–31], the frictionless contact problems [32–41], the frictional contact problems [42–47], the fretting contact problems [48–50] and the dynamic contact problems [51,52]. During nanoindentation tests, sharp indenter is widely used due to its higher resolution and the simplicity of the procedure [15]. As a typical sharp punch, the contact behaviors of piezoelectric materials indented by a conical punch have been widely investigated by many scholars. Chen et al. [21] studied the frictionless indentation problem of a piezoelectric solid punched by a rigid conical punch. Ding et al. [53] analyzed the frictional contact behavior between a piezoelectric solid and a rigid conical punch. Giannakopoulos and Suresh [22] developed a general theory for the axisymmetric indentation problem of transversely isotropic piezoelectric materials by using the Hankel integral transform technique. The closed-form solutions of physical quantities under the action of the rigid conducting and insulating conical punches were obtained, which later were generalized to piezoelectric film with finite thickness by [25,54]. Sridhar et al. [23] conducted an experimental investigation into the mechanical and electrical responses of piezoelectric solids indented by a rigid conducting conical punch with zero electric potential. Makagon et al. [24] analyzed the sliding frictional contact behavior between a piezoelectric solid and a rigid conical punch. Yang [26] obtained the general solutions of the piezoelectric solids punched by a rigid indenter with axisymmetric arbitrary profile and presented the closed-form solutions of the stress and electric displacement fields in the case of a rigid conical punch.

It is worth noting that the aforementioned works only focus on the macroscale contact behaviors of piezoelectric materials, and the influence of the adhesion effect was not taken into consideration. With the increasingly broad applications of piezoelectric materials in various micro-electro-mechanical systems (MEMS) devices, where the adhesion effect becomes very prominent due to the high surface-to volume ratio [17], the contact problems of piezoelectric materials at the micro/nanoscale have been studied by some researchers in the past few years. Chen and Yu [55] first extended the classical JKR model [56] and the M-D model [57] to study the adhesion behaviors of piezoelectric materials. The results indicated that the coupling effect between adhesion and piezoelectric effects lead to much more complicated adhesion behaviors than in the pure elastic case. Rogowski and Kalinski [58] studied the adhesion behaviors of a piezoelectric solid indented by a rigid circular punch and demonstrated the explicit expression of contact stresses, displacement outside the

contact zone, and electric physical quantities. Guo and Jin [59] established a generalized JKR model to study the adhesive contact problem between a piezoelectric solid and a rigid cylinder with constant electric potential. It was found that piezoelectric materials can be used to realize reversible adhesion. Jin et al. [60] developed the JKR-type adhesive contact model for the piezoelectric solid punched by a rigid indenter with an axisymmetric power-law profile. It is worth pointing out that all of the aforementioned works involved only single layer piezoelectric materials. However, layered structures have been widely used in various MEMS devices and structures [1,61]. To this end, the adhesion behaviors of layered piezoelectric structures were studied [62–64], which are helpful for revealing the adhesion mechanism of MEMS involving piezoelectric solids.

As typical multi-functional materials, multiferroic composite materials have been widely used in a variety of MEMS smart structures [65–67] due to their multi-field coupling effect. The contact behaviors of multiferroic composite media at micro/nanoscale have attracted some attention from researchers. Recently, with the use of the superposition principle and generalized potential theory, Wu et al. [68] first generalized the classical adhesive contact theories to multiferroic composite materials. They established corresponding JKR and M-D models for the multiferroic half-space under a spherical indenter with four different electric and magnetic properties. It was found that the electric potential and magnetic potential can be used to adjust the adhesion behaviors. More recently, Wu and Li [69] studied the frictionless adhesive contact behaviors between a rigid conical punch and a multiferroic half-space using the same approach. They found that the pull-off force can be adjusted by altering the half cone angle of the conical punch.

It is worth mentioning that the adhesion behaviors of multiferroic composite materials discussed in the above-mentioned two works [68,69] involved only one kind of material (i.e., $BaTiO_3$-$CoFe_2O_4$). Although the effects of the electric potential and the half cone angle of the conical punch on adhesion behaviors were discussed, whether these effects are dependent on different material properties is unclear. However, the nanoindentation technique has been widely used in characterizing the mechanical and electric properties of various piezoelectric materials [70–72]. For the two-dimensional adhesive contact of piezoelectric materials indent by a rigid cylinder, it has been verified that different types of piezoelectric materials share entirely different adhesion behaviors under an electric load [60], which reveals that the effect of the electric load on adhesion behaviors is sensitive to material properties. For the indentation problem of purely elastic materials under a conical punch, the existing results indicate that the half cone angle can significantly affect the calculation of mechanical properties in nanoindentation tests [15]. For the indentation behaviors of various piezoelectric materials indented by a rigid conical punch, it is unclear whether the effects of the electric potential and the half cone angle on adhesion behaviors are sensitive to different material properties, or whether the half cone angle has a significant effect on the characterization of mechanical properties of piezoelectric materials in nanoindentation tests. The current work is devoted to answer these queries.

It is well known that the classical adhesion theories include the JKR model [56], the DMT model [73], the M-D model [57] and the double-Hertz (D-H) model [74]. The M-D and D-H models are regarded as more general theories than the JKR and DMT models, since both the M-D and D-H models are applicable to the arbitrary Tabor parameter [75], whose applicable scope can vary between soft materials and extremely hard materials. The JKR and DMT models can be described as two limit cases derived from the M-D model, which thus can be used to verify the correctness of the M-D model. The JKR model is the most widely used theory in nanoindentation experiments due to its convenience and reasonability [16,76,77]. Based on the above considerations, the classical JKR and M-D models were generalized in the present study to investigate the adhesive contact behaviors of various piezoelectric materials indented by conical punches with different electric properties. Numerical analysis indicated that the effect of the electric potential on adhesion behaviors is sensitive to different material properties, while the effect of the half cone angle on adhesion behaviors is insensitive to different material properties, which

are not revealed in the existing studies into piezoelectric materials [60] and multiferroic composite materials [68,69]. Increasing the half cone angle can significantly enhance the adhesion effect, which suggests to us that a conical punch with a small half cone angle should be adopted in nanoindentation tests to reduce the effect of adhesion and improve the accuracy of characterization results. Furthermore, it was found that the load-displacement curves under conical punches with different half cone angles have very different slopes, which indicates that the half cone angle can significantly affect the characterization of mechanical properties of piezoelectric solids in nanoindentation tests.

2. Problem Description and Formulation

2.1. Problem Description

As shown in Figure 1, consider the axisymmetric frictionless adhesive contact problem of a transversely isotropic piezoelectric solid indented by a rigid conical punch with a constant electric potential, ϕ_0, which is acted on by an indentation force, P. The cylindrical coordinate (r, θ, z) is set up at the surface of the piezoelectric solid. The half cone angle of the rigid conical punch is denoted as α, and the contact radius is a, while h stands for the indentation depth and $p(r)$ represents the adhesion force. The piezoelectric solid is polarized with the positive z-axis.

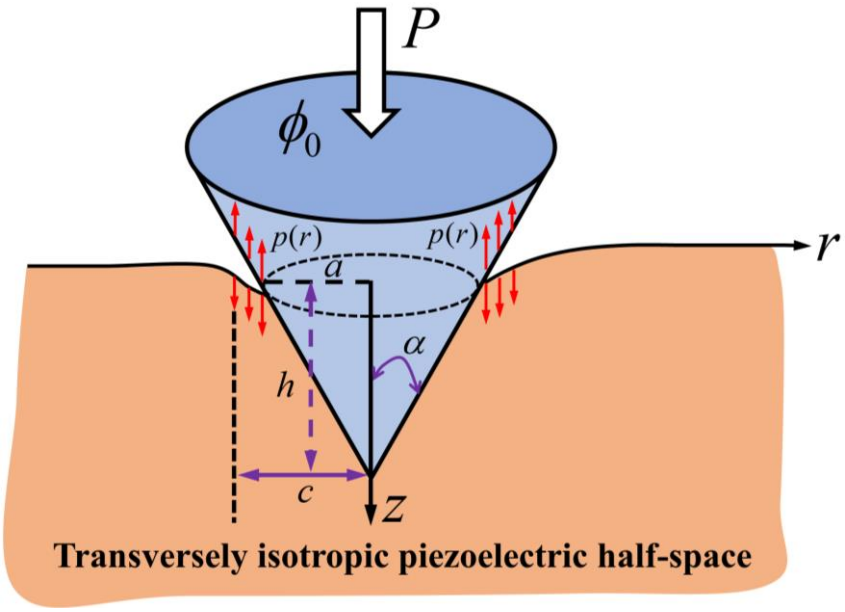

Figure 1. Schematic illustration of a piezoelectric solid in adhesive contact with a rigid conical punch under a normal force, P (negative when tensile). ϕ_0 denotes the constant electric potential; a, h, α, and $p(r)$ stand for the contact radius, the indentation depth, the half cone angle of the rigid conical punch, and the adhesion force, respectively. The poling direction of the piezoelectric solid corresponds with the positive z-axis.

2.2. Governing Equations

In the absence of body forces and body charges, the equilibrium equations and Gauss equation can be given as

$$\begin{aligned} &\frac{\partial \sigma_{rr}}{\partial r} + \frac{\partial \sigma_{rz}}{\partial z} + \frac{\sigma_{rr} - \sigma_{\theta\theta}}{r} = 0, \\ &\frac{\partial \sigma_{rz}}{\partial r} + \frac{\partial \sigma_{zz}}{\partial z} + \frac{\sigma_{rz}}{r} = 0, \\ &\frac{\partial D_r}{\partial r} + \frac{D_r}{r} + \frac{\partial D_z}{\partial z} = 0, \end{aligned} \tag{1}$$

where σ_{ij} and D_i denote the stress and electric displacement components, respectively.

In the cylindrical coordinates system, the constitutive equations can be expressed as

$$\begin{aligned}
\sigma_{rr} &= c_{11}\varepsilon_{rr} + c_{12}\varepsilon_{\theta\theta} + c_{13}\varepsilon_{zz} - e_{31}E_z,\\
\sigma_{\theta\theta} &= c_{12}\varepsilon_{rr} + c_{11}\varepsilon_{\theta\theta} + c_{13}\varepsilon_{zz} - e_{31}E_z,\\
\sigma_{zz} &= c_{13}(\varepsilon_{rr} + \varepsilon_{\theta\theta}) + c_{33}\varepsilon_{zz} - e_{33}E_z,\\
\sigma_{rz} &= 2c_{44}\varepsilon_{rz} - e_{15}E_r,\\
D_r &= 2e_{15}\varepsilon_{rz} + \in_{11} E_r,\\
D_z &= e_{31}(\varepsilon_{rr} + \varepsilon_{\theta\theta}) + e_{33}\varepsilon_{zz} + \in_{33} E_z,
\end{aligned} \tag{2}$$

where c_{ij}, e_{ij}, and $\in_{ij}$ represent the elastic, piezoelectric, and dielectric constants, respectively. Both ε_{ij} and E_i denote the strain and electric field components, respectively. The strain and electric field can be expressed by the mechanical displacements u_r, u_z, and the electric potential, ϕ, via the following relations:

$$\begin{aligned}
&\varepsilon_{rr} = \tfrac{\partial u_r}{\partial r},\ \varepsilon_{\theta\theta} = \tfrac{u_r}{r},\ \varepsilon_{zz} = \tfrac{\partial u_z}{\partial z},\\
&2\varepsilon_{rz} = \tfrac{\partial u_r}{\partial z} + \tfrac{\partial u_z}{\partial r},\ E_r = -\tfrac{\partial \phi}{\partial r},\ E_z = -\tfrac{\partial \phi}{\partial z}.
\end{aligned} \tag{3}$$

Through substitution of Equations (2) and (3) into Equation (1), one can obtain the following governing equations:

$$\begin{aligned}
&c_{11}\left(\tfrac{\partial^2 u_r}{\partial r^2} + \tfrac{1}{r}\tfrac{\partial u_r}{\partial r} - \tfrac{u_r}{r^2}\right) + c_{44}\tfrac{\partial^2 u_r}{\partial z^2} + (c_{13}+c_{44})\tfrac{\partial^2 u_z}{\partial r \partial z} + (e_{31}+e_{15})\tfrac{\partial^2 \phi}{\partial r \partial z} = 0,\\
&(c_{13}+c_{44})\left(\tfrac{\partial^2 u_r}{\partial r \partial z} + \tfrac{1}{r}\tfrac{\partial u_r}{\partial z}\right) + c_{44}\left(\tfrac{\partial^2 u_z}{\partial r^2} + \tfrac{1}{r}\tfrac{\partial u_z}{\partial r}\right) + c_{33}\tfrac{\partial^2 u_z}{\partial z^2}\\
&+e_{15}\left(\tfrac{\partial^2 \phi}{\partial r^2} + \tfrac{1}{r}\tfrac{\partial \phi}{\partial r}\right) + e_{33}\tfrac{\partial^2 \phi}{\partial z^2} = 0,\\
&(e_{31}+e_{15})\left(\tfrac{\partial^2 u_r}{\partial r \partial z} + \tfrac{1}{r}\tfrac{\partial u_r}{\partial z}\right) + e_{15}\left(\tfrac{\partial^2 u_z}{\partial r^2} + \tfrac{1}{r}\tfrac{\partial u_z}{\partial r}\right) + e_{33}\tfrac{\partial^2 u_z}{\partial z^2}\\
&- \in_{11}\left(\tfrac{\partial^2 \phi}{\partial r^2} + \tfrac{1}{r}\tfrac{\partial \phi}{\partial r}\right) - \in_{33}\tfrac{\partial^2 \phi}{\partial z^2} = 0.
\end{aligned} \tag{4}$$

2.3. General Solutions

The results shown in Equation (4) are the governing equations with respect to the mechanical displacement components and the electric potential. By solving Equation (4) and substituting the solutions into Equations (2) and (3), one can obtain the corresponding components of stress and electric displacement. Using the Hankel integral transform, and considering the frictionless contact boundary condition, the general solutions of the surface normal displacement, surface normal stress, and electric displacement can be obtained as follows [25]:

$$\begin{aligned}
u_z(r,0) &= \textstyle\int_0^\infty [M_1 A_1(\xi) + M_2 A_2(\xi)]\xi J_0(\xi r)d\xi,\\
\phi(r,0) &= \textstyle\int_0^\infty [M_3 A_1(\xi) + M_4 A_2(\xi)]\xi J_0(\xi r)d\xi,\\
\sigma_{zz}(r,0) &= \textstyle\int_0^\infty [M_5 A_1(\xi) + M_6 A_2(\xi)]\xi^2 J_0(\xi r)d\xi,\\
D_z(r,0) &= \textstyle\int_0^\infty [M_7 A_1(\xi) + M_8 A_2(\xi)]\xi^2 J_0(\xi r)d\xi,
\end{aligned} \tag{5}$$

where $M_i (i = 1, 2, \ldots, 8)$ represent the material constants related to the material properties of piezoelectric materials, whose explicit expressions were given by Appendix (A.8) in [25]; $A_i(\xi)$ $(i = 1, 2)$ denote the undetermined constants that can be obtained with use of the corresponding boundary conditions; and $J_0(\xi r)$ denotes the Bessel function of the first kind of zero order. In order to obtain the general solutions shown in Equation (5), the regularity condition of the piezoelectric solid at infinity is considered, i.e., $u_r, u_z, \phi \to 0$, $\sqrt{r^2 + z^2} \to 0$.

For the frictionless contact problem between a piezoelectric solid and a rigid axisymmetric punch with arbitrary profile, whose shape function can be denoted as $f(r)$, the solutions of the surface mechanical displacement, stress, and electric displacement of the piezoelectric solid can be obtained with use of Equation (5) and the corresponding boundary

conditions. It is worth mentioning that the electrical boundary conditions for conducting and insulating indenters are different.

First, whether for the conducting or insulating indenter, the mechanical boundary conditions can be described as

$$\begin{cases} u_z(r,0) = h - f(r), & 0 \le r \le a, \\ \sigma_{zz}(r,0) = 0, & r > a, \end{cases} \tag{6}$$

where h, $f(r)$, and a stand for the indentation depth, the shape function of the punch, and the contact radius, respectively. For the three typical indenters (the flat-ended cylindrical, the conical, and the spherical punches), the shape functions are denoted as

$$f(r) = \begin{cases} 0, & (0 \le r \le a) \text{ (flat-endedcircular punch)}, \\ r\cot\alpha, & (0 \le r \le a) \text{ (conical punch)}, \\ r^2/(2R), & (0 \le r \le a) \text{ (spherical punch)}. \end{cases} \tag{7}$$

For the electrically conducting indenter, the electrical boundary conditions are given as

$$\begin{cases} \phi(r,0) = \phi_0, & 0 \le r \le a, \\ D_z(r,0) = 0, & r > a, \end{cases} \tag{8}$$

where ϕ_0 is a constant denoting the constant electric potential.

For the electrically insulating indenter, the corresponding electrical boundary condition is expressed as

$$D_z(r,0) = 0, \quad r \ge 0. \tag{9}$$

In addition, for both the conducting and insulating indenters, the following equilibrium condition should be satisfied:

$$P = -2\pi \int_0^a r\sigma_{zz}(r,0)dr, \tag{10}$$

where P is the indentation load. For the conducting indenter, one can further obtain

$$Q = -2\pi \int_0^a rD_z(r,0)dr, \tag{11}$$

where Q stands for the total electric charge.

3. The Solution of the JKR Model

In this section, the classical JKR model [56] is generalized to investigate the adhesive contact problem of a piezoelectric solid indented by a rigid conical punch.

3.1. Boundary Conditions for the JKR Model

In the classical JKR model, only the adhesion force within the contact area was taken into consideration. According to the different electric properties of the indenters, the mixed boundary conditions for the conducting and insulating punches can be described as follows:

Case I: electrically conducting punch

$$\begin{aligned} &u_z(r,0) = h - r\cot\alpha, \ \phi(r,0) = \phi_0, && 0 \le r < a, \\ &\sigma_{zz}(r,0) = D_z(r,0) = 0, && r > a, \\ &\sigma_{rz}(r,0) = 0, && r \ge 0. \end{aligned} \tag{12}$$

Case II: electrically insulating punch

$$\begin{aligned} u_z(r,0) &= h - r\cot\alpha, & 0 \le r < a,\\ \sigma_{zz}(r,0) &= 0, & r > a,\\ \sigma_{zr}(r,0) &= D_z(r,0) = 0, & r \ge 0. \end{aligned} \tag{13}$$

Referring to the establishment process of the classical JKR model, the solutions for piezoelectric materials can be derived by superposing the corresponding piezoelectric Hertz contact solution under the conical punch, and the Boussinesq contact solution under the flat-ended circular punch, as shown in Figure 2a,b. Using the general solutions presented in Equation (5) and combining the corresponding boundary conditions shown in Equations (12) and (13), one can obtain the closed-form analytical solutions of the contact problems of the piezoelectric solid indented by the rigid conical punch and flat-ended cylindrical punch, respectively. For the convenience of subsequent analysis, the solutions of the above-mentioned two subproblems are listed in Appendices A and B.

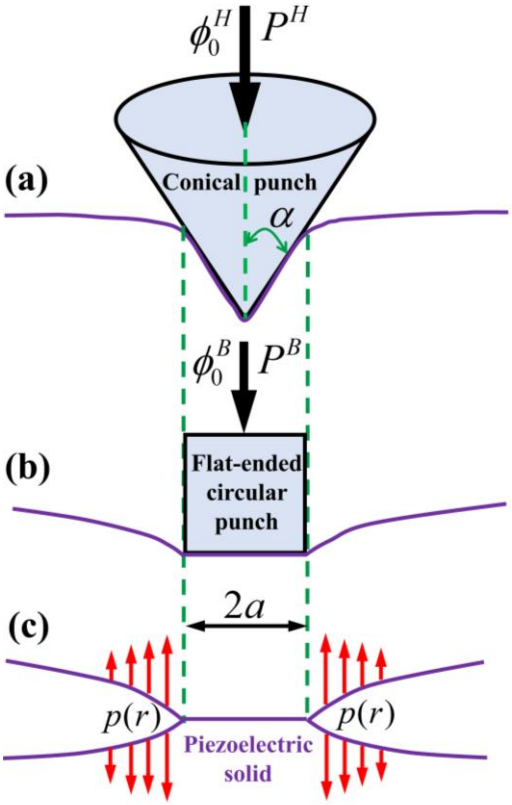

Figure 2. Illustration of the M-D model of a conical punch on a piezoelectric solid: (**a**) Hertz piezoelectric contact for a conical punch. (**b**) Boussinesq piezoelectric contact for a flat-ended circular punch. (**c**) An axisymmetric external crack in an infinite piezoelectric body.

3.2. The Solution of Case I: Electrically Conducting Punch

Using the Hertz solutions in Equations (A2)–(A6) and the corresponding Boussinesq solutions in Equations (A14)–(A18), the solutions of the JKR model for a piezoelectric solid indented by a rigid conducting conical punch can be obtained as

$$h^{JKR} = \frac{\pi a}{4}\cot\alpha - B_3\phi_0 + \frac{P}{4B_4 a}, \tag{14}$$

$$\sigma_{zz}^{JKR}(r,0) = -B_4\cot\alpha\cosh^{-1}\left(\frac{a}{r}\right) + \frac{\pi a^2 B_4\cot\alpha - P}{2\pi a\sqrt{a^2 - r^2}}, \tag{15}$$

$$D_z^{JKR}(r,0) = \frac{2B_5(B_6+B_3)\phi_0}{\pi\sqrt{a^2-r^2}} - B_5\cot\alpha\cosh^{-1}\left(\frac{a}{r}\right) + \frac{B_5}{B_4}\frac{\pi a^2 B_4\cot\alpha - P}{2\pi a\sqrt{a^2-r^2}}, \tag{16}$$

$$u_z^{JKR}(r,0) = \begin{cases} h^{JKR} - r\cot\alpha, & 0 \le r \le a, \\ \frac{2}{\pi}h^{JKR}\sin^{-1}\left(\frac{a}{r}\right) + \left(\sqrt{r^2-a^2} - r\right)\cot\alpha, & r > a, \end{cases} \tag{17}$$

$$\phi^{JKR}(r,0) = \begin{cases} \phi_0, & 0 \le r \le a, \\ \frac{2}{\pi}\phi_0\sin^{-1}\left(\frac{a}{r}\right), & r > a. \end{cases} \tag{18}$$

According to the establishment procedure of the classical JKR model, the total energy method should be adopted to obtain the relationship between the indentation force and contact radius. The total free energy of the contact system can be expressed as

$$U_T = U_E + U_D + U_P + U_S, \tag{19}$$

where U_T, U_E, U_D, U_P, and U_S denote the total free energy, the elastic strain energy, the electrostatic field energy, the mechanical energy, and the surface energy of the contact system, respectively, which are defined as

$$U_E = -\frac{1}{2}\int_0^{2\pi}\int_0^a \sigma_{zz}^{JKR}(r,0)u_z^{JKR}(r,0)\, r dr d\theta, \tag{20}$$

$$U_D = -\frac{1}{2}\int_0^{2\pi}\int_0^a D_z^{JKR}(r,0)\phi^{JKR}(r,0) r dr d\theta, \tag{21}$$

$$U_P = -Ph^{JKR},\ U_S = -\pi a^2\Delta\gamma, \tag{22}$$

where $\Delta\gamma$ is the surface energy denoting the work of adhesion for per unit area needed to separate two contacting objects from equilibrium state to infinity.

Substituting Equations (14)–(18) into Equations (20)–(22) yields that

$$\begin{aligned} &U_E = \frac{P^2}{8B_4 a} + \frac{\pi^2\cot^2\alpha B_4 a^3}{24} - \frac{PB_3\phi_0}{2},\ U_D = \frac{B_5}{2B_4}P\phi_0 - 2B_5(B_6+B_3)a\phi_0^2, \\ &U_P = -\frac{\pi\cot\alpha}{4}Pa - \frac{P^2}{4aB_4} + PB_3\phi_0. \end{aligned} \tag{23}$$

In order to obtain the results presented in Equation (23), the following integral results were utilized [69]:

$$\begin{aligned} &\int_0^a \frac{r}{\sqrt{a^2-r^2}}dr = a,\ \int_0^a \frac{r^2}{\sqrt{a^2-r^2}}dr = \frac{\pi}{4}a^2, \\ &\int_0^a r\cosh^{-1}\frac{a}{r}dr = \frac{1}{2}a^2,\ \int_0^a r^2\cosh^{-1}\frac{a}{r}dr = \frac{\pi a^3}{12}. \end{aligned} \tag{24}$$

The equilibrium state of the contact system should satisfy the following condition:

$$\left.\frac{\partial U_T}{\partial a}\right|_P = 0, \tag{25}$$

By substituting Equation (23) into Equation (19) and then inserting the corresponding result into Equation (25), one can obtain

$$P = \pi\cot\alpha B_4 a^2 \pm 4a\sqrt{\pi B_4\Delta\gamma a + B_4B_5(B_6+B_3)\phi_0^2}. \tag{26}$$

The stable equilibrium state of the contact system should satisfy the condition $\frac{\partial^2 U_T}{\partial a^2} > 0$, in which case

$$P^{JKR} = \pi B_4 a^2 \cot\alpha - 4a\sqrt{\pi B_4 \Delta\gamma a + B_4 B_5 (B_6 + B_3)\phi_0^2}. \tag{27}$$

If the rigid conical punch has zero electric potential (i.e., $\phi_0 = 0$), Equation (27) degenerates into the following form:

$$P = \pi \cot\alpha B_4 a^2 - 4a\sqrt{\pi B_4 \Delta\gamma a}, \tag{28}$$

which is the same as the result of Equation (3.16) obtained in [60].

When a piezoelectric material degenerates into a isotropic elastic solid, considering $B_4 = E^*/2$ (where E^* denotes the equivalent elastic modulus), Equation (28) can be rewritten as

$$P = \frac{\pi \cot\alpha E^*}{2} a^2 - \sqrt{8\pi E^* \Delta\gamma a^3}, \tag{29}$$

which is in agreement with the result of Equation (17) derived from [78].

By substituting Equation (27) into Equations (14)–(16), one can obtain

$$\begin{aligned} h^{JKR} &= \tfrac{\pi a}{2}\cot\alpha - B_3\phi_0 - \tfrac{1}{B_4}\sqrt{B_4\pi\Delta\gamma a + B_4 B_5(B_6+B_3)\phi_0^2}, \\ \sigma_{zz}^{JKR}(r,0) &= -B_4\cot\alpha \cosh^{-1}\tfrac{a}{r} + \tfrac{2}{\pi}\sqrt{\tfrac{\pi B_4\Delta\gamma a + B_4 B_5(B_6+B_3)\phi_0^2}{a^2-r^2}}, \\ D_z^{JKR}(r,0) &= \tfrac{2B_5(B_6+B_3)\phi_0}{\pi\sqrt{a^2-r^2}} - B_5\cot\alpha\cosh^{-1}\tfrac{a}{r} \\ &+ \tfrac{2B_5}{\pi B_4}\sqrt{\tfrac{\pi B_4\Delta\gamma a + B_4 B_5(B_6+B_3)\phi_0^2}{a^2-r^2}}. \end{aligned} \tag{30}$$

In adhesive contact problems, the pull-off force is regarded as the maximum external pulling force needed to separate two contacting objects, which is a vital physical quantity. In order to obtain the explicit expression of the pull-off force, one must consider the following condition:

$$\frac{dP}{da} = 0. \tag{31}$$

Inserting Equation (27) into Equation (31) yields

$$\chi_1 a^3 + \chi_2 a^2 + \chi_3 a + \chi_4 = 0, \tag{32}$$

where

$$\begin{aligned} &\chi_1 = \pi^3 B_4^3 \cot^2\alpha\Delta\gamma,\ \chi_2 = \pi^2 B_4^3 B_5(B_6+B_3)\cot^2\alpha\phi_0^2 - 9\pi^2 B_4^2\Delta\gamma^2, \\ &\chi_3 = -12\pi B_4^2 B_5(B_6+B_3)\Delta\gamma\phi_0^2,\ \chi_4 = -4B^2\phi_0^4. \end{aligned} \tag{33}$$

Using the Cardans formula, one can derive

$$\Delta = \left(\frac{q}{2}\right)^2 + \left(\frac{p}{3}\right)^3 = -\frac{4B^3\phi_0^6}{B_4^4\pi^6\cot^2\alpha}\left(\frac{B^2\phi_0^4}{27\Delta\gamma^4} + \frac{B\phi_0^2}{3\Delta\gamma^2} + \frac{1}{\cot^4\alpha}\right), \tag{34}$$

where $B = B_4 B_5(B_6 + B_3)$, and p and q are defined as

$$p = \frac{\chi_3}{\chi_1} - \frac{\chi_2^2}{3\chi_1^2},\ q = \frac{\chi_4}{\chi_1} + \frac{2\chi_2^3}{27\chi_1^3} - \frac{\chi_2\chi_3}{3\chi_1^2}. \tag{35}$$

The numerical results indicate that $B > 0$ for several common piezoelectric materials (e.g., PZT-4, PZT-5A, $BaTiO_3$, and $Ba_{0.917}Ca_{0.083}TiO_3$); hence, one can obtain that $\Delta < 0$, and Equation (32) has three real roots given as follows:

$$\begin{aligned} a_1 &= \frac{2\sqrt{-3p}}{3}\cos\frac{\beta}{3} - \frac{1}{3}\left(\frac{BB_4^2\pi^2\cot^2\alpha\phi_0^2 - 9\pi^2B_4^2\Delta\gamma^2}{\pi^3B_4^3\cot^2\alpha\Delta\gamma}\right), \\ a_2 &= -\frac{\sqrt{-3p}}{3}\left(\cos\frac{\beta}{3} - \sqrt{3}\sin\frac{\beta}{3}\right) - \frac{1}{3}\left(\frac{BB_4^2\pi^2\cot^2\alpha\phi_0^2 - 9\pi^2B_4^2\Delta\gamma^2}{\pi^3B_4^3\cot^2\alpha\Delta\gamma}\right), \\ a_3 &= -\frac{\sqrt{-3p}}{3}\left(\cos\frac{\beta}{3} + \sqrt{3}\sin\frac{\beta}{3}\right) - \frac{1}{3}\left(\frac{BB_4^2\pi^2\cot^2\alpha\phi_0^2 - 9\pi^2B_4^2\Delta\gamma^2}{\pi^3B_4^3\cot^2\alpha\Delta\gamma}\right), \end{aligned} \tag{36}$$

where

$$\beta = \arccos\left(-\frac{3q\sqrt{-3p}}{2p^2}\right),\ 0 \le \beta \le \pi. \tag{37}$$

From Equation (37), one can find that $0 \le \beta/3 \le \pi/3$. Therefore, the three roots in Equation (36) satisfy the following orders

$$a_3 \le a_2 \le a_1. \tag{38}$$

In addition, from Equation (36), one can obtain the following relation:

$$\begin{aligned} a_1 &= \frac{2\sqrt{-3p}}{3}\cos\frac{\beta}{3} - \frac{1}{3}\left(\frac{BB_4^2\pi^2\cot^2\alpha\phi_0^2 - 9\pi^2B_4^2\Delta\gamma^2}{\pi^3B_4^3\cot^2\alpha\Delta\gamma}\right) \\ &\ge \frac{\sqrt{-3p}}{3} - \frac{1}{3}\left(\frac{BB_4^2\pi^2\cot^2\alpha\phi_0^2 - 9\pi^2B_4^2\Delta\gamma^2}{\pi^3B_4^3\cot^2\alpha\Delta\gamma}\right) \\ &= \frac{1}{3}\left[\sqrt{\frac{36B\phi_0^2}{\pi^2B_4^2\cot^2\alpha} + \left(\frac{BB_4^2\pi^2\cot^2\alpha\phi_0^2 - 9\pi^2B_4^2\Delta\gamma^2}{\pi^3B_4^3\cot^2\alpha\Delta\gamma}\right)^2}\right. \\ &\quad \left. - \frac{BB_4^2\pi^2\cot^2\alpha\phi_0^2 - 9\pi^2B_4^2\Delta\gamma^2}{\pi^3B_4^3\cot^2\alpha\Delta\gamma}\right] \ge 0, \end{aligned} \tag{39}$$

$$\begin{aligned} a_3 &= -\frac{\sqrt{-3p}}{3}\left(\cos\frac{\beta}{3} + \sqrt{3}\sin\frac{\beta}{3}\right) - \frac{1}{3}\left(\frac{BB_4^2\pi^2\cot^2\alpha\phi_0^2 - 9\pi^2B_4^2\Delta\gamma^2}{\pi^3B_4^3\cot^2\alpha\Delta\gamma}\right) \\ &\le -\frac{\sqrt{-3p}}{3} - \frac{1}{3}\left(\frac{BB_4^2\pi^2\cot^2\alpha\phi_0^2 - 9\pi^2B_4^2\Delta\gamma^2}{\pi^3B_4^3\cot^2\alpha\Delta\gamma}\right) \\ &= -\frac{1}{3}\left[\sqrt{\frac{36B\phi_0^2}{\pi^2B_4^2\cot^2\alpha} + \left(\frac{BB_4^2\pi^2\cot^2\alpha\phi_0^2 - 9\pi^2B_4^2\Delta\gamma^2}{\pi^3B_4^3\cot^2\alpha\Delta\gamma}\right)^2}\right. \\ &\quad \left. + \frac{BB_4^2\pi^2\cot^2\alpha\phi_0^2 - 9\pi^2B_4^2\Delta\gamma^2}{\pi^3B_4^3\cot^2\alpha\Delta\gamma}\right] < 0. \end{aligned} \tag{40}$$

It should be noted that the contact radius a should be a non-negative real quantity. Therefore, a_1 should be selected as the critical contact radius at the pull-off moment. One can obtain

$$P_{\text{pull-off}} = \pi\cot\alpha B_4 a_{\text{pull-off}}^2 - 4a_{\text{pull-off}}\sqrt{\pi B_4\Delta\gamma a_{\text{pull-off}} + B_4B_5(B_6 + B_3)\phi_0^2}, \tag{41}$$

where

$$a_{\text{pull-off}} = a_1 = \frac{2\sqrt{-3p}}{3}\cos\frac{\beta}{3} - \frac{1}{3}\left(\frac{BB_4^2\pi^2\cot^2\alpha\phi_0^2 - 9\pi^2B_4^2\Delta\gamma^2}{\pi^3B_4^3\cot^2\alpha\Delta\gamma}\right). \tag{42}$$

By adopting the same solution procedures as those of Case I, one can also obtain the JKR solutions for Case II, and the solutions of Case II have similar mathematical structures to Case I. The corresponding solutions for Case II are presented in Appendix C.

4. The Solution of M-D Model

In this section, the classical M-D model is generalized to investigate the adhesive contact behaviors of a piezoelectric solid indented by a rigid conical punch. The adhesive contact problem in classical M-D adhesion theory was divided into three subproblems, i.e., the Hertz contact problem, the Boussinesq contact problem, and the external circular crack problem, as shown in Figure 2. This solution approach will also be adopted here to establish the M-D adhesive contact model for piezoelectric materials.

4.1. Boundary Conditions for the M-D Model

In the classical M-D model [57], the sophisticated adhesion force is simplified as a constant in an annular zone by using the Dugdale model [79]. In this case, the boundary conditions for the two cases of the M-D model can be expressed as follows:
Case I: electrically conducting punch

$$\begin{aligned} &\sigma_{zz}(r,0) = \begin{cases} \sigma_0, & a < r < c, \\ 0, & c < r < \infty, \end{cases} \\ &u_z(r,0) = h - r\cot\alpha,\ \phi(r,0) = \phi_0, \quad 0 \le r < a, \\ &D_z(r,0) = 0, \qquad\qquad\qquad\quad r > a, \\ &\sigma_{zr}(r,0) = 0, \qquad\qquad\qquad\quad r \ge 0. \end{aligned} \tag{43}$$

Case II: electrically insulating punch

$$\begin{aligned} &\sigma_{zz}(r,0) = \begin{cases} \sigma_0, & a < r < c, \\ 0, & c < r < \infty, \end{cases} \\ &u_z(r,0) = h - r\cot\alpha, \qquad 0 \le r < a, \\ &\sigma_{zr}(r,0) = D_z(r,0) = 0, \qquad r \ge 0. \end{aligned} \tag{44}$$

Note that in Equations (43) and (44), σ_0 denotes the constant adhesion force outside of the contact region, which is the theoretical adhesion strength of the material.

Using the general solutions obtained in Equation (5) and combining the corresponding boundary conditions presented in Equations (43) and (44), the solutions of the three subproblems can be obtained. The corresponding Hertz contact solutions and the Boussinesq contact solutions are presented in Appendices A and B, respectively. The solutions of the axisymmetric external circular crack problem in an infinite piezoelectric solid are given in Appendix E.

4.2. The Solution of Case I: Electrically Conducting Punch

The JKR solutions under a rigid conducting conical punch are presented in Section 4. Introducing the following stress and electric displacement intensity factors:

$$K_I = \frac{P_1 - P}{2a\sqrt{\pi a}},\ K_D = \frac{2B_5(B_6 + B_3)\phi_0}{\sqrt{\pi a}}, \tag{45}$$

where P_1 denotes the corresponding apparent Hertz load, then Equations (14)–(16)can be rewritten as follows:

$$h^{JKR} = \frac{\pi a}{2}\cot\alpha - B_3\phi_0 - \frac{\sqrt{\pi a}K_I}{2B_4}, \tag{46}$$

$$\sigma_{zz}^{JKR}(r,0) = -B_4\cot\alpha\cosh^{-1}\frac{a}{r} + \frac{K_I}{\sqrt{\pi a}}\frac{a}{\sqrt{a^2 - r^2}},\ 0 \le r < a. \tag{47}$$

$$D_z^{JKR}(r,0) = \sqrt{\frac{a}{\pi}}\frac{K_D}{\sqrt{a^2-r^2}} - B_5\cot\alpha\cosh^{-1}\frac{a}{r} + \frac{B_5}{B_4}\sqrt{\frac{a}{\pi}}\frac{K_I}{\sqrt{a^2-r^2}},\ 0 \le r < a. \tag{48}$$

Substituting Equation (46) into Equation (17), one can obtain

$$u_z^{JKR}(r,0) = \begin{cases} \frac{\pi a}{2}\cot\alpha - B_3\phi_0 - \frac{\sqrt{\pi a}K_I}{2B_4} - r\cot\alpha, & 0 \le r < a, \\ -\sqrt{\frac{a}{\pi}}\frac{K_I}{B_4}sin^{-1}\frac{a}{r} + \frac{2}{\pi}\left(\frac{\pi a}{2}\cot\alpha - B_3\phi_0\right)\sin^{-1}\frac{a}{r} & \\ +\left(\sqrt{r^2-a^2} - r\right)\cot\alpha, & r > a. \end{cases} \tag{49}$$

Using Equations (18) and (49), the discontinuity of the displacement and the electric potential outside the contact region can be defined as

$$\begin{aligned} &\left[u_z^{JKR}(r,0)\right] = f\left(\tfrac{r}{a}\right) - \delta + u_z(r,0) \\ &= \tfrac{K_I\sqrt{\pi a}}{B_4\pi}\cos^{-1}\tfrac{a}{r} + \left(\tfrac{2B_3\phi_0}{\pi} - a\cot\alpha\right)\cos^{-1}\tfrac{a}{r} + \sqrt{r^2-a^2}\cot\alpha,\ r > a, \end{aligned} \tag{50}$$

and

$$\left[\phi^{JKR}(r,0)\right] = \frac{2}{\pi}\phi_0\sin^{-1}\frac{a}{r} - \phi_0 = -\frac{2\phi_0}{\pi}\cos^{-1}\frac{a}{r},\ r > a, \tag{51}$$

respectively.

The solutions of the external circular crack subjected to constant normal pressure, p_0, at the crack surfaces are presented in Appendix E. By inserting $p_0 = -\sigma_0$ into Equation (A111) and Equations (A114)–(A117) and combining the result in Equation (A91), one can obtain

$$\sigma_{zz}(r,0) = \begin{cases} \frac{K_m}{\sqrt{\pi a}}\frac{a}{\sqrt{a^2-r^2}} + \frac{2\sigma_0}{\pi}\tan^{-1}\sqrt{\frac{c^2-a^2}{a^2-r^2}}, & r < a, \\ \sigma_0, & a < r < c, \end{cases} \tag{52}$$

$$D_z(r,0) = \frac{B_5}{B_4\pi}\frac{K_m\sqrt{\pi a} + 2\sigma_0\sqrt{c^2-a^2}}{\sqrt{a^2-r^2}},\ r < a, \tag{53}$$

$$\begin{aligned} u_T &= -\tfrac{2\sigma_0}{B_1\pi a}\left[\sqrt{(c^2-a^2)(r^2-a^2)} - ac^2\textstyle\int_a^{\min(r,c)}\frac{\sqrt{r^2-t^2}}{t^2\sqrt{c^2-t^2}}dt\right] \\ &+ \tfrac{K_m\sqrt{\pi a}+2\sigma_0\sqrt{c^2-a^2}}{B_4\pi}\cos^{-1}\tfrac{a}{r},\ r > a, \end{aligned} \tag{54}$$

$$\phi_T = -\frac{2B_2\sigma_0}{B_1\pi a}\left[\sqrt{(c^2-a^2)(r^2-a^2)} - ac^2\int_a^{\min(r,c)}\frac{\sqrt{r^2-t^2}}{t^2\sqrt{c^2-t^2}}dt\right],\ r > a, \tag{55}$$

$$\delta' = \frac{\sigma_0}{2B_4}\left(\frac{c^2}{a}\cos^{-1}\frac{a}{c} - \sqrt{c^2-a^2}\right), \tag{56}$$

where

$$K_m = -\frac{\sigma_0}{\sqrt{\pi a}}\left(\sqrt{c^2-a^2} + \frac{c^2}{a}\cos^{-1}\frac{a}{c}\right). \tag{57}$$

By superposing Equations (47) and (48) and Equations (52) and (53), one can determine that

$$\sigma_{zz}^{M-D}(r,0) = \begin{cases} -B_4\cot\alpha\cosh^{-1}\frac{a}{r} + \frac{a}{\sqrt{\pi a}}\frac{K_I+K_m}{\sqrt{a^2-r^2}} \\ +\frac{2\sigma_0}{\pi}\tan^{-1}\sqrt{\frac{c^2-a^2}{a^2-r^2}},\ r < a, \\ \sigma_0,\ a < r < c. \end{cases} \tag{58}$$

$$\begin{aligned} D_z^{\mathrm{M-D}}(r,0) &= \tfrac{K_D}{\sqrt{\pi a}}\tfrac{a}{\sqrt{a^2-r^2}} - B_5\cot\alpha\cosh^{-1}\tfrac{a}{r} \\ &+\tfrac{B_5}{B_4}\tfrac{K_I+K_m}{\sqrt{\pi a}}\tfrac{a}{\sqrt{a^2-r^2}} + \tfrac{2B_5\sigma_0}{B_4\pi}\sqrt{\tfrac{c^2-a^2}{a^2-r^2}}, r<a. \end{aligned} \tag{59}$$

According to the classical M-D theory [57], in order to eliminate the stress singularity at the fringe of the contact zone, the following continuity condition should be satisfied:

$$K_I + K_m = 0 \Rightarrow K_I = \frac{P_1 - P}{2a\sqrt{\pi a}} = -K_m = \frac{\sigma_0}{\sqrt{\pi a}}\left(\sqrt{c^2-a^2} + \frac{c^2}{a}\cos^{-1}\frac{a}{c}\right). \tag{60}$$

From Equation (60), one can obtain

$$\begin{aligned} P &= P_1 - 2\sigma_0 a\left(\sqrt{c^2-a^2} + \tfrac{c^2}{a}\cos^{-1}\tfrac{a}{c}\right) \\ &= \pi a^2 B_4\cot\alpha - 2\sigma_0 a\left(\sqrt{c^2-a^2} + \tfrac{c^2}{a}\cos^{-1}\tfrac{a}{c}\right). \end{aligned} \tag{61}$$

Using the continuity condition in Equation (60), Equations (58) and (59) can be simplified as

$$\sigma_{zz}^{\mathrm{M-D}}(r,0) = \begin{cases} -B_4\cot\alpha\cosh^{-1}\tfrac{a}{r} + \tfrac{2\sigma_0}{\pi}\tan^{-1}\sqrt{\tfrac{c^2-a^2}{a^2-r^2}}, & r<a, \\ \sigma_0, & a<r<c. \end{cases} \tag{62}$$

and

$$D_z^{\mathrm{M-D}}(r,0) = \frac{K_D}{\sqrt{\pi a}}\frac{a}{\sqrt{a^2-r^2}} - B_5\cot\alpha\cosh^{-1}\frac{a}{r} + \frac{2B_5\sigma_0}{B_4\pi}\sqrt{\frac{c^2-a^2}{a^2-r^2}},\ r<a, \tag{63}$$

respectively.

For the indentation depth, by superposing Equations (14) and (56) and combining the result presented in Equation (61), one can obtain

$$h^{\mathrm{M-D}} = \frac{\pi a}{2}\cot\alpha - \frac{\sigma_0}{B_4}\sqrt{c^2-a^2} - B_3\phi_0. \tag{64}$$

Using Equations (50) and (54), and considering the continuity condition in Equation (60), the discontinuity displacement outside the contact region can be obtained as

$$\begin{aligned} \left[u_z^{\mathrm{M-D}}(r,0)\right] &= \left(\tfrac{2B_3\phi_0}{\pi} - a\cot\alpha\right)\cos^{-1}\tfrac{a}{r} \\ &+\sqrt{r^2-a^2}\cot\alpha + \tfrac{2\sigma_0\sqrt{c^2-a^2}}{\pi B_4}\cos^{-1}\tfrac{a}{r} \\ &-\tfrac{2\sigma_0}{B_1\pi a}\left[\sqrt{(c^2-a^2)(r^2-a^2)} - ac^2\textstyle\int_a^{\min(r,c)}\tfrac{\sqrt{r^2-t^2}}{t^2\sqrt{c^2-t^2}}dt\right]. \end{aligned} \tag{65}$$

The discontinuity of the displacement can be given as

$$\begin{aligned} \delta_t = \left[u_z^{\mathrm{M-D}}(c,0)\right] &= \left[\sqrt{m^2-1} - \cos^{-1}\left(\tfrac{1}{m}\right)\right]a\cot\alpha \\ &+\tfrac{2B_3\phi_0}{\pi}\cos^{-1}\left(\tfrac{1}{m}\right) + \tfrac{2\sigma_0 a}{\pi}\left[\tfrac{1}{B_4}\sqrt{m^2-1}\cos^{-1}\left(\tfrac{1}{m}\right) - \tfrac{1}{B_1}(m-1)\right], \end{aligned} \tag{66}$$

where $m = c/a$.

By superposing Equations (51) and (55), the discontinuity of electric potential can be derived as

$$\begin{aligned} \left[\phi^{\mathrm{M-D}}(r,0)\right] &= -\tfrac{2\phi_0}{\pi}\cos^{-1}\tfrac{a}{r} \\ &-\tfrac{2B_2\sigma_0}{B_1\pi a}\left[\sqrt{(c^2-a^2)(r^2-a^2)} - ac^2\textstyle\int_a^{\min(r,c)}\tfrac{\sqrt{r^2-t^2}}{t^2\sqrt{c^2-t^2}}dt\right]. \end{aligned} \tag{67}$$

where $a < r < c$, one can determine that

$$\begin{array}{l}\left[\phi^{\mathrm{M-D}}(r,0)\right] = -\frac{2\phi_0}{\pi}\cos^{-1}\frac{a}{r} \\ -\frac{2B_2\sigma_0}{B_1\pi a}\left[\sqrt{(c^2-a^2)(r^2-a^2)} - ac^2\int_a^r \frac{\sqrt{r^2-t^2}}{t^2\sqrt{c^2-t^2}}dt\right].\end{array} \tag{68}$$

by virtue of the following integral results [57]:

$$\int_a^r \frac{\sqrt{r^2-t^2}}{t^2\sqrt{c^2-t^2}}dt = \frac{1}{a}\sqrt{\frac{r^2-a^2}{c^2-a^2}} - \frac{1}{c}E(\zeta,t), \tag{69}$$

where

$$E(\zeta,t) = \int_0^\zeta \sqrt{1-t^2\sin^2\theta}d\theta \tag{70}$$

is the elliptic integral of the second kind, and

$$\zeta = \arcsin\left(\frac{c}{r}\sqrt{\frac{r^2-a^2}{c^2-a^2}}\right),\ t = \frac{r}{c}. \tag{71}$$

Equation (68) can be simplified as

$$\begin{array}{l}\left[\phi^{\mathrm{M-D}}(r,0)\right] = -\frac{2\phi_0}{\pi}\cos^{-1}\frac{a}{r} \\ -\frac{2B_2\sigma_0}{B_1\pi a}\left[\sqrt{(c^2-a^2)(r^2-a^2)} - c^2\sqrt{\frac{r^2-a^2}{c^2-a^2}} + acE(\zeta,t)\right].\end{array} \tag{72}$$

When $\rho_0 \to 0$, from Equations (63) and (72), one can determine that

$$D_z^{\mathrm{M-D}}(a-\rho_0,0) \approx \frac{2B_5(B_6+B_3)\phi_0}{\pi\sqrt{2a\rho_0}} + \frac{B_5}{B_4}\frac{2\sigma_0}{\pi}\sqrt{\frac{c^2-a^2}{2a\rho_0}}. \tag{73}$$

$$\begin{array}{l}\left[\phi^{\mathrm{M-D}}(a+\rho_0,0)\right] \approx -\frac{2\phi_0}{\pi}\cos^{-1}\frac{a}{a+\rho_0} \\ -\frac{2B_2\sigma_0}{B_1\pi a}\left[\sqrt{(c^2-a^2)2a\rho_0} - c^2\sqrt{\frac{2a\rho_0}{c^2-a^2}} + acE(\zeta,t)\right].\end{array} \tag{74}$$

In the case of $\rho_0 \to 0$, using the following results [68]:

$$\cos^{-1}\frac{a}{a+\rho_0} \approx \sqrt{\frac{2\rho_0}{a}},\ E(\zeta,t) \approx \frac{\sqrt{2a\rho_0}}{c}\left(\frac{a}{\sqrt{c^2-a^2}} + \frac{\sqrt{c^2-a^2}}{a}\right), \tag{75}$$

Equation (74) can be simplified as

$$\left[\phi^{\mathrm{M-D}}(a+\rho_0,0)\right] = -\frac{2}{\pi}\left(\phi_0 + \frac{B_2}{B_1}\sigma_0\sqrt{c^2-a^2}\right)\sqrt{\frac{2\rho_0}{a}}. \tag{76}$$

Using the virtual crack closure integral technique [68,69], the energy release rate of the piezoelectric solid can be calculated as

$$G = \sigma_0\delta_t + \lim_{\delta\to 0}\frac{1}{\delta}\int_0^\delta \frac{1}{2}D_z^{\mathrm{M-D}}(a-\rho_0,0)\left[\phi^{\mathrm{M-D}}(a+\delta-\rho_0,0)\right]d\rho_0. \tag{77}$$

By substituting Equations (73) and (76) into Equation (77), and using the following integral result [80]:

$$\lim_{\delta\to 0}\frac{1}{\delta}\int_0^\delta \sqrt{\frac{\delta-\rho_0}{\rho_0}}d\rho_0 = \frac{\pi}{2}, \tag{78}$$

the energy release rate can be derived as

$$\begin{aligned} G = &\left[\sqrt{m^2-1} - \cos^{-1}\left(\tfrac{1}{m}\right)\right]\sigma_0 a \cot\alpha + \tfrac{2B_3\phi_0\sigma_0}{\pi}\cos^{-1}\left(\tfrac{1}{m}\right) \\ &+\tfrac{2\sigma_0^2 a}{\pi}\left[\tfrac{1}{B_4}\sqrt{m^2-1}\cos^{-1}\left(\tfrac{1}{m}\right) - \tfrac{1}{B_1}(m-1)\right] - \tfrac{B_5(B_3+B_6)\phi_0^2}{\pi a} \\ &-\tfrac{1}{\pi}\left[\tfrac{B_5}{B_4} + \tfrac{B_2B_5(B_3+B_6)}{B_1}\right]\phi_0\sigma_0\sqrt{m^2-1} - \tfrac{B_2B_5}{B_1B_4}\tfrac{\sigma_0^2 a}{\pi}(m^2-1). \end{aligned} \tag{79}$$

Using the Griffith energy balance criterion, one can determine that

$$\begin{aligned} &\left[\sqrt{m^2-1} - \cos^{-1}\left(\tfrac{1}{m}\right)\right]\sigma_0 a \cot\alpha + \tfrac{2B_3\phi_0\sigma_0}{\pi}\cos^{-1}\left(\tfrac{1}{m}\right) \\ &+\tfrac{2\sigma_0^2 a}{\pi}\left[\tfrac{1}{B_4}\sqrt{m^2-1}\cos^{-1}\left(\tfrac{1}{m}\right) - \tfrac{1}{B_1}(m-1)\right] - \tfrac{B_5(B_3+B_6)\phi_0^2}{\pi a} \\ &-\tfrac{1}{\pi}\left[\tfrac{B_5}{B_4} + \tfrac{B_2B_5(B_3+B_6)}{B_1}\right]\phi_0\sigma_0\sqrt{m^2-1} - \tfrac{B_2B_5}{B_1B_4}\tfrac{\sigma_0^2 a}{\pi}(m^2-1) = \Delta\gamma, \end{aligned} \tag{80}$$

where $\Delta\gamma$ denotes the work of adhesion.

The correctness of the above results can be verified by checking whether the corresponding JKR solutions obtained in Section 3.2 can be derived as the limit case from them, and the detailed procedures can be found in Appendix F. This verified method was also adopted in the classical M-D theory [81].

By adopting the same solution procedures as those of Case I, one can also obtain the corresponding solutions for Case II, and the solutions of Case II have the similar mathematical structures to Case I. The corresponding solutions for Case II are presented in Appendix D.

5. Numerical Results and Discussion

In this section, the effects of the electric potential, the half cone angle of the conical punch, and different material properties on the adhesion behaviors will be revealed. In the following numerical analysis, the corresponding numerical results were computed by Mathematica software. The material properties of the four different piezoelectric materials examined here are listed in Table 1. For the sake of convenience, the following dimensionless physical parameters are defined:

$$\begin{aligned} &P^* = P\Big/\left(\tfrac{\Delta\gamma^2}{B_4}\right),\ a^* = a\Big/\left(\tfrac{\Delta\gamma}{B_4}\right),\ h^* = h\Big/\left(\tfrac{\Delta\gamma}{B_4}\right), \\ &\phi^* = B_3\phi_0\Big/\left(\tfrac{\Delta\gamma}{B_4}\right),\ m = \tfrac{c}{a},\ \lambda = \tfrac{\sigma_0}{B_4}. \end{aligned} \tag{81}$$

5.1. JKR Solutions

Based on the JKR theory, the variations of the dimensionless contact radius, a^*, with the dimensionless indentation force, P^*, for the four different piezoelectric materials are shown in Figure 3. From Figure 3a, one can see that the electric potential has a prominent effect on the adhesive contact behavior. For the electrically conducting punch, the pull-off force increases with the electric potential. In the case of $Ba_{0.917}Ca_{0.083}TiO_3$, as the dimensionless electric potential, ϕ^*, increases from 0 to 3, the corresponding pull-off force increases by about six times, which indicates that the adhesion effect can be strengthened by applying electric potential. This conclusion is in good agreement with the experimental results derived by [82]. Furthermore, the above result also suggests that as typical functional materials, piezoelectric materials offer a new approach to achieve reversible adhesion.

Table 1. Material constants of the four piezoelectric materials.

	PZT-4	PZT-5A	$BaTiO_3$	$(Ba_{0.917}Ca_{0.083})TiO_3$
Elastic coefficients (GPa)				
c_{11}	139.00	121.00	150.00	158.00
c_{33}	115.00	111.00	146.00	150.00
c_{44}	25.60	21.10	44.00	45.00
c_{12}	77.80	75.40	66.00	69.00
c_{13}	74.30	75.20	66.00	67.50
Piezoelectric coefficients (C/m^2)				
e_{31}	−5.200	−5.400	−4.350	−3.100
e_{33}	15.10	15.80	17.50	13.50
e_{15}	12.70	12.30	11.40	10.90
Dielectric constants (10^{-9} F/m)				
$\in_{11}$	6.461	8.107	9.868	8.850
$\in_{33}$	5.620	7.346	11.151	8.054
Material coefficients				
B_1 (GPa)	56.41	47.88	70.68	71.48
B_2 (10^9 V/m)	1.246	1.0196	0.8645	0.8787
B_3 (10^{-10} m/V)	2.501	3.035	1.668	1.312
B_4 (GPa)	43.00	36.56	61.77	64.09
B_5 (C/m^2)	10.756	11.097	10.302	8.411
B_6 (10^{-10} m/V)	8.027	9.807	11.567	11.381

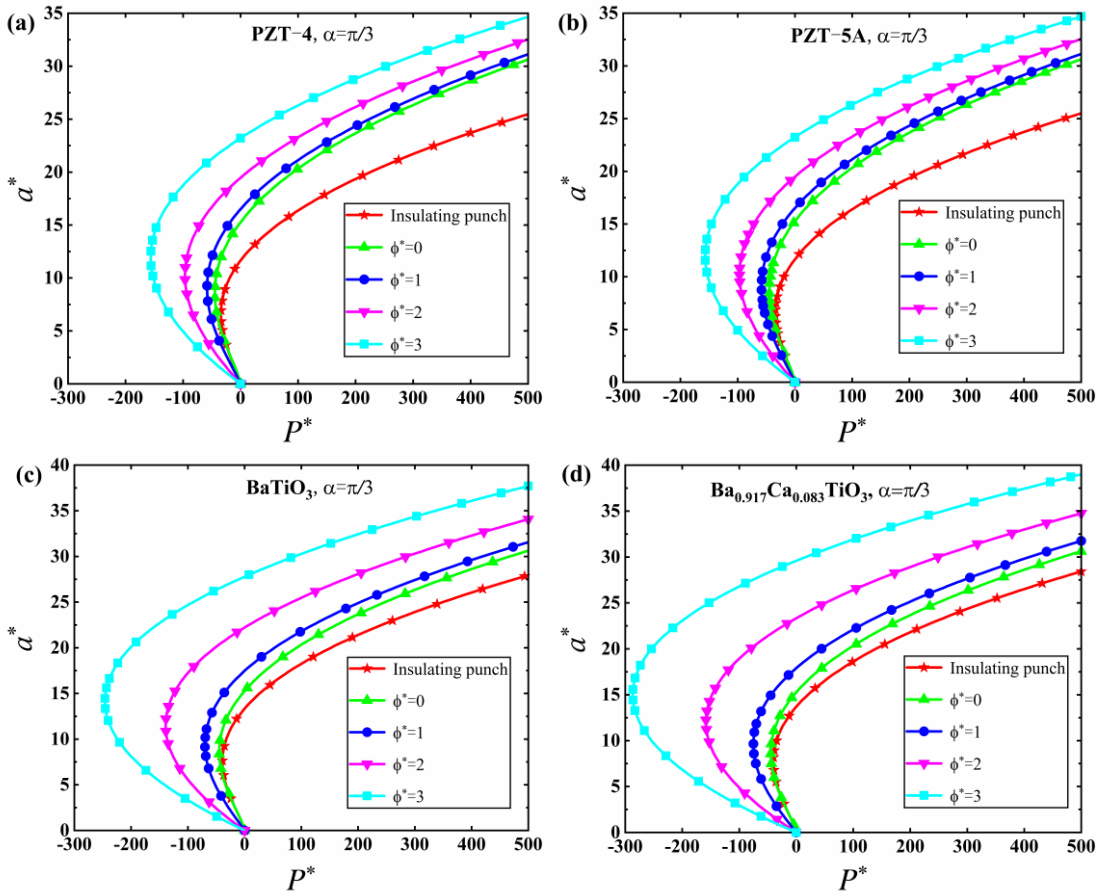

Figure 3. The dimensionless contact radius, a^*, as a function of the dimensionless indentation force, P^*, at a fixed value of $\alpha = \pi/3$ for the JKR model. (**a**) PZT-4. (**b**) PZT-5A. (**c**) $BaTiO_3$. (**d**) $Ba_{0.917}Ca_{0.083}TiO_3$.

For a given indentation force, one can determine from Figure 3 that the larger the exerted electric potential, the larger the contact radius, which reveals that it is easier

to obtain a larger contact area for a conducting punch with higher electric potential. It is worth noting that the $P^* - a^*$ curves of the insulating punch are always below the corresponding curves for the conducting punch. This result indicates that the minimum pull-off force is obtained for the insulating punch, and for a given indentation force, the contact radius under the action of the insulating punch is always smaller than the counterpart value induced by the conducting punch. In addition, comparing the results displayed in Figure 3a–d, one can determine that under the action of the same electric potential, the adhesion strengthening effect induced by the electric potential for the $BaTiO_3$ and $Ba_{0.917}Ca_{0.083}TiO_3$ was more prominent than that for the PZT-4 and PZT-5A, which stems from different material properties between them. This reveals that the effect of the electric potential on the $a^* \sim P^*$ curve is sensitive to different material properties, which was not suggested in the existing studies on piezoelectric materials [60] and multiferroic composite materials [68,69].

Figures 4 and 5 display the effect of the half cone angle of the rigid conical punch on the adhesion behaviors of the four different piezoelectric materials. It can be seen in Figure 4 that whether for the insulating punch or the conducting punch with zero electric potential, the pull-off force increases with the half cone angle of the rigid conical punch. For a given indentation force, the larger the half cone angle, the larger the contact radius. It is worth mentioning that the curves of the conducting punch with zero electric potential are always above the corresponding curves for the insulating punch, which indicates that for conical punches with the same half cone angle, the contact radius induced by the conducting punch is always larger than the counterpart value under the insulating punch when both of them are subjected to the same indentation force.

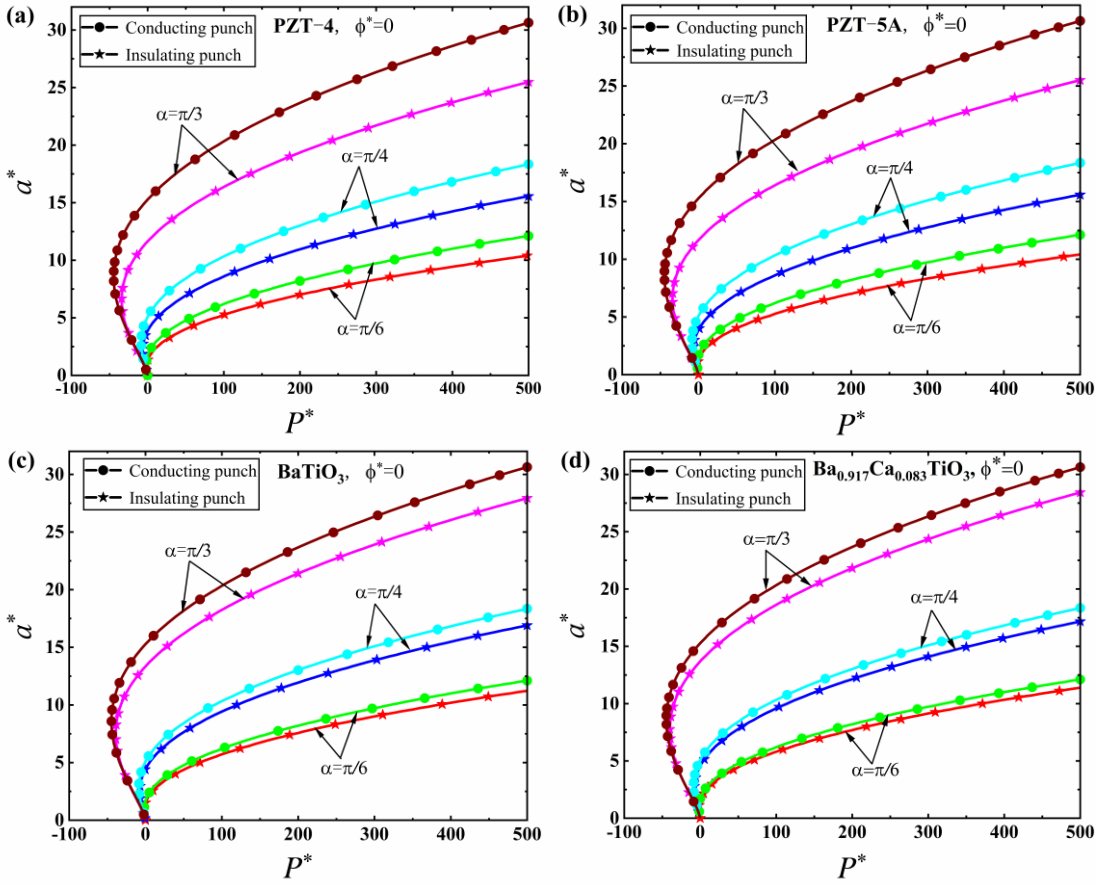

Figure 4. Variation of the dimensionless contact radius, a^*, with the dimensionless indentation force, P^*, at the different values of $\alpha = \pi/6, \pi/4$ and $\pi/3$ for the conducting punch with zero electric potential and insulating punch. (**a**) PZT-4. (**b**) PZT-5A. (**c**) $BaTiO_3$. (**d**) $Ba_{0.917}Ca_{0.083}TiO_3$.

According to the results presented in Figures 3 and 4, one can find that increasing the electric potential or increasing the half cone angle of the conical punch can enhance the adhesion effect. Therefore, it can be found from Figures 4 and 5 that the pull-off force and the contact radius under the action of the same indentation force for a conducting punch with non-zero electric potential are obviously larger than the counterpart values induced by a conducting punch with zero potential. Furthermore, one can see from Figure 5 that for the conducting punch with non-zero electric potential, the adhesion strengthening effect induced by increasing the half cone angle was very prominent. For example, for the PZT-4 subjected to the dimensionless electric potential $\phi^* = 2$, as the half cone angle of the conical punch changes from $\pi/6$ to $\pi/3$, the pull-off force of the contact system increases by about seven times, which suggests to us that a conical punch with a small cone angle should be adopted in nanoindentation tests in order to reduce the effect of adhesion on the results of characterization. From Figures 4 and 5, one can determine that the $a^* \sim P^*$ curves for the four different piezoelectric materials examined here are not very distinct, which reveals that the effect of the half cone angle on the adhesion behavior is insensitive to the material properties. This conclusion was obtained for the first time in our work and was not given in the existing studies on piezoelectric materials [60] and multiferroic composite materials [68,69].

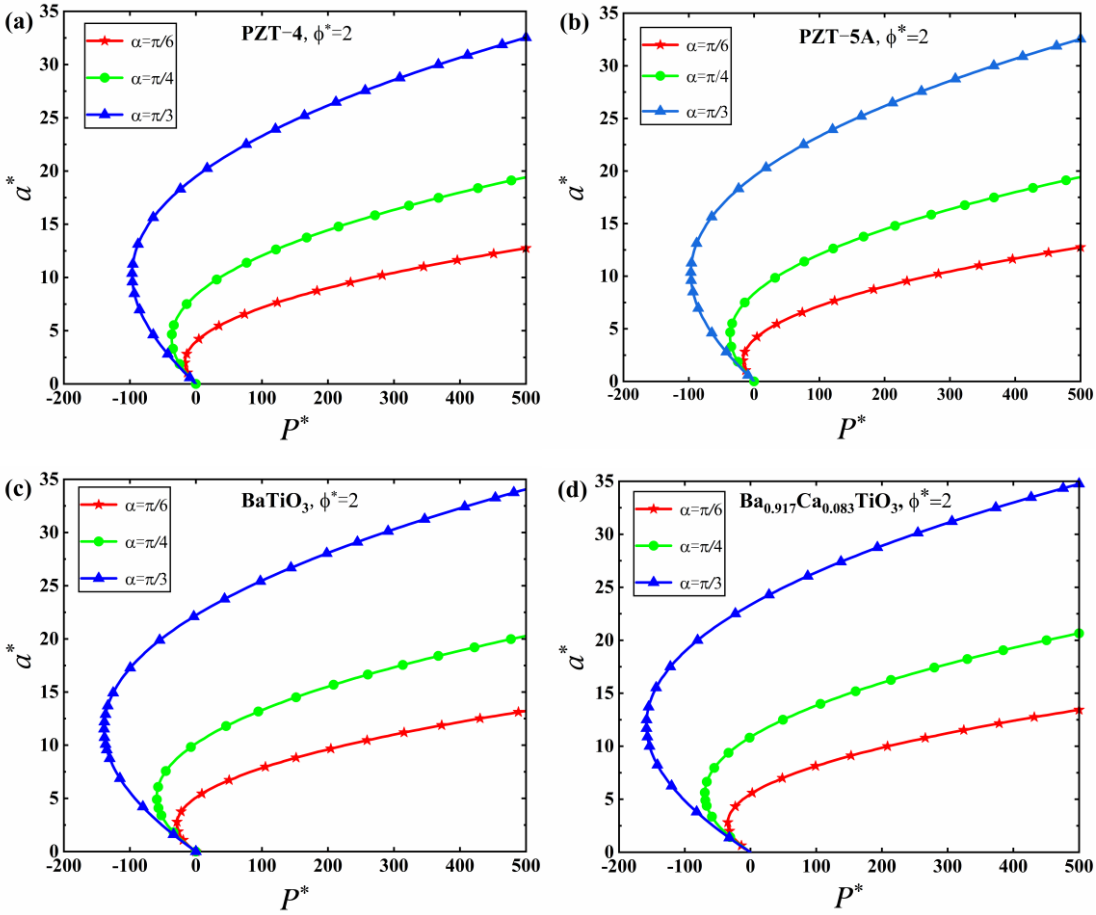

Figure 5. Variation of the dimensionless contact radius, a^*, with the dimensionless indentation force, P^*, at the different values of $\alpha = \pi/6, \pi/4$ and $\pi/3$ for the conducting punch with non-zero electric potential ($\phi^* = 2$). (**a**) PZT-4. (**b**) PZT-5A. (**c**) $BaTiO_3$. (**d**) $Ba_{0.917}Ca_{0.083}TiO_3$.

The scanning probe microscope and nanoindentation technique play significant roles in characterizing the mechanical properties of various materials. During the nanoindentation testing technique, the sample is pressed by a small indenter tip and the force and displacement are continuously measured as a function of time with high accuracy and pre-

cision, which can be used to evaluate the mechanical properties of the materials. Therefore, the indentation force-displacement curve $P^* \sim h^*$ is the key theoretical foundation of the nanoindentation technique. When a piezoelectric solid is indented by a rigid conducting or insulating conical punch, the dimensionless indentation force, P^*, as a function of the dimensionless indentation depth, h^*, for the four different piezoelectric materials is shown in Figure 6. We found that the pull-off force of the conducting punch under force control increases with increases in the electric potential. The sign of the electric potential has little effect on the magnitude of pull-off force. Furthermore, one may notice that the critical indentation depth at the pull-off moment in the case of a negative electric potential is always larger than the counterpart value when the punch is subjected to positive electric potential.

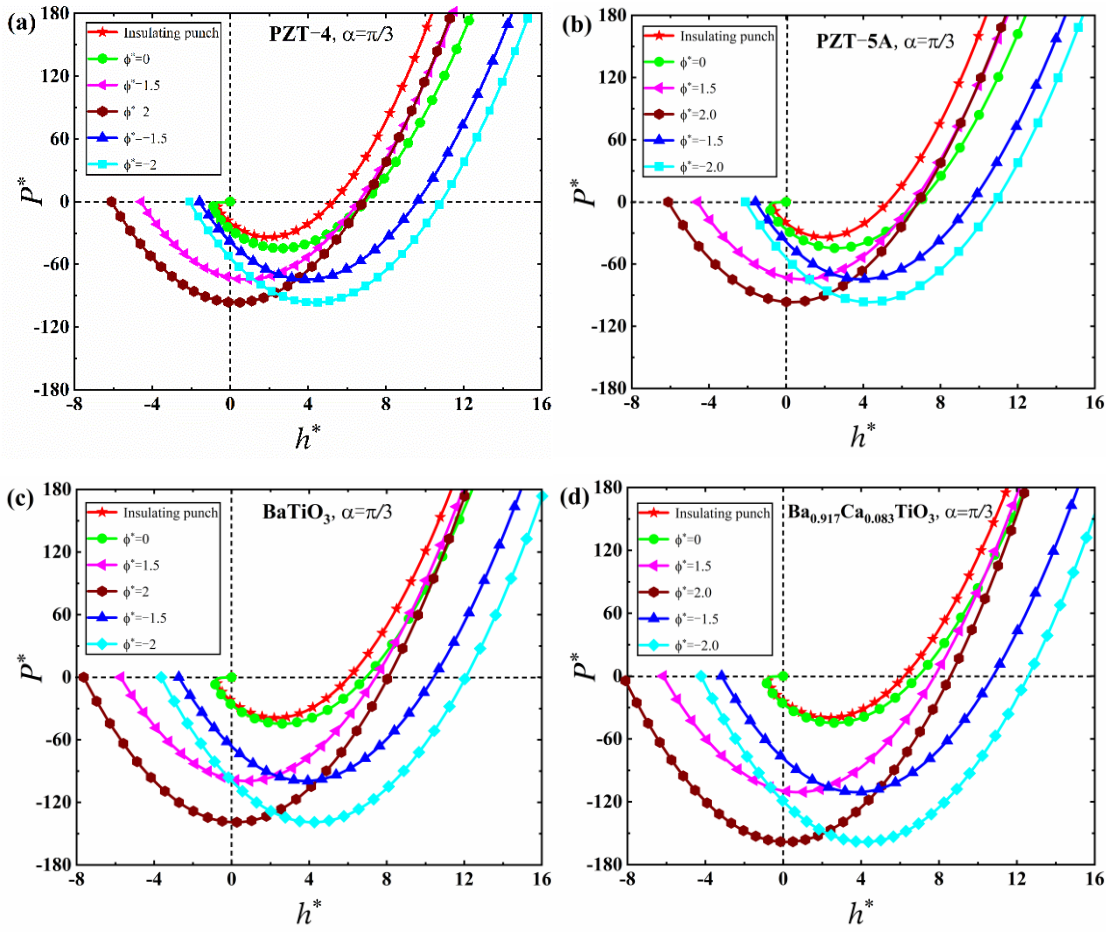

Figure 6. The dimensionless indentation force, P^*, as a function of the dimensionless indentation depth, h^*, at a fixed value of $\alpha = \pi/3$ for the JKR model. (**a**) PZT-4. (**b**) PZT-5A. (**c**) $BaTiO_3$. (**d**) $Ba_{0.917}Ca_{0.083}TiO_3$.

It can be seen from Figure 6 that the $P^* \sim h^*$ curves of the conducting punch are always below the corresponding curves of the insulating punch, which yields two main conclusions. First, the pull-off force under force control for the conducting punch is always larger than the counterpart value of the insulating punch, which is consistent with the conclusions derived from Figures 3 and 4. Second, for a given indentation force, the indentation depth under the action of the insulating punch is always smaller than the counterpart value for the conducting punch. In contrast, for a given indentation depth, the indentation force exerted on the insulating punch is larger than the counterpart value applied to the conducting punch. The above results can serve as the theoretical foundation for the nanoindentation technique in characterizing the mechanical and adhesion properties of piezoelectric materials. By comparing the results shown in Figure 6a–d, one can

conclude that the effect of the electric potential on the adhesion behaviors of $BaTiO_3$ and $Ba_{0.917}Ca_{0.083}TiO_3$ was more prominent than that on PZT-4 and PZT-5A, which is attributed to the different material properties of the four piezoelectric materials examined here. This also reveals that the effect of the electric potential on $P^* \sim h^*$ curve is largely dependent on different material properties, which was not derived in the existing studies on piezoelectric materials [60] and multiferroic composite materials [68,69].

Figures 7 and 8 present the effect of the half cone angle of a conical punch on the variation of the dimensionless indentation force, P^*, with the dimensionless indentation depth, h^*. One can see in Figure 7 that the pull-off force increases with the half cone angle for both the insulating and conducting conical punches, which is consistent with the conclusions obtained from Figures 4 and 5. It is noteworthy that the $P^* \sim h^*$ curve lies almost entirely on the positive semi-axis of P^* for the very sharp punch (i.e., $\alpha \leq \pi/6$), which suggests that the adhesion effect is very weak in this case. Therefore, a conical punch with a small half cone angle should be adopted in nanoindentation tests, as this can weaken the adhesion effect and improve the accuracy of the results of characterization.

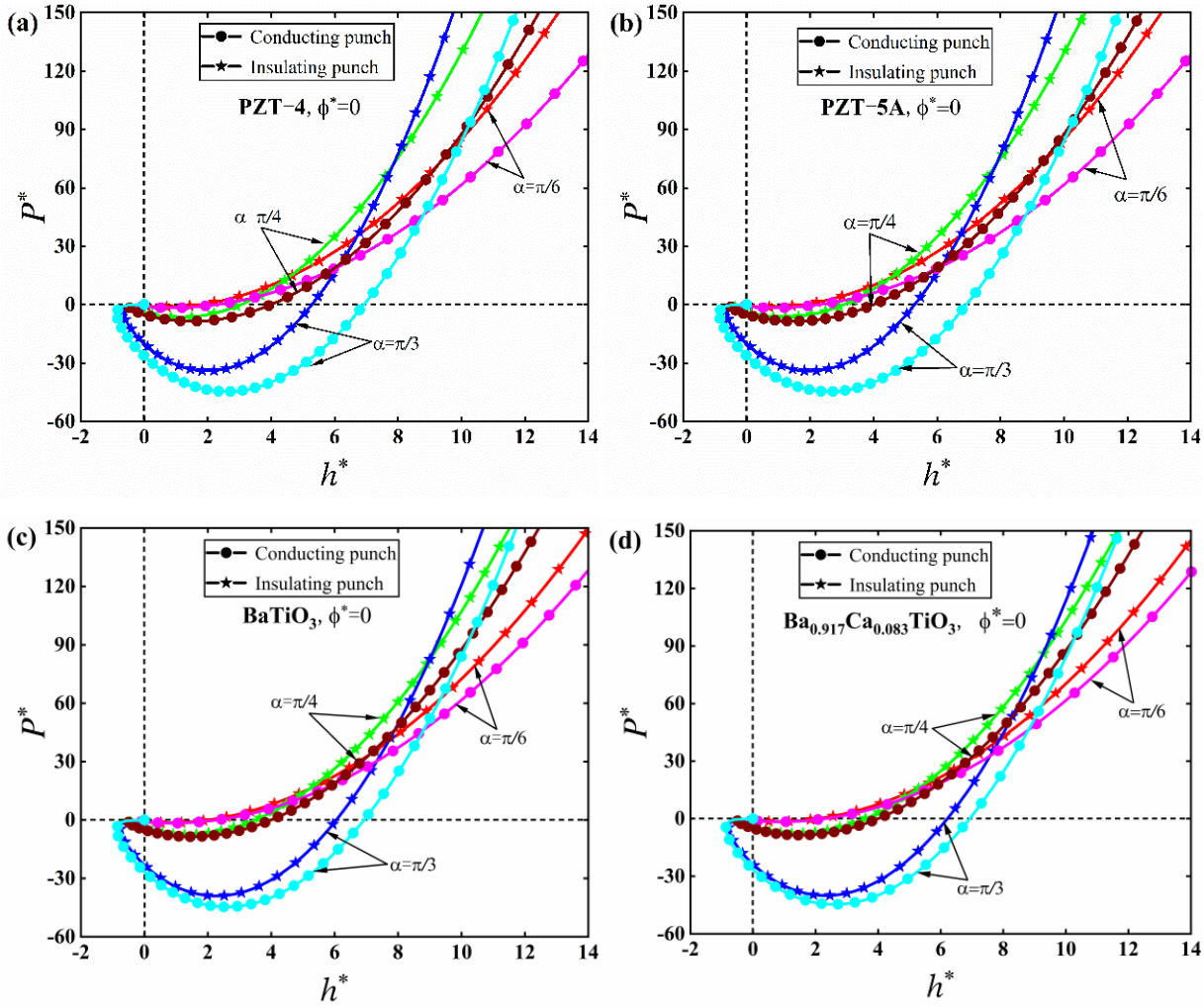

Figure 7. Variation of the dimensionless indentation force, P^*, with the dimensionless indentation depth h^* at the different values of $\alpha = \pi/6, \pi/4$ and $\pi/3$ for the conducting punch with zero electric potential and the insulating punch. (**a**) PZT-4. (**b**) PZT-5A. (**c**) $BaTiO_3$. (**d**) $Ba_{0.917}Ca_{0.083}TiO_3$.

For the conducting punch with non-zero electric potential, the results shown in Figure 8 reveal that the adhesion strengthening effect induced by increasing the half cone angle of the conical punch becomes more prominent. It can be seen in Figures 7 and 8 that the $P^* \sim h^*$ curves for the four different piezoelectric materials examined here are very similar, which

suggests that the effect of the half cone angle on the load-displacement curves is insensitive to material properties, which was not revealed in the existing studies on piezoelectric materials [60] and multiferroic composite materials [68,69]. Furthermore, one can see from Figure 7 that the load-displacement curves under the conical indenters with different half cone angles have very different slopes, which indicates that the half cone angle can significantly affect the characterization of mechanical properties in nanoindentation tests.

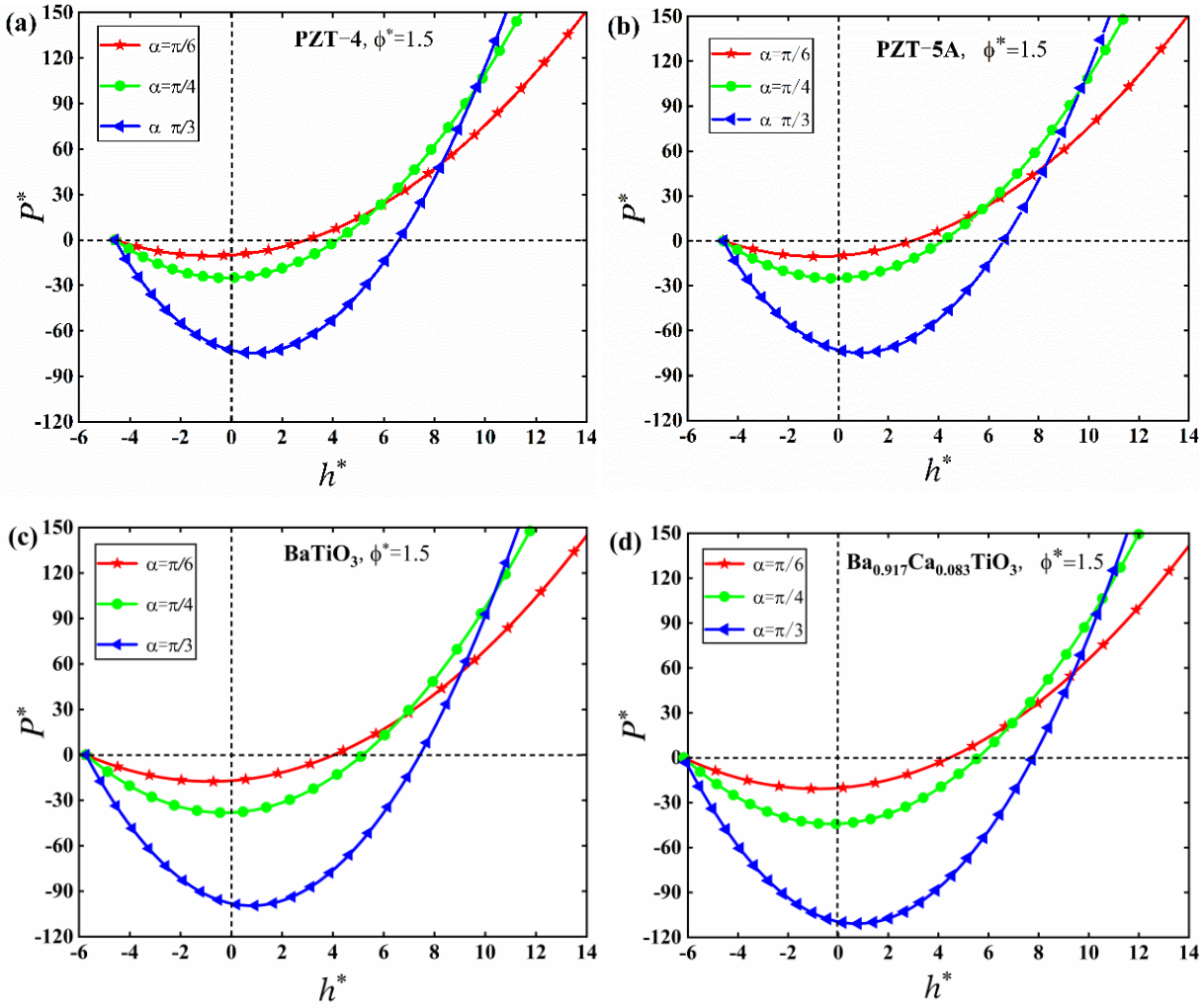

Figure 8. The dimensionless indentation force, P^*, as a function of the dimensionless indentation, h^*, at the different values of $\alpha = \pi/6, \pi/4$ and $\pi/3$ for the conducting punch with non-zero electric potential ($\phi^* = 1.5$). (**a**) PZT-4. (**b**) PZT-5A. (**c**) $BaTiO_3$. (**d**) $Ba_{0.917}Ca_{0.083}TiO_3$.

Figure 9 illustrates the influence of the dimensionless electric potential, ϕ^*, on the variation of the dimensionless contact radius, a^*, with the dimensionless indentation depth, h^*. The results reveal that the electric potential has a prominent effect on the relation between the contact radius and the indentation depth. It is worth noting that the $a^* \sim h^*$ curves for the conducting punch are always above the corresponding curve for the insulating punch, which indicates that for a given indentation depth, the contact radius under the action of the conducting punch is always larger than the counterpart value of the insulating punch. Furthermore, for the insulating punch and the conducting punch with zero electric potential, one can determine that the critical contact radius at pull-off moment is a finite value under displacement control. In contrast, the pull-off moment happens when the contact radius decreases to zero for the conducting punch. However, the correctness of these conclusions should be verified by corresponding experimental studies in the future.

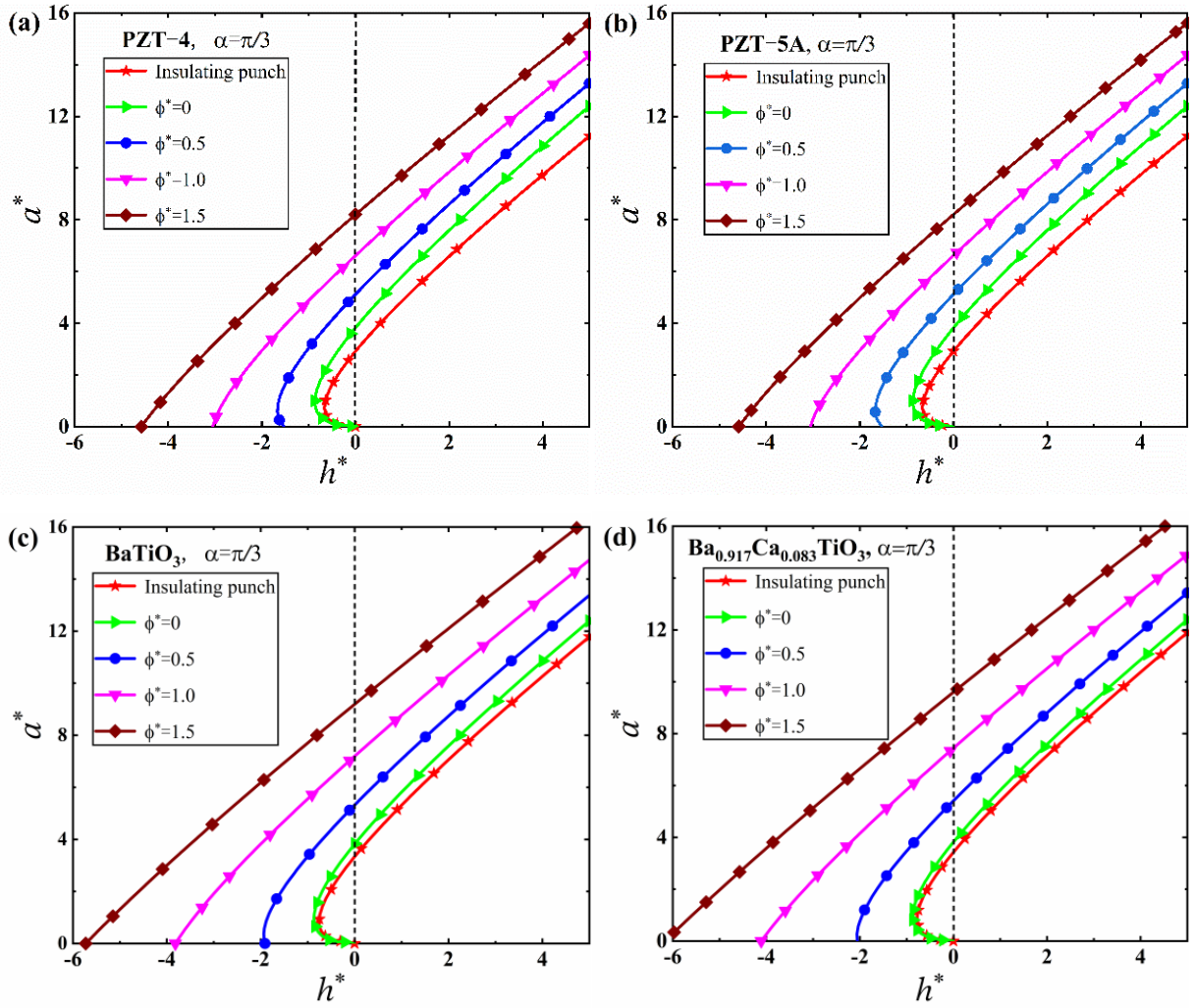

Figure 9. The dimensionless contact radius, a^*, as a function of the dimensionless indentation depth, h^*, at a fixed value of $\alpha = \pi/3$ for the JKR model. (**a**) PZT-4. (**b**) PZT-5A. (**c**) $BaTiO_3$. (**d**) $Ba_{0.917}Ca_{0.083}TiO_3$.

The effect of the half cone angle on the variation of the dimensionless contact radius as a function of the dimensionless indentation depth is shown in Figures 10 and 11. It can be seen in Figure 10 that for a given indentation depth, the larger the half cone angle, the larger the contact radius for both the insulating and conducting punches, which is easy to understand. In the case of a punch with the same half cone angle and indentation depth, the contact radius for the conducting punch is always larger than the counterpart value for the insulating punch, and the difference between them increases with increases in the half cone angle. By comparing the results displayed in Figures 10 and 11, one can determine that the half cone angle has a more prominent effect on the variation of the dimensionless contact radius with the dimensionless indentation depth when a piezoelectric solid is indented by a conducting punch with non-zero electric potential. Furthermore, the $a^* \sim h^*$ curves for the four different piezoelectric materials presented in Figures 10 and 11 are very similar, which also means that the effect of the half cone angle on the relation between the contact radius and indentation depth is insensitive to material properties.

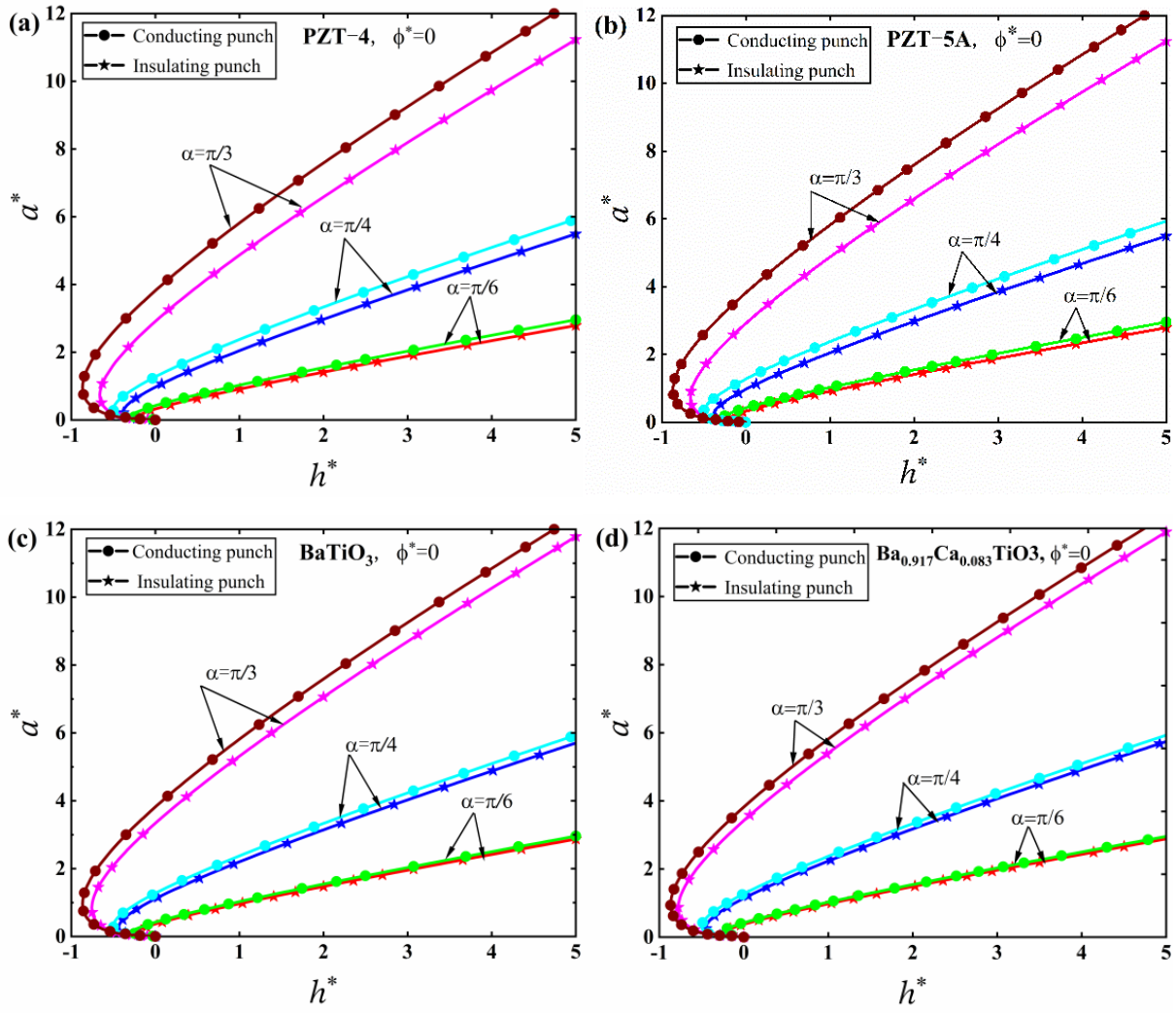

Figure 10. Variation of the dimensionless contact radius, a^*, with the dimensionless indentation depth, h^*, at the different values of $\alpha = \pi/6, \pi/4$ and $\pi/3$ for the conducting punch with zero electric potential and the insulating punch. (**a**) PZT-4. (**b**) PZT-5A. (**c**) $BaTiO_3$. (**d**) $Ba_{0.917}Ca_{0.083}TiO_3$.

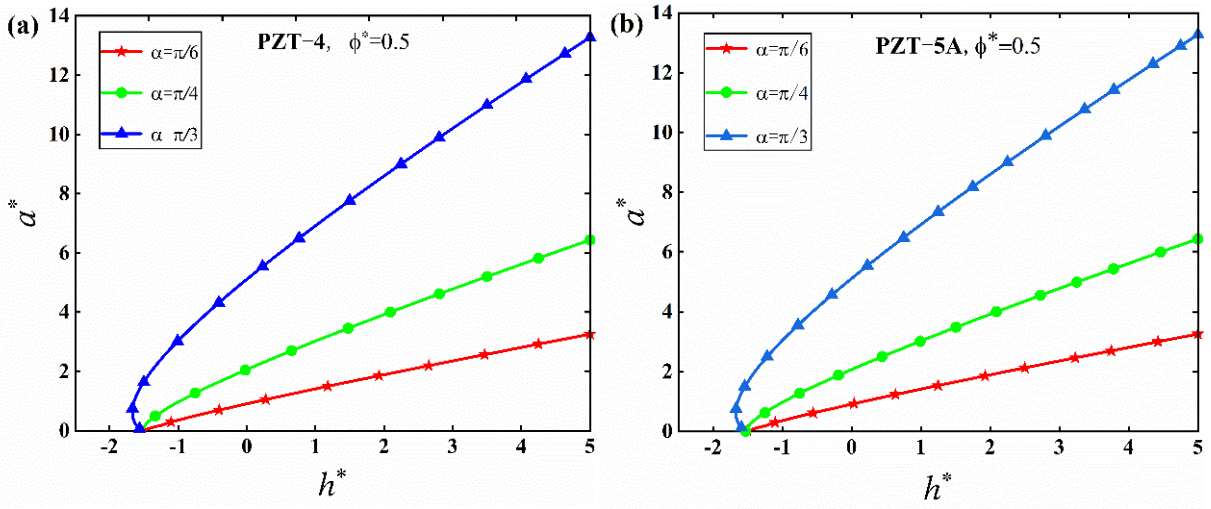

Figure 11. *Cont.*

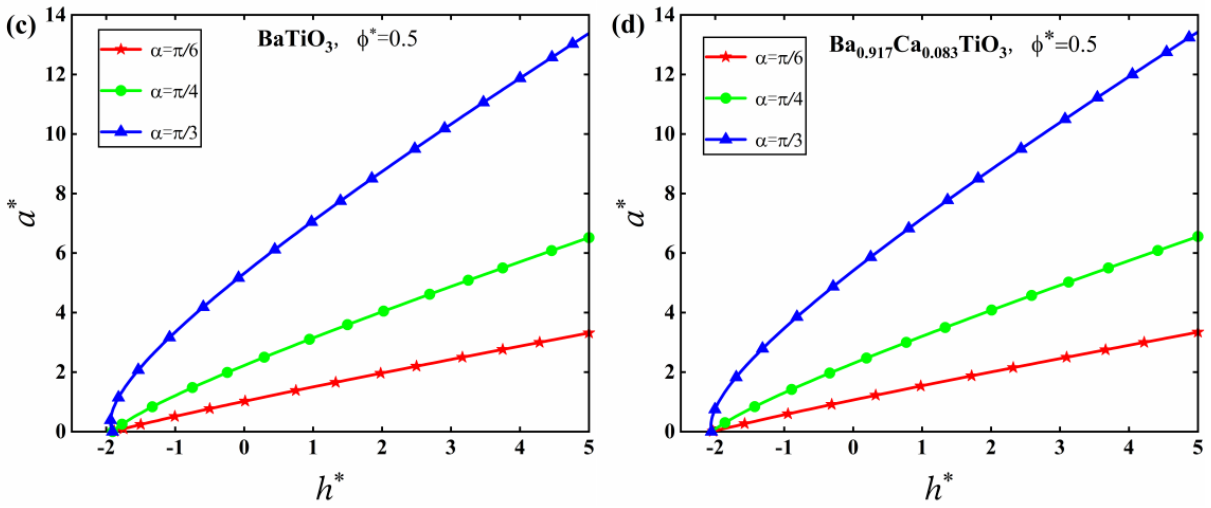

Figure 11. Variation of the dimensionless contact radius, a^*, with the dimensionless indentation depth, h^*, at different values of $\alpha = \pi/6, \pi/4$ and $\pi/3$ for the conducting punch with non-zero electric potential ($\phi^* = 0.5$). (**a**) PZT-4. (**b**) PZT-5A. (**c**) $BaTiO_3$. (**d**) $Ba_{0.917}Ca_{0.083}TiO_3$.

Figure 12 presents the effect of the electric potential on the pull-off force of different piezoelectric adhesion systems. It can be seen in Figure 12 that the electric potential has a very significant effect on the pull-off force of the piezoelectric adhesion system. For the four different piezoelectric materials considered here, the dimensionless pull-off force increases by more than two times as the absolute value of the dimensionless electric potential increases from 0 to 2. This result embodies the adhesion strengthening effect induced by the electric potential, which is in agreement with the experimental result given by [82]. In addition, one can also determine that the pull-off force for the conducting punch is always larger than the counterpart value of the insulating punch. The variation of the dimensionless pull-off force as a function of the half cone angle of the conical punch is shown in Figure 13. The results reveal that the magnitude of the pull-off force increases with the half cone angle and finally approaches infinity in the limit case $\alpha = \pi/2$, which is consistent with the result given by a multiferroic half-space indented by a rigid conical punch [69]. In the limit case of $\alpha = \pi/2$, the rigid conical punch becomes the semi-infinite rigid punch. By comparing the results presented in Figure 13a–d, one can conclude that the effect of the half cone angle on the pull-off force is insensitive to the material properties.

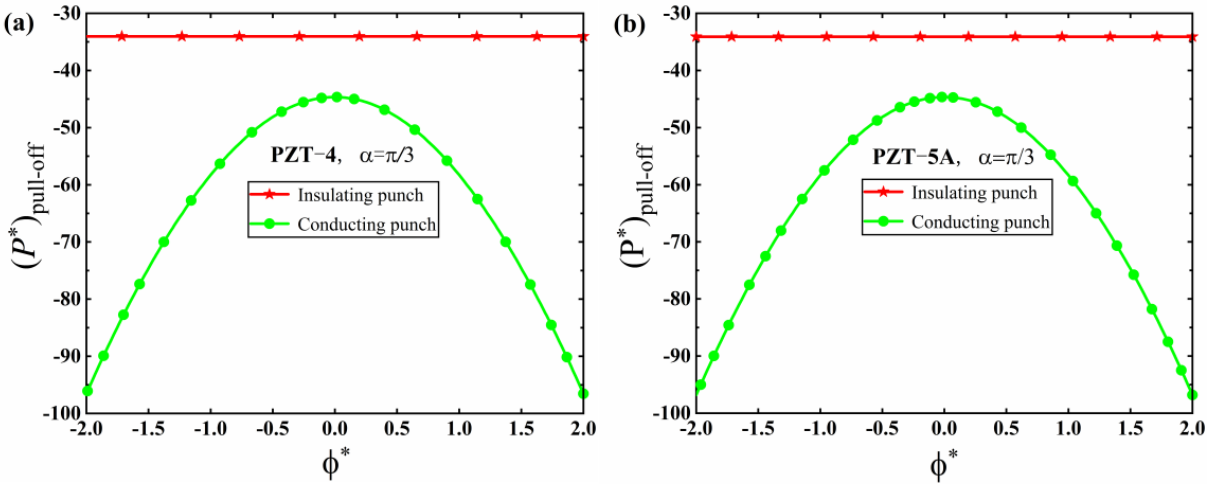

Figure 12. *Cont.*

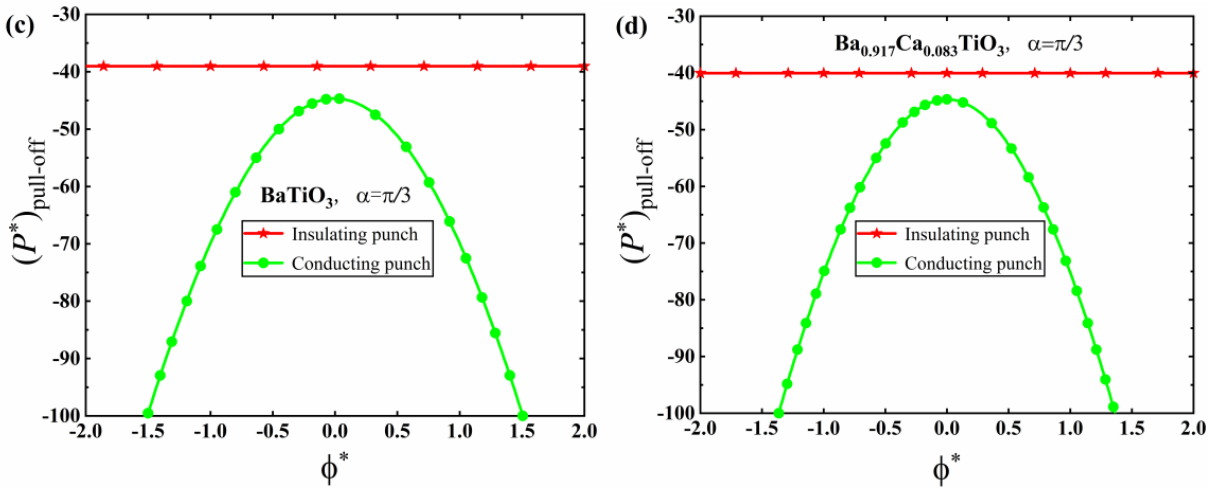

Figure 12. Variation of the dimensionless pull-off force, $P^*_{\text{pull-off}}$, with the dimensionless electric potential, ϕ^*, at a fixed value of $\alpha = \pi/3$. (**a**) PZT-4. (**b**) PZT-5A. (**c**) $BaTiO_3$. (**d**) $Ba_{0.917}Ca_{0.083}TiO_3$.

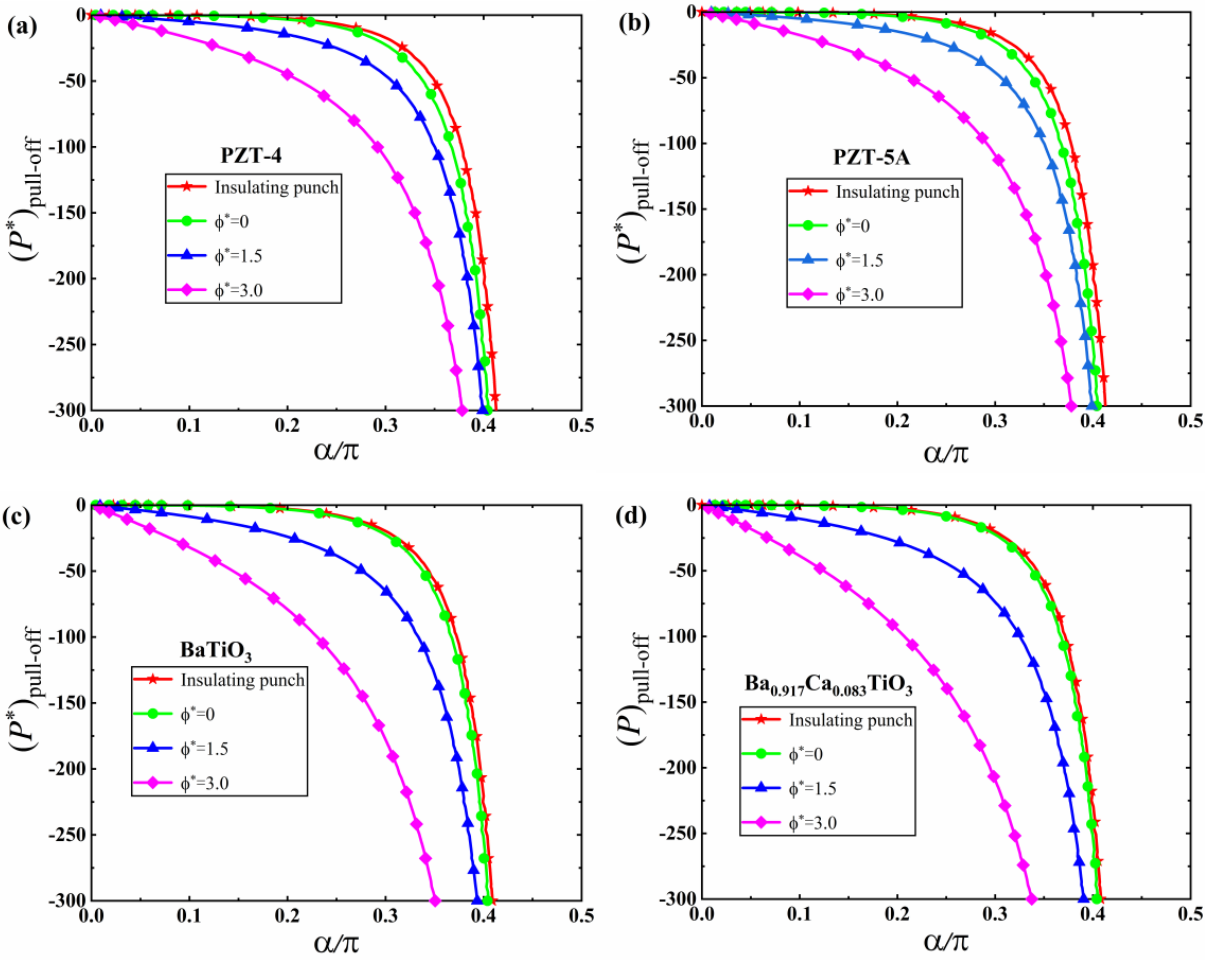

Figure 13. The dimensionless pull-off force, $P^*_{\text{pull-off}}$, as a function of the half cone angle of the rigid conical punch, α/π, for the JKR model. (**a**) PZT-4. (**b**) PZT-5A. (**c**) $BaTiO_3$. (**d**) $Ba_{0.917}Ca_{0.083}TiO_3$.

5.2. M-D Solutions

Figure 14 displays the variation of the dimensionless parameter $m = c/a$ as a function of the dimensionless contact radius, a^*, for the M-D model. It is shown that the transition parameter, λ, and the dimensionless electric potential, ϕ^*, have significant effects on

the physical quantity, m, whose value reflects the size of the cohesive zone. The results presented in Figure 14a indicate that the dimensionless parameter, m, diminishes as the transition parameter, λ, and the dimensionless contact radius, a^*, increase. When the transition parameter, λ, increases, which can be understood as the adhesion force increasing, then the dimensionless parameter, m, decreases, i.e., the cohesive zone outside the contact region diminishes. In Figure 14b, one can see that for a given transition parameter, λ, and a dimensionless contact radius, a^*, the larger the electric potential, the larger the value of m is, which reveals that the adhesion effect can be strengthened by applying the electric potential.

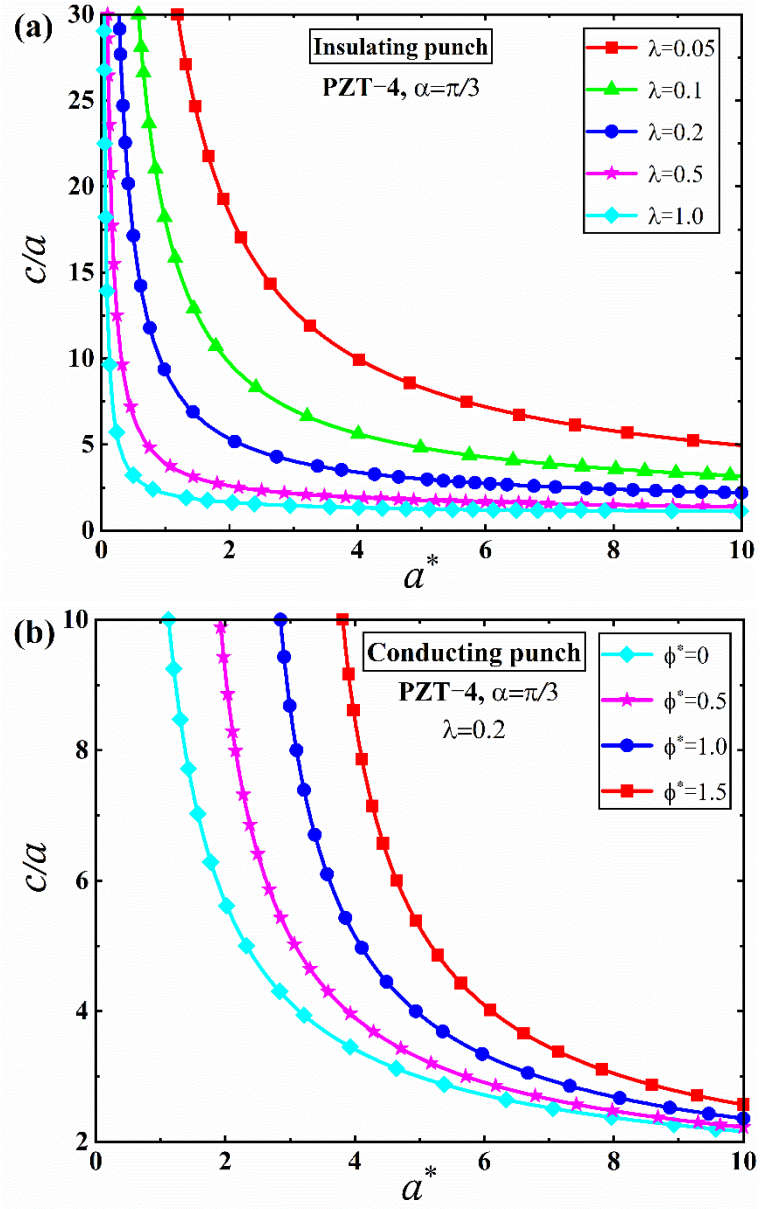

Figure 14. Variation of c/a with the dimensionless contact radius, a^*. (**a**) The effect of the transition parameter, λ. (**b**) The effect of the dimensionless electric potential, ϕ^*.

Figures 15 and 16 illustrate the variation of the dimensionless contact radius, a^*, with the dimensionless indentation force, P^*, under the action of the insulating punch and the conducting punch with non-zero electric potential based on the M-D model, respectively. It can be found that for both the insulating punch and the conducting punch with non-zero electric potential, as the transition parameter, λ, increases from 0.1 to 2.0, the $a^* \sim P^*$ curve for the M-D model then can be approximated by the corresponding curve in the JKR model. This suggests that the $a^* \sim P^*$ curve in the JKR model can be regarded as the limit case

of the corresponding solution for the M-D model, which has been verified by theoretical derivation in Appendix F.

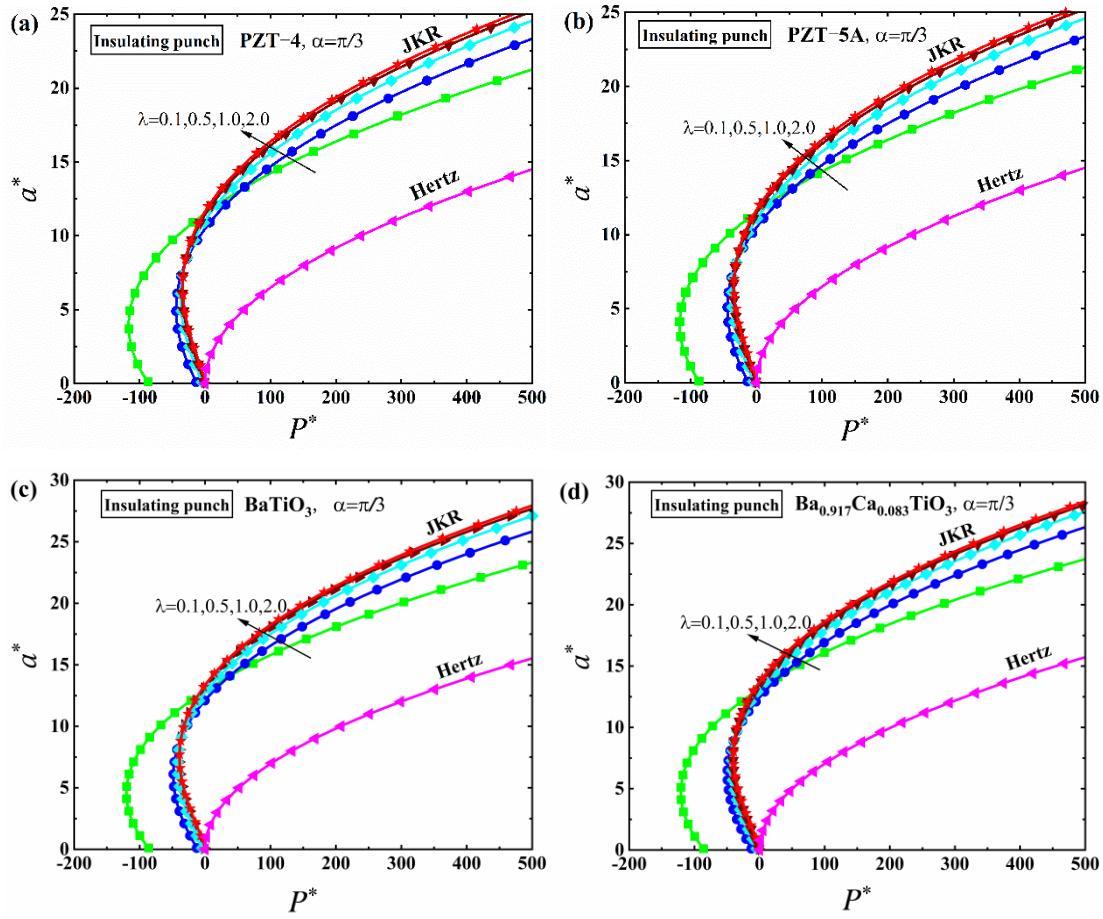

Figure 15. The dimensionless contact radius, a^*, as a function of the dimensionless indentation force, P^*, under the action of an insulating punch for the M-D model. (**a**) PZT-4. (**b**) PZT-5A. (**c**) $BaTiO_3$. (**d**) $Ba_{0.917}Ca_{0.083}TiO_3$.

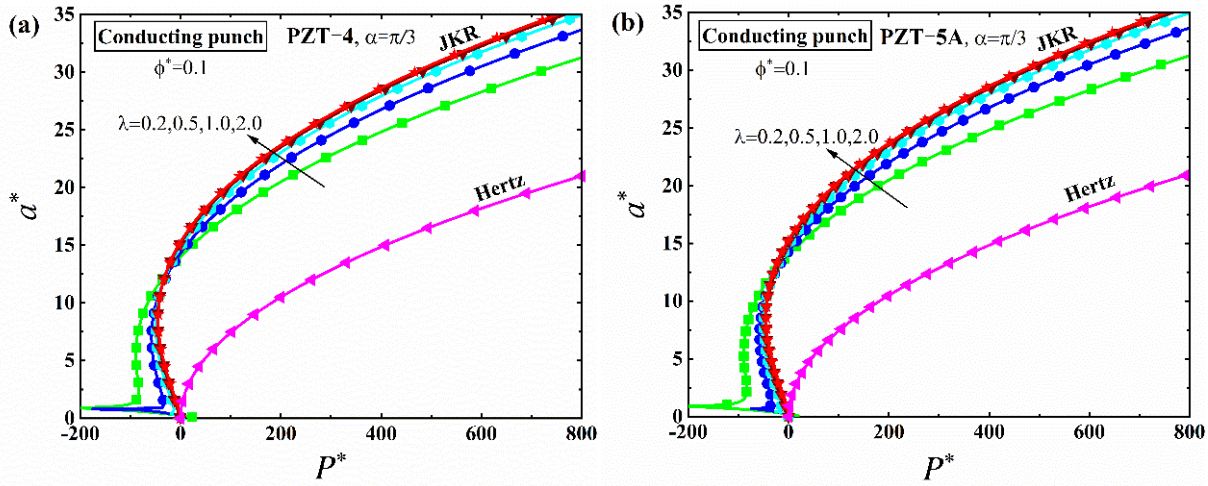

Figure 16. *Cont.*

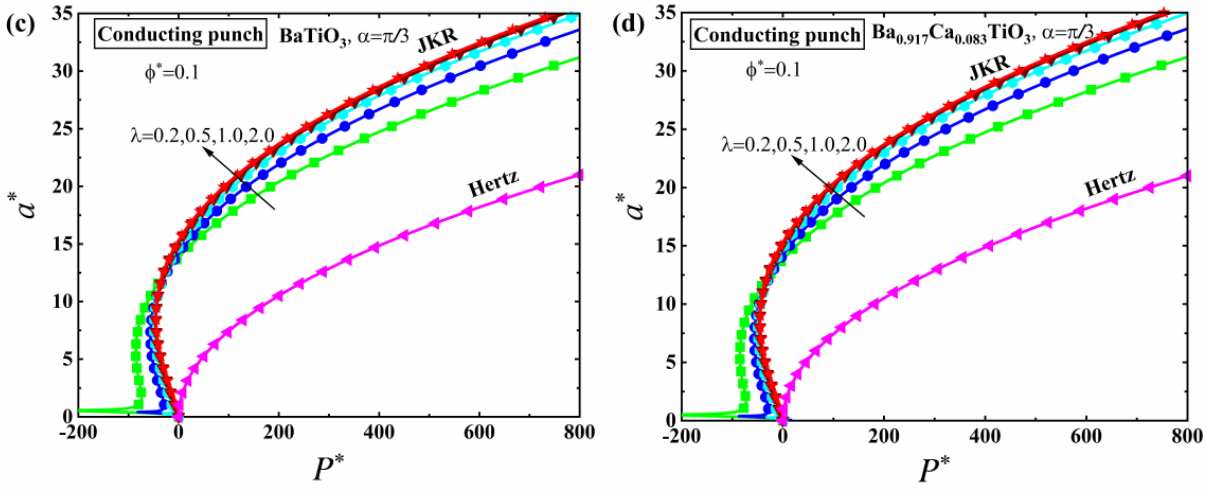

Figure 16. The dimensionless indentation force, P^*, as a function of the dimensionless indentation depth, h^*, under the action of a conducting punch for the M-D model. (**a**) PZT-4. (**b**) PZT-5A. (**c**) $BaTiO_3$. (**d**) $Ba_{0.917}Ca_{0.083}TiO_3$.

The variations of the dimensionless indentation force, P^*, with the dimensionless indentation depth, h^*, for the insulating punch and the conducting punch with a constant electric potential are shown in Figures 17 and 18, respectively. It is seen that for both the insulating punch and the conducting punch with non-zero electric potential, when the transition parameter, λ, changes from 0.2 to 2.0, the $P^* \sim h^*$ curves for the M-D model can be approximated by the corresponding curves in the JKR model. Similarly, the $a^* \sim h^*$ curves for the M-D model can also be replaced by the corresponding results in the JKR model when the transition parameter changes from 0.2 to 2.0, as shown in Figures 19 and 20. This reveals that the JKR solutions can be regarded as the limit case, which can be degenerated from the corresponding solutions in M-D model. This conclusion has also been verified through rigorous theoretical derivation in Appendix F.

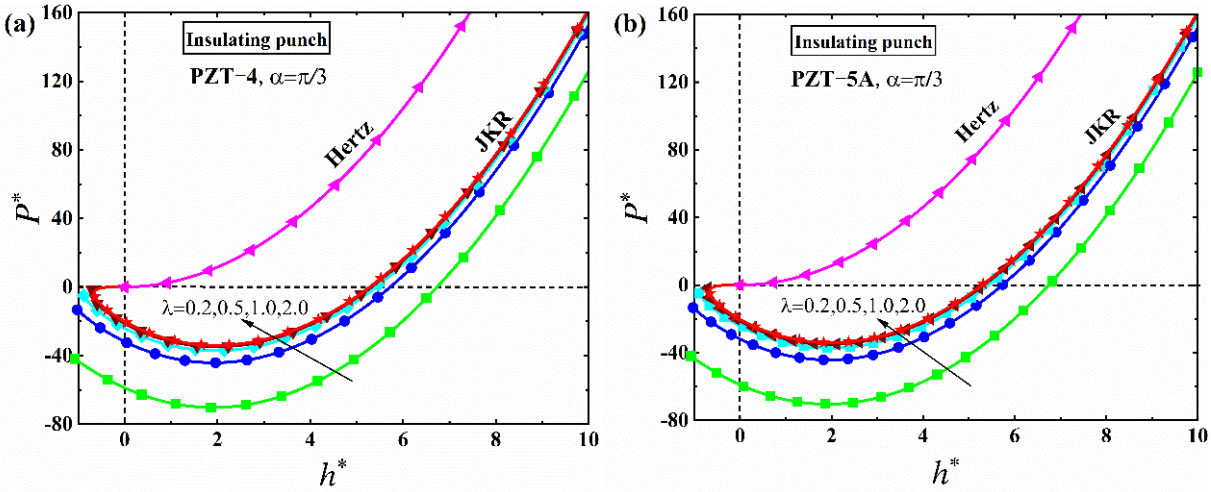

Figure 17. *Cont.*

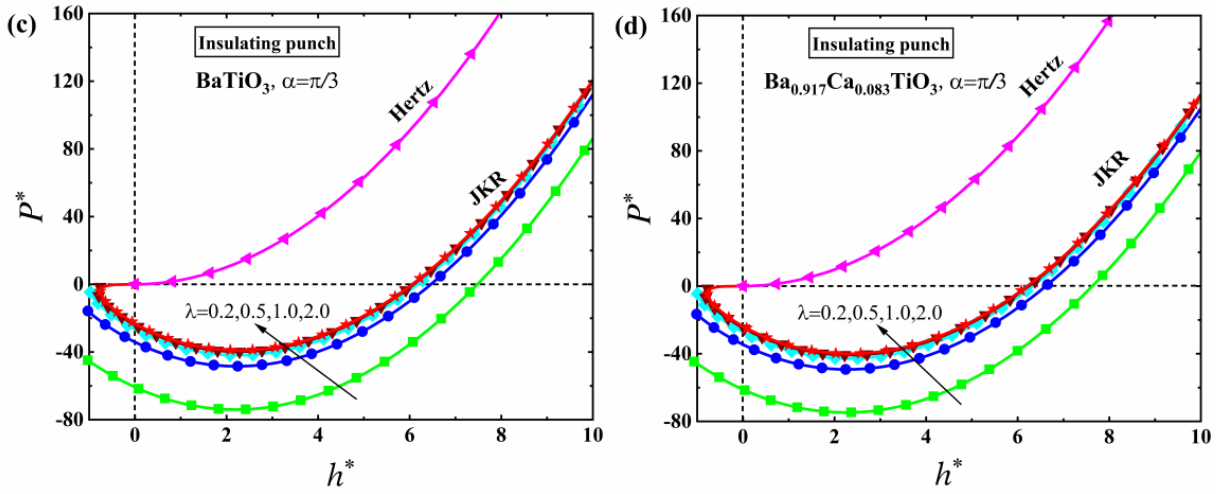

Figure 17. The dimensionless indentation force, P^*, as a function of the dimensionless indentation depth, h^*, under the action of an insulating punch for the M-D model. (**a**) PZT-4. (**b**) PZT-5A. (**c**) $BaTiO_3$. (**d**) $Ba_{0.917}Ca_{0.083}TiO_3$.

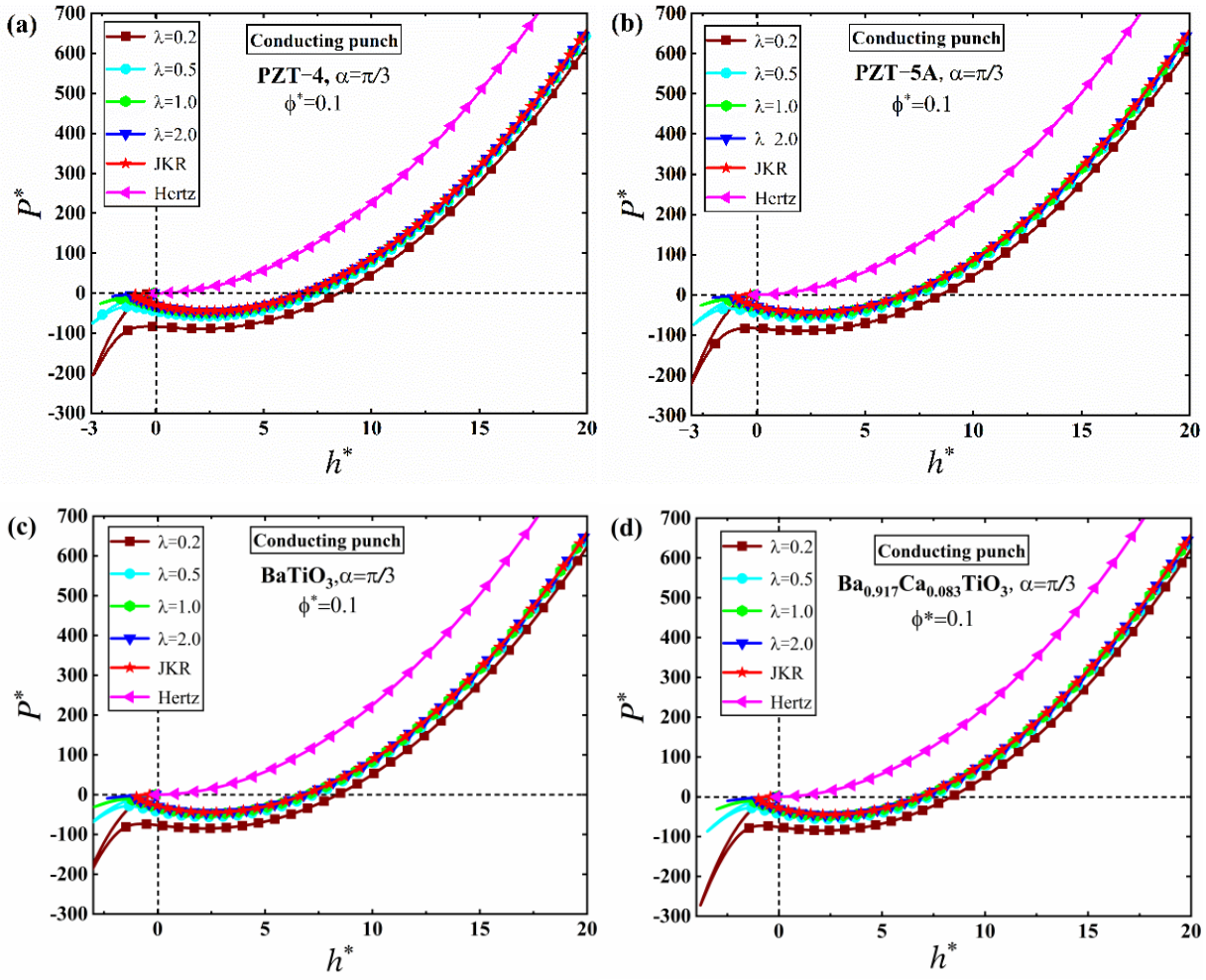

Figure 18. The dimensionless indentation force, P^*, as a function of the dimensionless indentation depth, h^*, under the action of a conducting punch for the M-D model. (**a**) PZT-4. (**b**) PZT-5A. (**c**) $BaTiO_3$. (**d**) $Ba_{0.917}Ca_{0.083}TiO_3$.

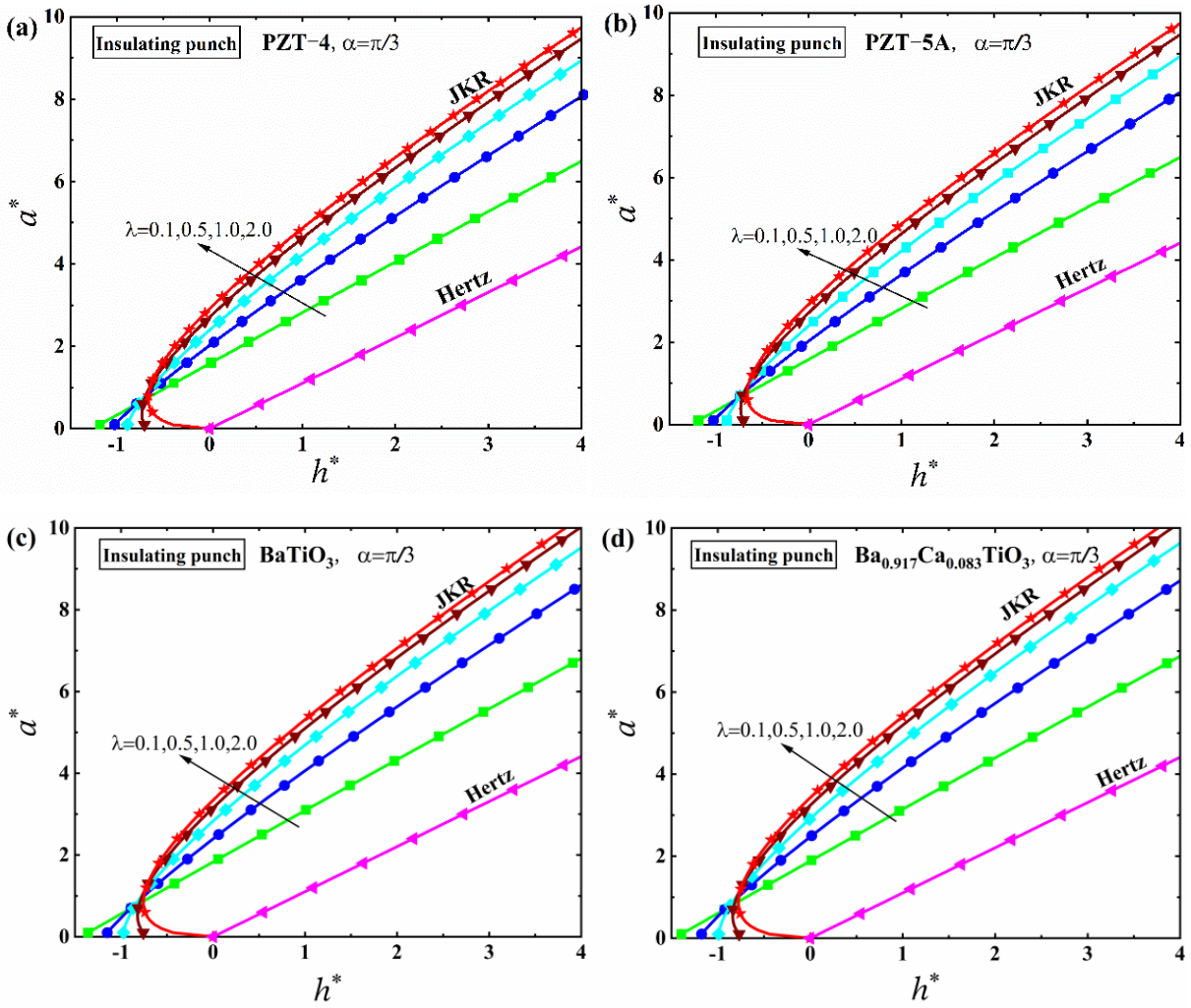

Figure 19. The dimensionless contact radius, a^*, as a function of the dimensionless indentation depth, h^*, under the action of an insulating punch for the M-D model. (**a**) PZT-4. (**b**) PZT-5A. (**c**) $BaTiO_3$. (**d**) $Ba_{0.917}Ca_{0.083}TiO_3$.

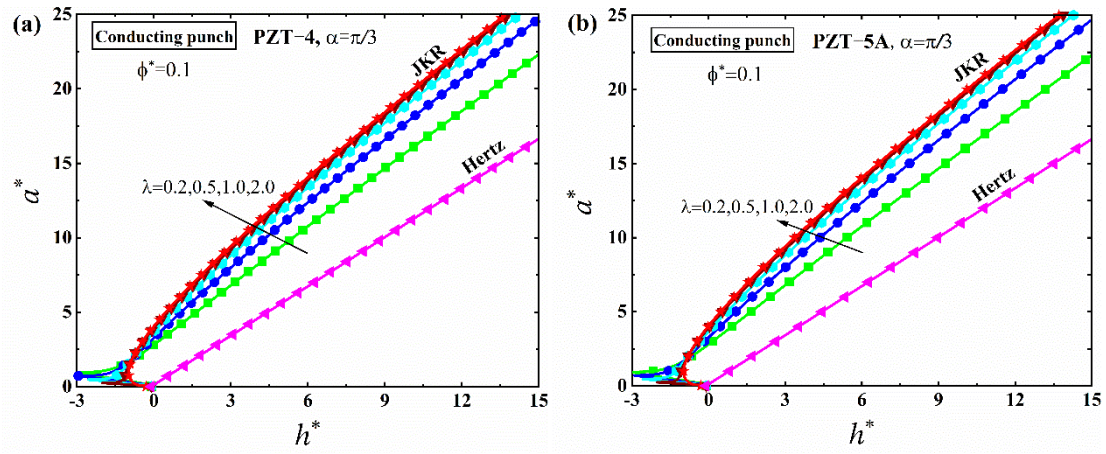

Figure 20. *Cont.*

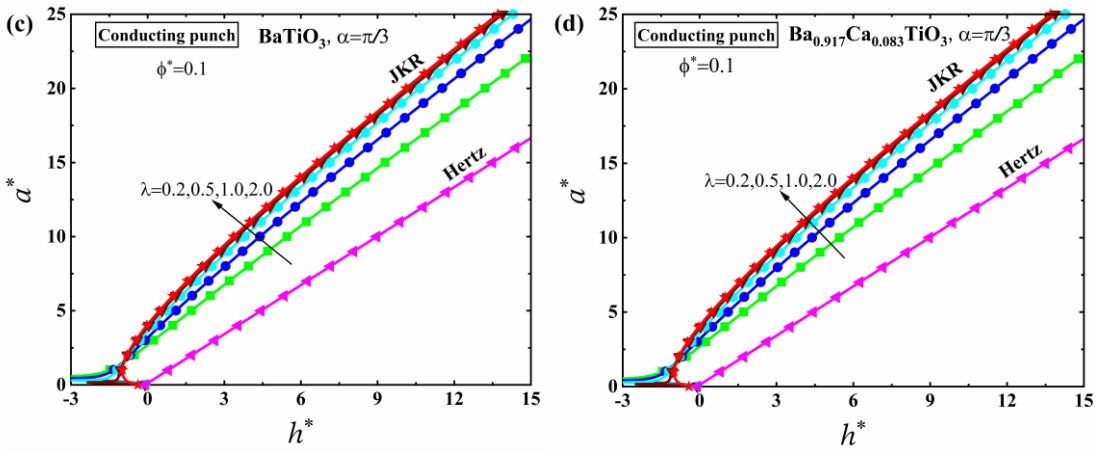

Figure 20. The dimensionless contact radius, a^*, as a function of the dimensionless indentation depth, h^*, under the action of a conducting punch for the M-D model. (**a**) PZT-4. (**b**) PZT-5A. (**c**) $BaTiO_3$. (**d**) $Ba_{0.917}Ca_{0.083}TiO_3$.

6. Conclusions

The adhesive contact problem between a rigid conical punch and a transversely isotropic piezoelectric solid was studied in this work. The classical adhesion theories were extended to investigate the contact behaviors of various piezoelectric materials indented by conical punches with different electric properties. The closed-form solutions for the JKR and M-D models were obtained by virtue of the Hankel integral transform, dual integral equations, and the superposing principle. The contribution of the electrical energy to the energy release rate under the conducting punch was taken into consideration. The relationships between the contact radius, the indentation load, and the indentation depth were established using the total energy method for the JKR model and the Griffith energy balance for the M-D model. The main conclusions can be summarized as follows:

(1) The adhesion effect between the tip of the conical punch and the piezoelectric solid can be enhanced by increasing the electric potential and the half cone angle of the punch, which suggests that a conical punch with a small half cone angle should be adopted in nanoindentation tests in order to reduce the effect of adhesion and improve the accuracy of characterization results.

(2) The effect of electric potential on adhesion behaviors is sensitive to different material properties, while the effect of the half cone angle of the conical punch on adhesion behaviors is insensitive to different material properties. These conclusions were made for the first time in this work.

(3) The load-displacement curves under the conical punch with different half cone angles have very different slopes, which indicates that the half cone angle of the conical punch can significantly affect the characterization of mechanical properties of piezoelectric solids in nanoindentation tests.

The results obtained from this paper can not only serve as the theoretical foundation for nanoindentation tests in characterizing the material properties of piezoelectric solids, but also offer new approaches to achieving reversible adhesion.

Author Contributions: Conceptualization, Y.Z., L.W. and S.D.; Methodology, Q.L. and Y.Z.; Investigation, Q.L.; Writing—original draft, Q.L.; Writing—review & editing, Q.L., Y.Z., L.W. and S.D.; Funding acquisition, Y.Z. All authors have read and agreed to the published version of the manuscript.

Funding: This work was supported by the National Natural Science Foundation of China (11972257, 12272269, 11832014 and 11472193), the China Scholarship Council (CSC), and the Fundamental Research Funds for the Central Universities (22120180223).

Conflicts of Interest: The authors declare no conflict of interest.

Appendix A. The Hertz Contact Solution

For the Hertz contact problem of a piezoelectric solid indented by a rigid punch, the analytical solutions of the full fields were obtained by [25]. For the convenience of referring and using, the corresponding results are presented in this section. The explicit expressions of the material constants $B_i (i = 1, 2, \ldots, 6)$ involved in this section and the following sections (Appendices B–E) are given as follows [25]:

$$\begin{aligned} B_1 &= \tfrac{M_6M_7 - M_5M_8}{M_1M_8 - M_2M_7}, \quad B_2 = \tfrac{M_3M_8 - M_4M_7}{M_1M_8 - M_2M_7}, \quad B_3 = \tfrac{M_1M_6 - M_2M_5}{M_4M_5 - M_3M_6}, \\ B_4 &= \tfrac{M_6M_3 - M_5M_4}{M_1M_4 - M_2M_3}, \quad B_5 = \tfrac{M_3M_8 - M_4M_7}{M_1M_4 - M_2M_3}, \quad B_6 = \tfrac{M_1M_8 - M_2M_7}{M_3M_8 - M_4M_7}, \end{aligned} \tag{A1}$$

where the explicit expressions of $M_i (i = 1, 2, \ldots, 8)$ can be found in Equation (A8) of [25].

Case I: electrically conducting punch

For the electrically conducting punch, the Hertz contact solutions can be obtained using the following equations:

$$\sigma_{zz}^H(r, 0) = -B_4 \cot\alpha \cosh^{-1}\frac{a}{r}, \tag{A2}$$

$$D_z^H(r, 0) = -B_5\left[\cot\alpha \cosh^{-1}\frac{a}{r} - \frac{2(B_3 + B_6)\phi_0}{\pi\sqrt{a^2 - r^2}}\right], \tag{A3}$$

$$h^H = \frac{\pi}{2} a \cot\alpha - B_3\phi_0, \; P^H = B_4\pi a^2 \cot\alpha, \tag{A4}$$

$$u_z^H(r, 0) = \begin{cases} h^H - r\cot\alpha, & 0 \le r \le a, \\ \frac{2h^H}{\pi}\sin^{-1}\frac{a}{r} + \cot\alpha\left(\sqrt{r^2 - a^2} - r\right), & r > a, \end{cases} \tag{A5}$$

$$\phi^H(r, 0) = \begin{cases} \phi_0, \; 0 \le r \le a, \\ \frac{2\phi_0}{\pi}\sin^{-1}\frac{a}{r}, \; r > a, \end{cases} \tag{A6}$$

$$\begin{aligned} \left[u_z^H(r, 0)\right] &= f(r) - \delta + u_z^H(r, 0) \\ &= \left(\tfrac{2B_3\phi_0}{\pi} - a\cot\alpha\right)\cos^{-1}\tfrac{a}{r} + \sqrt{r^2 - a^2}\cot\alpha, \; r > a, \end{aligned} \tag{A7}$$

$$\left[\phi^H(r, 0)\right] = \phi^H(r, 0) - \phi_0 = -\frac{2\phi_0}{\pi}\cos^{-1}\frac{a}{r}, \; r > a. \tag{A8}$$

Case II: electrically insulating punch

When the rigid conical punch is electrically insulating, the corresponding solutions can be defined as

$$\sigma_{zz}^H(r, 0) = -B_1 \cot\alpha \cosh^{-1}\frac{a}{r}, \; 0 \le \; r < a \tag{A9}$$

$$h^H = \frac{\pi a \cot\alpha}{2}, \; P^H = \pi a^2 B_1 \cot\alpha, \tag{A10}$$

$$u_z^H(r, 0) = \begin{cases} h^H - r\cot\alpha, & 0 \le r \le a, \\ \frac{2h^H}{\pi}\left(\sqrt{\frac{r^2}{a^2} - 1} - \frac{r}{a} + \sin^{-1}\frac{a}{r}\right), & r > a, \end{cases} \tag{A11}$$

$$\phi^H(r, 0) = \begin{cases} B_2(h^H - r\cot\alpha), & 0 \le r \le a, \\ \frac{2B_2h^H}{\pi}\left(\sqrt{\frac{r^2}{a^2} - 1} - \frac{r}{a} + \sin^{-1}\frac{a}{r}\right), & r > a. \end{cases} \tag{A12}$$

$$\left[u_z^H(r,0)\right] = \sqrt{r^2-a^2}\cot\alpha - a\cot\alpha\cos^{-1}\frac{a}{r}. \tag{A13}$$

Appendix B. The Boussinesq Contact Solution

For the Boussinesq contact problem, the corresponding solutions can be obtained as follows:

Case I: electrically conducting punch

$$\sigma_{zz}^B(r,0) = -\frac{P^B}{2\pi a\sqrt{a^2-r^2}},\ r<a, \tag{A14}$$

$$D_z^B(r,0) = -\frac{2B_5(h^B - B_6\phi_0)}{\pi\sqrt{a^2-r^2}},\ r<a, \tag{A15}$$

$$P^B = 4aB_4(h^B + B_3\phi_0), \tag{A16}$$

$$u_z^B(r,0) = \begin{cases} h^B, & r\le a, \\ \frac{2h^B}{\pi}\sin^{-1}\frac{a}{r}, & r>a, \end{cases} \tag{A17}$$

$$\phi^B(r,0) = \begin{cases} \phi_0, & r\le a, \\ \frac{2\phi_0}{\pi}\sin^{-1}\frac{a}{r}, & r>a. \end{cases} \tag{A18}$$

Case II: electrically insulating punch

$$\sigma_{zz}^B(r,0) = -\frac{P^B}{2\pi a\sqrt{a^2-r^2}},\ r<a, \tag{A19}$$

$$P^B = 4aB_1h^B, \tag{A20}$$

$$u_z^B(r,0) = \begin{cases} h^B, & r\le a, \\ \frac{2h^B}{\pi}\sin^{-1}\frac{a}{r}, & r>a, \end{cases} \tag{A21}$$

$$\phi^B(r,0) = \begin{cases} B_2h^B, & r\le a, \\ \frac{2B_2h^B}{\pi}\sin^{-1}\frac{a}{r}, & r>a. \end{cases} \tag{A22}$$

Appendix C. The Solutions of the JKR Model for Case II

When the conical punch is electrically insulating, by superposing the Hertz contact solutions from Equations (A9)–(A13) and the Boussinesq contact solutions from Equations (A19)–(A22), one can determine that

$$h^{JKR} = \frac{\pi a\cot\alpha}{4} + \frac{P}{4B_1a}, \tag{A23}$$

$$\sigma_{zz}^{JKR}(r,0) = -B_1\cot\alpha\cosh^{-1}\frac{a}{r} + \frac{B_1\cot\alpha\pi a^2 - P}{2\pi a\sqrt{a^2-r^2}}, \tag{A24}$$

$$u_z^{JKR}(r,0) = \begin{cases} h^{JKR} - r\cot\alpha, & r\le a, \\ \frac{2}{\pi}h^{JKR}\sin^{-1}\frac{a}{r} + \left(\sqrt{r^2-a^2}-r\right)\cot\alpha, & r>a, \end{cases} \tag{A25}$$

$$\phi^{JKR}(r,0) = \begin{cases} B_2(h^{JKR} - r\cot\alpha), & r\le a, \\ B_2\left[\frac{2}{\pi}h^{JKR}\sin^{-1}\frac{a}{r} + \left(\sqrt{r^2-a^2}-r\right)\cot\alpha\right], & r>a, \end{cases} \tag{A26}$$

$$\begin{aligned}\left[u_z^{JKR}(r,0)\right] &= f(r) - h^{JKR} + u_z^{JKR}(r,0)\\ &= \sqrt{r^2-a^2}\cot\alpha - \tfrac{2}{\pi}h^{JKR}\cos^{-1}\tfrac{a}{r},\ r>a.\end{aligned} \tag{A27}$$

For the rigid insulating indenter, the contribution of the electrical energy to the total free energy of the contact system is nil due to the lack of electric displacement within the contact region. Under these circumstances, the total free energy, U_T, is composed of three parts, including the elastic strain energy, U_E, the mechanical potential energy, U_P and the surface energy, U_S. As such, one can deduce that

$$U_T = U_E + U_P + U_S, \tag{A28}$$

They can be calculated as

$$U_E = -\frac{1}{2}\int_0^{2\pi}\int_0^a \sigma_{zz}(r,\theta,0)u_z^{JKR}(r,\theta,0)\ rdrd\theta = \frac{B_1\pi^2\cot^2\alpha a^3}{24} + \frac{P^2}{8B_1 a}, \tag{A29}$$

$$U_P = -\frac{\pi\cot\alpha}{4}Pa - \frac{P^2}{4B_1 a}, \tag{A30}$$

$$U_S = -\pi a^2\Delta\gamma, \tag{A31}$$

In order to obtain the result in Equation (A29), the integral results shown in Equation (24) were used.

The equilibrium state of the contact system should satisfy the following condition:

$$\left.\frac{\partial U_T}{\partial a}\right|_P = 0. \tag{A32}$$

By inserting the results presented in Equations (A28)–(A31) into Equation (A32), one can obtain

$$P = \pi B_1\cot\alpha a^2 \pm 4\sqrt{\pi\Delta\gamma B_1 a^3}. \tag{A33}$$

The stable equilibrium state of the contact system should satisfy the condition $\frac{\partial^2 U_T}{\partial a^2} > 0$, then one can determine that

$$P = \pi B_1\cot\alpha a^2 - 4\sqrt{\pi\Delta\gamma B_1 a^3}. \tag{A34}$$

When piezoelectric materials degenerate into isotropic elastic solids, i.e., $B_1 = E^*/2$ (E^* is the equivalent elastic modulus), Equation (A34) can be rewritten as

$$P = \frac{\pi E^*\cot\alpha}{2}a^2 - \sqrt{8\pi\Delta\gamma E^* a^3}, \tag{A35}$$

which is the same as the result of Equation (17) obtained in [78].

Considering the following condition:

$$\frac{dP}{da} = 0, \tag{A36}$$

substituting Equation (A34) into Equation (A36) yields

$$a_{\text{pull-off}} = \frac{9\Delta\gamma}{\pi B_1\cot^2\alpha}, \tag{A37}$$

which is the critical contact radius at the pull-off moment. By inserting this result into Equation (A34), one can define the explicit expression of the pull-off force as

$$P_{\text{pull-off}} = -\frac{27\Delta\gamma^2}{\pi B_1 \cot^3\alpha}. \tag{A38}$$

If the piezoelectric materials degenerate into isotropic elastic solids, one can obtain

$$P_{\text{pull-off}} = -\frac{54\Delta\gamma^2}{\pi E^* \cot^3\alpha}, \tag{A39}$$

This result is consistent with that of Equation (16) defined in [78].

Appendix D. The Solutions of the M-D Model for Case II

The JKR solutions for a piezoelectric solid indented by a rigid insulating conical punch are presented in Equations (A23)–(A27). If we define that

$$K_I = \lim_{r\to a}\sqrt{2\pi(a-r)}\sigma_{zz}(r,0) = \frac{P^H - P}{2a\sqrt{\pi a}}, \tag{A40}$$

where P^H is the apparent Hertz load, then the stress distribution in Equation (A24) can be rewritten as follows:

$$\sigma_{zz}^{JKR}(r,0) = -B_1 \cot\alpha \cosh^{-1}\frac{a}{r} + \frac{K_I}{\sqrt{\pi a}}\frac{a}{\sqrt{a^2-r^2}}. \tag{A41}$$

The solutions of the external circular crack subjected to a uniform pressure, p_0, on the crack surfaces are presented in Appendix E. By substituting $p_0 = -\sigma_0$ into Equations (A98), (A102), and (A106), one can obtain

$$\sigma_{zz}(r,0) = \begin{cases} \frac{K_m}{\sqrt{\pi a}}\frac{a}{\sqrt{a^2-r^2}} + \frac{2\sigma_0}{\pi}\tan^{-1}\sqrt{\frac{c^2-a^2}{a^2-r^2}}, & r < a, \\ \sigma_0, & a < r < c, \end{cases} \tag{A42}$$

$$u_T = -\frac{2\sigma_0}{B_1\pi}\left[\sqrt{c^2-a^2}\left(\sqrt{\frac{r^2}{a^2}-1} - \cos^{-1}\frac{a}{r}\right) - c^2\int_a^{\min(r,c)}\frac{\sqrt{r^2-t^2}}{t^2\sqrt{c^2-t^2}}dt\right] + \frac{K_m\sqrt{\pi a}}{B_1\pi}\cos^{-1}\frac{a}{r},\ r > a, \tag{A43}$$

$$\delta' = \frac{\sigma_0 a}{2B_1}\left(\frac{c^2}{a^2}\cos^{-1}\frac{a}{c} - \sqrt{\frac{c^2}{a^2}-1}\right), \tag{A44}$$

where

$$K_m = -\frac{\sigma_0}{\sqrt{\pi a}}\left(\sqrt{c^2-a^2} + \frac{c^2}{a}\cos^{-1}\frac{a}{c}\right). \tag{A45}$$

Superposing Equations (A41) and (A42) yields

$$\sigma_{zz}^{\text{M-D}}(r,0) = \begin{cases} \frac{K_m+K_I}{\sqrt{\pi a}}\frac{a}{\sqrt{a^2-r^2}} - B_1\cot\alpha\cosh^{-1}\frac{a}{r} \\ +\frac{2\sigma_0}{\pi}\tan^{-1}\sqrt{\frac{c^2-a^2}{a^2-r^2}} & r < a, \\ \sigma_0, & a < r < c. \end{cases} \tag{A46}$$

According to the classical M-D theory [57], in order to eliminate the stress singularity at the contact periphery, the following condition should be satisfied:

$$K_I + K_m = 0 \Rightarrow K_I = -K_m \Rightarrow \frac{P^H - P}{2a\sqrt{\pi a}} = \frac{\sigma_0}{\sqrt{\pi a}}\left(\sqrt{c^2-a^2} + \frac{c^2}{a}\cos^{-1}\frac{a}{c}\right). \tag{A47}$$

From Equation (A47), one can obtain

$$\begin{aligned} P^{\mathrm{M-D}} &= P^{H} - 2\sigma_0 a\left(\sqrt{c^2-a^2} + \tfrac{c^2}{a}\cos^{-1}\tfrac{a}{c}\right) \\ &= B_1 \cot\alpha \pi a^2 - 2\sigma_0 a\left(\sqrt{c^2-a^2} + \tfrac{c^2}{a}\cos^{-1}\tfrac{a}{c}\right). \end{aligned} \tag{A48}$$

Using the continuity condition in Equation (A47), the stress distribution given by Equation (A46) can be simplified as follows:

$$\sigma_{zz}^{\mathrm{M-D}}(r,0) = \begin{cases} -B_1 \cot\alpha \cos\mathrm{h}^{-1}\tfrac{a}{r} + \tfrac{2\sigma_0}{\pi}\tan^{-1}\sqrt{\tfrac{c^2-a^2}{a^2-r^2}}, & r < a, \\ \sigma_0, \ a < r < c. \end{cases} \tag{A49}$$

By adding Equation (A23) to Equation (A28) and using the result in Equation (A48), one obtains

$$\begin{aligned} h^{\mathrm{M-D}} &= \tfrac{\pi a \cot\alpha}{4} + \tfrac{P}{4B_1 a} + \tfrac{\sigma_0 a}{2B_1}\left(\tfrac{c^2}{a^2}\cos^{-1}\tfrac{a}{c} - \sqrt{\tfrac{c^2}{a^2}-1}\right) \\ &= \tfrac{\pi a \cot\alpha}{2} - \tfrac{\sigma_0}{B_1}\sqrt{c^2-a^2}. \end{aligned} \tag{A50}$$

Using the result in Equation (A40), Equation (A23) can be rewritten as

$$h^{JKR} = \frac{\pi a \cot\alpha}{2} - \frac{K_I\sqrt{\pi a}}{2B_1}. \tag{A51}$$

Inserting Equation (A51) into Equation (A27), one can obtain

$$\begin{aligned} \left[u_z^{JKR}(r,0)\right] &= \sqrt{r^2-a^2}\cot\alpha - a\cot\alpha\cos^{-1}\tfrac{a}{r} \\ &+ \tfrac{K_I\sqrt{\pi a}}{B_1\pi}\cos^{-1}\tfrac{a}{r}, \ r > a. \end{aligned} \tag{A52}$$

By superposing Equation (A43) and (A52), considering the continuity condition in Equation (A47), one obtains

$$\begin{aligned} &\left[u_z^{\mathrm{M-D}}(r,0)\right] = \sqrt{r^2-a^2}\cot\alpha - a\cot\alpha\cos^{-1}\tfrac{a}{r} \\ &-\tfrac{2\sigma_0}{B_1\pi}\left[\sqrt{c^2-a^2}\left(\sqrt{\tfrac{r^2}{a^2}-1} - \cos^{-1}\tfrac{a}{r}\right) - c^2\int_a^{\min(r,c)}\tfrac{\sqrt{r^2-t^2}}{t^2\sqrt{c^2-t^2}}dt\right], \ r > a. \end{aligned} \tag{A53}$$

Using Equation (A53), the discontinuity displacement can be defined as

$$\begin{aligned} \delta_t &= \left[u_z^{M-D}(c,0)\right] = \left(\sqrt{m^2-1} - \cos^{-1}\tfrac{1}{m}\right)a\cot\alpha \\ &+ \tfrac{2\sigma_0 a}{B_1\pi}\left(\sqrt{m^2-1}\cos^{-1}\tfrac{1}{m} - m + 1\right), \end{aligned} \tag{A54}$$

where $m = c/a$.

Using the relation in Equation (A121), Equation (A54) can be rewritten as

$$\begin{aligned} \delta_t &= \left(\sqrt{m^2-1} - \tan^{-1}\sqrt{m^2-1}\right)a\cot\alpha \\ &+ \tfrac{2\sigma_0 a}{B_1\pi}\left(\sqrt{m^2-1}\tan^{-1}\sqrt{m^2-1} - m + 1\right). \end{aligned} \tag{A55}$$

When the complicated adhesion force is simplified by using the Dugdale cohesive model [79], one can obtain the following relation:

$$J = G = \sigma_0\delta_t = \Delta\gamma, \tag{A56}$$

where J, G and $\Delta\gamma$ denote the J-integral, energy release rate and work of adhesion, respectively.

By substituting Equation (A55) into Equation (A56), one can obtain

$$\begin{aligned}&\left(\sqrt{m^2-1}-\tan^{-1}\sqrt{m^2-1}\right)\sigma_0 a\cot\alpha\\&+\tfrac{2\sigma_0^2 a}{B_1\pi}\left(\sqrt{m^2-1}\tan^{-1}\sqrt{m^2-1}-m+1\right)=\Delta\gamma.\end{aligned}\tag{A57}$$

In the subsequent analysis, the correctness of these solutions will be verified by checking whether the corresponding JKR solutions presented in Appendix C can be degenerated as the limiting case from the M-D solutions obtained in this section.

First, from Equation (A47), one can obtain

$$K_I=\frac{\sigma_0}{\sqrt{\pi a}}\left(\sqrt{c^2-a^2}+\frac{c^2}{a}\cos^{-1}\frac{a}{c}\right)=\frac{\sigma_0 a}{\sqrt{\pi a}}\left(\sqrt{m^2-1}+m^2\cos^{-1}\frac{1}{m}\right).\tag{A58}$$

Using the relation in Equation (A121), Equation (A58) can be rewritten as

$$\frac{K_I\sqrt{\pi a}}{\sigma_0 a}=\sqrt{m^2-1}+m^2\tan^{-1}\sqrt{m^2-1}.\tag{A59}$$

When $m\to 1$, $\tan^{-1}\sqrt{m^2-1}\sim\sqrt{m^2-1}$, then

$$\frac{K_I\sqrt{\pi a}}{\sigma_0 a}\approx 2\sqrt{m^2-1}.\tag{A60}$$

Using Equation (A60), the stress distribution in Equation (A49) can be expressed as follows:

$$\sigma_{zz}^{\mathrm{M-D}}(\rho,0)=\begin{cases}-B_1\cot\alpha\cosh^{-1}\frac{1}{\rho}+\frac{2\sigma_0}{\pi}\tan^{-1}\sqrt{\frac{m^2-1}{1-\rho^2}},\ \rho<1,\\ \sigma_0,\ 1<\rho<m,\end{cases}\tag{A61}$$

where $\rho=r/a$.

It can be seen in Equation (A60) that $m\to 1$ as $\sigma_0\to\infty$. Under these circumstances, Equation (A61) can be simplified as follows:

$$\sigma_{zz}(\rho,0)=-B_1\cot\alpha\cosh^{-1}\frac{1}{\rho}+\frac{K_I}{\sqrt{\pi a}}\frac{1}{\sqrt{1-\rho^2}},\ \rho<1,\tag{A62}$$

which is consistent with the corresponding JKR solution presented in Equation (A24).

From Equation (A59), one can find that $\sigma_0\to 0$ as $m\to\infty$, and as such, Equation (A61) degenerates into the following form:

$$\sigma_{zz}(r,0)=-B_1\cot\alpha\cosh^{-1}\frac{a}{r},\ r<a,\tag{A63}$$

which is in agreement with the corresponding Hertz solution obtained in Equation (A9).

The discontinuity displacement outside the contact region in Equation (A53) can be expressed as follows:

$$\begin{aligned}&\left[u_z^{\mathrm{M-D}}(r,0)\right]=\sqrt{r^2-a^2}\cot\alpha-a\cot\alpha\cos^{-1}\tfrac{a}{r}\\&-\tfrac{2\sigma_0 a}{B_1\pi}\left[\sqrt{m^2-1}\left(\sqrt{\tfrac{r^2}{a^2}-1}-\cos^{-1}\tfrac{a}{r}\right)-m^2\int_1^{\min(\rho,m)}\tfrac{\sqrt{\rho^2-t^2}}{t^2\sqrt{m^2-t^2}}dt\right].\end{aligned}\tag{A64}$$

As $m\to\infty$, Equation (A64) can be simplified as [57]:

$$\left[u_z(r,0)\right]=\sqrt{r^2-a^2}\cot\alpha-a\cot\alpha\cos^{-1}\frac{a}{r},\tag{A65}$$

which is the same as the corresponding Hertz solution shown in Equation (A13).

When $m \to 1$, Equation (A65) can be expressed as follows:

$$\begin{aligned}\left[u_z^{\mathrm{M-D}}(r,0)\right] &= \sqrt{r^2-a^2}\cot\alpha - a\cot\alpha\cos^{-1}\tfrac{a}{r} + \tfrac{2\sigma_0 a\sqrt{m^2-1}}{B_1\pi}\cos^{-1}\tfrac{a}{r} \\ &- \tfrac{2\sigma_0 a}{B_1\pi}\left[\sqrt{m^2-1}\sqrt{\tfrac{r^2}{a^2}-1} - m^2\int_1^{\min(\rho,m)}\tfrac{\sqrt{\rho^2-t^2}}{t^2\sqrt{m^2-t^2}}dt\right],\ r>a.\end{aligned} \tag{A66}$$

Substituting Equation (A60) into Equation (A66) yields

$$\begin{aligned}\left[u_z^{\mathrm{M-D}}(r,0)\right] &= \sqrt{r^2-a^2}\cot\alpha - a\cot\alpha\cos^{-1}\tfrac{a}{r} + \tfrac{K_I\sqrt{\pi a}}{B_1\pi}\cos^{-1}\tfrac{a}{r} \\ &- \tfrac{2\sigma_0 a}{B_1\pi}\left[\sqrt{m^2-1}\sqrt{\tfrac{r^2}{a^2}-1} - m^2\int_1^{\min(\rho,m)}\tfrac{\sqrt{\rho^2-t^2}}{t^2\sqrt{m^2-t^2}}dt\right],\ r>a.\end{aligned} \tag{A67}$$

Using the integral result in Equation (A128), Equation (A67) can be simplified as

$$\left[u_z(r,0)\right] = \sqrt{r^2-a^2}\cot\alpha - a\cot\alpha\cos^{-1}\frac{a}{r} + \frac{K_I\sqrt{\pi a}}{B_1\pi}\cos^{-1}\frac{a}{r},\ r>a, \tag{A68}$$

which is consistent with the corresponding JKR solution obtained in Equation (A27).

By virtue of the relation in Equation (A132), the indentation depth in Equation (A50) can be expressed as

$$h^{M-D} = \frac{\pi a\cot\alpha}{4} + \frac{P}{4B_1 a} + \frac{\sigma_0 a}{2B_1}\left(m^2\tan^{-1}\sqrt{m^2-1} - \sqrt{m^2-1}\right). \tag{A69}$$

From Equation (A47), one can obtain the following result:

$$\sigma_0 a = \frac{B_1\pi a^2\cot\alpha - P}{2a\left(\sqrt{m^2-1} + m^2\tan^{-1}\sqrt{m^2-1}\right)}. \tag{A70}$$

By substituting Equation (A70) into Equation (A69), one can obtain

$$\begin{aligned}h^{M-D} &= \tfrac{\pi a\cot\alpha}{4} + \tfrac{P}{4B_1 a} \\ &+ \tfrac{B_1\pi a^2\cot\alpha - P}{4B_1 a}\tfrac{m^2\tan^{-1}\sqrt{m^2-1} - \sqrt{m^2-1}}{m^2\tan^{-1}\sqrt{m^2-1} + \sqrt{m^2-1}}.\end{aligned} \tag{A71}$$

When $m \to 1$, by combining the results obtained in Equation (A134), Equation (A71) can be simplified as

$$h = \frac{\pi a\cot\alpha}{4} + \frac{P}{4B_1 a}, \tag{A72}$$

which is the same as the corresponding JKR solution presented in Equation (A23).

When $m \to \infty$, Equation (A71) can be simplified as:

$$h = \frac{\pi a\cot\alpha}{2}, \tag{A73}$$

which is identical to the Hertz solution obtained in Equation (A10).

The energy release rate can be derived from Equation (A56) as follows:

$$\begin{aligned}G &= \left(\sqrt{m^2-1} - \tan^{-1}\sqrt{m^2-1}\right)\sigma_0 a\cot\alpha \\ &+ \tfrac{2\sigma_0^2 a}{B_1\pi}\left(\sqrt{m^2-1}\tan^{-1}\sqrt{m^2-1} - m + 1\right).\end{aligned} \tag{A74}$$

Inserting Equation (A70) into Equation (A74) yields

$$\begin{aligned} G = & \frac{(P^H-P)\cot\alpha}{2a}\frac{\sqrt{m^2-1}-\tan^{-1}\sqrt{m^2-1}}{\sqrt{m^2-1}+m^2\tan^{-1}\sqrt{m^2-1}} \\ & +\frac{(P^H-P)^2}{2\pi B_1 a^3}\frac{\sqrt{m^2-1}\tan^{-1}\sqrt{m^2-1}-m+1}{\left(\sqrt{m^2-1}+m^2\tan^{-1}\sqrt{m^2-1}\right)^2}. \end{aligned} \tag{A75}$$

In the limit case, as $m \to 1$, letting $m = 1+\varepsilon$ and using the result in Equation (A144), one can obtain

$$G \approx \frac{(P^H-P)^2}{16\pi B_1 a^3}. \tag{A76}$$

Using the energy balance relation, one can obtain

$$P = P^H \pm 4\sqrt{\pi B_1 \Delta\gamma a^3}. \tag{A77}$$

Considering the stable equilibrium condition of the contact system, one can determine that

$$P = P^H - 4\sqrt{\pi B_1 \Delta\gamma a^3} = B_1\cot\alpha\pi a^2 - 4\sqrt{\pi B_1\Delta\gamma a^3}, \tag{A78}$$

which is in agreement with the corresponding JKR solution obtained in Equation (A34).

Therefore, the above results indicate that the JKR solutions of a piezoelectric solid indented by a rigid insulating conical punch can be regarded as the limiting case, which can be degenerated from the corresponding M-D solutions. The correctness of the corresponding solutions is verified.

Appendix E. External Circular Crack Problem

In this section, we will investigate the external circular crack problem in an infinite piezoelectric solid, as shown in Figure A1. The prescribed normal pressure, $p(r)$, is symmetrically exerted on the upper and lower crack surfaces. The considered problem can be formulated by

$$\begin{cases} u_z(r,0) = 0, \phi(r,0) = 0, & 0 \le r \le a, \\ \sigma_{zz}(r,0) = -p(r), D_z(r,0) = 0, & r > a, \\ \sigma_{rz}(r,0) = 0, & r \ge 0. \end{cases} \tag{A79}$$

It should be noted that $p(r)$ is positive for compression and negative for tension.

The general solutions of the axisymmetric problem for the piezoelectric solids are presented in Equation (5). By substituting Equation (5) into Equation (A79), one can obtain

$$\begin{cases} \int_0^\infty A_1(\xi)\xi J_0(\xi r)d\xi = 0, & 0 < r < a, \\ \int_0^\infty A_1(\xi)\xi^2 J_0(\xi r)d\xi = -\frac{M_8 p(r)}{M_5M_8-M_6M_7}, & r > a, \end{cases} \tag{A80}$$

$$\begin{cases} \int_0^\infty A_2(\xi)\xi J_0(\xi r)d\xi = 0, & 0 < r < a, \\ \int_0^\infty A_2(\xi)\xi^2 J_0(\xi r)d\xi = \frac{M_7 p(r)}{M_5M_8-M_6M_7}, & r > a. \end{cases} \tag{A81}$$

Equations (A80) and (A81) are a pair of dual integral equations with respect to the undetermined constants $A_1(\xi)$ and $A_2(\xi)$. The explicit expressions of $A_1(\xi)$ and $A_2(\xi)$ can be obtained by solving Equations (A80) and (A81) using the same method adopted in [83,84], and then, by inserting the corresponding solutions into Equation (5), one can obtain the solutions for the external circular crack problem. In order to save space,

the detailed solution procedures are omitted here, and we only present the final results as follows:

$$\begin{cases} u_z(r,0) = \frac{2}{B_1\pi}\int_a^r \frac{g(t)}{\sqrt{r^2-t^2}}dt, & r > a, \\ \phi(r,0) = \frac{B_2}{B_1}\frac{2}{\pi}\int_a^r \frac{g(t)}{\sqrt{r^2-t^2}}dt, & r > a, \\ \sigma_{zz}(r,0) = \frac{2}{\pi}\left[\frac{g(a)}{\sqrt{a^2-r^2}} + \int_a^\infty \frac{g^{'}(t)}{\sqrt{t^2-r^2}}dt\right], & r < a, \\ D_z(r,0) = 0, & r \geq 0, \end{cases} \tag{A82}$$

where B_1 and B_2 are material constants defined in Equation (A1), and

$$g(t) = \int_t^\infty \frac{sp(s)}{\sqrt{s^2-t^2}}ds. \tag{A83}$$

When the surface of external crack is subjected to the prescribed uniform pressure, p_0, one has the following equation from [81]:

$$g(t) = \int_t^\infty \frac{sp(s)}{\sqrt{s^2-t^2}}ds = \begin{cases} p_0\sqrt{c^2-t^2}, & a < t < c, \\ 0, & t \geq c, \end{cases} \tag{A84}$$

and one can the determine that

$$g^{'}(t) = \begin{cases} -\frac{p_0 t}{\sqrt{c^2-t^2}}, & a < t < c, \\ 0, & t \geq c. \end{cases} \tag{A85}$$

Inserting Equations (A84) and (A85) into $(82)_3$ yields

$$\sigma_{zz}(r,0) = \frac{2p_0}{\pi}\left(\sqrt{\frac{c^2-a^2}{a^2-r^2}} - \tan^{-1}\sqrt{\frac{c^2-a^2}{a^2-r^2}}\right),\ r < a, \tag{A86}$$

and the stress distribution at the crack surface can obtained as

$$\sigma_{zz}(r,0) = \begin{cases} \frac{2p_0}{\pi}\left(\sqrt{\frac{c^2-a^2}{a^2-r^2}} - \tan^{-1}\sqrt{\frac{c^2-a^2}{a^2-r^2}}\right), & r < a, \\ -p_0, & a < r < c, \\ 0, & r > c. \end{cases} \tag{A87}$$

By substituting of Equation (A84) into Equations $(A82)_1$ and $(A82)_2$, can obtain

$$u_z(r,0) = \frac{2p_0}{B_1\pi}\left[\frac{\sqrt{c^2-a^2}\sqrt{r^2-a^2}}{a} - c^2\int_a^{\min(r,c)} \frac{\sqrt{r^2-t^2}}{t^2\sqrt{c^2-t^2}}dt\right],\ r > a, \tag{A88}$$

$$\phi(r,0) = \frac{B_2}{B_1}\frac{2p_0}{\pi}\left[\frac{\sqrt{c^2-a^2}\sqrt{r^2-a^2}}{a} - c^2\int_a^{\min(r,c)} \frac{\sqrt{r^2-t^2}}{t^2\sqrt{c^2-t^2}}dt\right],\ r > a. \tag{A89}$$

respectively.

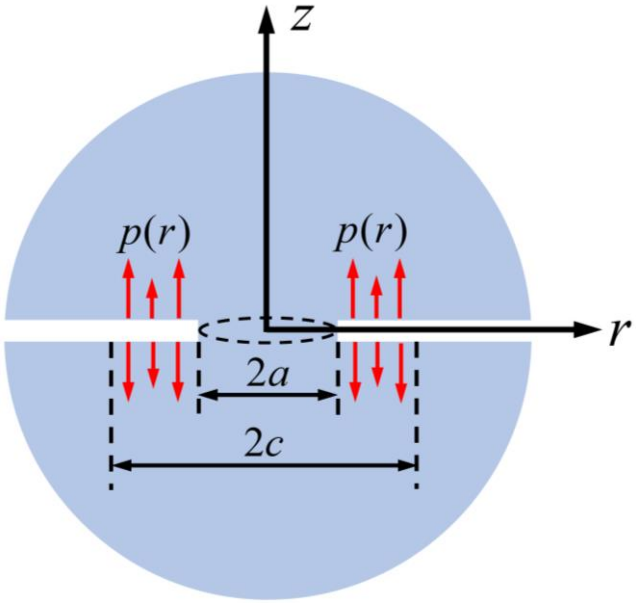

Figure A1. Schematic illustration of an external circular crack contained in an infinite transversely isotropic piezoelectric solid.

It is worth noting that the stresses at the crack surface are not self-equilibrated since the force

$$\int_0^a \sigma_{zz}(r,0)2\pi r dr = p_0\pi(c^2-a^2) - 2p_0a^2\left[\frac{c^2}{a^2}\cos^{-1}\left(\frac{a}{c}\right) - \sqrt{\frac{c^2}{a^2}-1}\right] \tag{A90}$$

does not equilibrate with the force $p_0\pi(c^2-a^2)$ exerted on the crack surface. Therefore, an additional force of

$$P' = 2p_0a^2\left[\frac{c^2}{a^2}\cos^{-1}\left(\frac{a}{c}\right) - \sqrt{\frac{c^2}{a^2}-1}\right] > 0 \tag{A91}$$

is thus exerted at infinity which permits $u_z(r,\infty)$ to be zero.

In order to satisfy the force equilibrium condition, keeping the radius, a, constant, exerting the force $-P^{'}$ (tensile force) at infinity, which will give rise to a displacement like the Boussinesq flat punch and introduce in the ligament a stress distribution. According to the different electric properties of the punch, two cases will be discussed separately in the following:

Case (a): superposing the solutions of a rigid insulating circular punch

The solutions to the Boussinesq problem under the action of a rigid insulating circular punch are presented in Equations (A19)–(A22). By inserting $-P^{'}$ into Equations (A19)–(A22), one can obtain

$$\sigma_{zz}^B(r,0) = \frac{P'}{2\pi a\sqrt{a^2-r^2}}, \quad r<a, \tag{A92}$$

$$h^B = -\frac{P'}{4B_1a}, \tag{A93}$$

$$u_z^B(r,0) = \begin{cases} -\frac{P'}{4B_1a}, & 0\le r\le a, \\ -\frac{P'}{2B_1\pi a}sin^{-1}\left(\frac{a}{r}\right), & r>a, \end{cases} \tag{A94}$$

$$\phi^B(r,0) = \begin{cases} -\frac{B_2 P'}{4B_1 a}, & 0 \le r \le a, \\ -\frac{B_2 P'}{2B_1 \pi a} sin^{-1}\left(\frac{a}{r}\right), & r > a. \end{cases} \tag{A95}$$

By superposing Equations (A87)$_1$ and (A92), and combining the results in Equation (A91), one obtains

$$\sigma_{zz}(r,0) = \frac{K_m}{\sqrt{\pi a}} \frac{a}{\sqrt{a^2 - r^2}} - \frac{2p_0}{\pi} \tan^{-1} \sqrt{\frac{c^2 - a^2}{a^2 - r^2}}, \; r < a, \tag{A96}$$

where

$$K_m = \frac{p_0}{\sqrt{\pi a}} \left[\sqrt{c^2 - a^2} + \frac{c^2}{a} \cos^{-1}\left(\frac{a}{c}\right) \right]. \tag{A97}$$

By considering Equations (A87) and (A96), the stress distribution of the circular external crack subjected to the uniform pressure, p_0, on crack surfaces can be defined as

$$\sigma_{zz}(r,0) = \begin{cases} \frac{K_m}{\sqrt{\pi a}} \frac{a}{\sqrt{a^2 - r^2}} - \frac{2p_0}{\pi} \tan^{-1} \sqrt{\frac{c^2 - a^2}{a^2 - r^2}}, & r < a, \\ -p_0, & a < r < c, \\ 0, & r > c. \end{cases} \tag{A98}$$

By substituting Equation (A91) into Equations (A94) and (A95), one can obtain

$$u_z^B(r,0) = \begin{cases} -\frac{p_0 a}{2B_1} \left[\frac{c^2}{a^2} \cos^{-1}\left(\frac{a}{c}\right) - \sqrt{\frac{c^2}{a^2} - 1} \right], & 0 \le r \le a, \\ -\frac{p_0 a}{B_1 \pi} \left[\frac{c^2}{a^2} \cos^{-1}\left(\frac{a}{c}\right) - \sqrt{\frac{c^2}{a^2} - 1} \right] \sin^{-1}\left(\frac{a}{r}\right), & r > a. \end{cases} \tag{A99}$$

$$\phi^B(r,0) = \begin{cases} -\frac{B_2 p_0 a}{2B_1} \left[\frac{c^2}{a^2} \cos^{-1}\left(\frac{a}{c}\right) - \sqrt{\frac{c^2}{a^2} - 1} \right], & 0 \le r \le a, \\ -\frac{B_2 p_0 a}{B_1 \pi} \left[\frac{c^2}{a^2} \cos^{-1}\left(\frac{a}{c}\right) - \sqrt{\frac{c^2}{a^2} - 1} \right] \sin^{-1}\left(\frac{a}{r}\right), & r > a. \end{cases} \tag{A100}$$

respectively.

In Boussinesq's theory, the profile of the surface is given by [81]:

$$u_B = -\frac{p_0 a}{B_1 \pi} \left[\frac{c^2}{a^2} \cos^{-1}\left(\frac{a}{c}\right) - \sqrt{\frac{c^2}{a^2} - 1} \right] \sin^{-1}\left(\frac{a}{r}\right), \; r \ge a, \tag{A101}$$

and the "penetration" of the punch is defined by

$$\delta_B = -\frac{p_0 a}{2B_1} \left[\frac{c^2}{a^2} \cos^{-1}\left(\frac{a}{c}\right) - \sqrt{\frac{c^2}{a^2} - 1} \right] < 0. \tag{A102}$$

Taking the origin of displacement at the tip of the crack, one has

$$u_z'(r,0) = \delta_B - u_B, \tag{A103}$$

Substitution of Equations (A101) and (A102) into Equation (A103) yields

$$u_z'(r,0) = \frac{p_0 a}{B_1 \pi} \left(\sqrt{\frac{c^2}{a^2} - 1} - \frac{c^2}{a^2} \cos^{-1} \frac{a}{c} \right) \cos^{-1} \frac{a}{r} < 0. \tag{A104}$$

Similarly, one can obtain

$$\phi^{'}(r,0) = \frac{B_2 p_0 a}{B_1 \pi}\left(\sqrt{\frac{c^2}{a^2}-1} - \frac{c^2}{a^2}\cos^{-1}\frac{a}{c}\right)\cos^{-1}\frac{a}{r} < 0. \tag{A105}$$

Adding the displacement and electric potential shown in Equations (A104) and (A105) to the corresponding results given by Equations (A88) and (A89), respectively, we obtain

$$\begin{aligned} u_T &= u_z(r,0) - u_z^{'} \\ &= \frac{2p_0}{B_1\pi}\left[\sqrt{c^2-a^2}\left(\sqrt{\frac{r^2}{a^2}-1} - \cos^{-1}\frac{a}{r}\right) - c^2\int_a^{\min(r,c)}\frac{\sqrt{r^2-t^2}}{t^2\sqrt{c^2-t^2}}dt\right] \\ &+ \frac{K_m\sqrt{\pi a}}{B_1\pi}\cos^{-1}\frac{a}{r}, \end{aligned} \tag{A106}$$

$$\begin{aligned} \phi_T &= \phi(r,0) - \phi^{'} \\ &= \frac{2B_2 p_0}{B_1\pi}\left[\sqrt{c^2-a^2}\left(\sqrt{\frac{r^2}{a^2}-1} - \cos^{-1}\frac{a}{r}\right) - c^2\int_a^{\min(r,c)}\frac{\sqrt{r^2-t^2}}{t^2\sqrt{c^2-t^2}}dt\right] \\ &+ \frac{B_2 K_m\sqrt{\pi a}}{B_1\pi}\cos^{-1}\frac{a}{r}. \end{aligned} \tag{A107}$$

When a piezoelectric material degenerates into an isotropic elastic solid, $B_1 = E^*/2 = E/2(1-\nu^2)$ (where E and ν are the elastic modulus and the Poisson's ratio of the isotropic elastic material, respectively), Equation (A106) can be rewritten as

$$\begin{aligned} u_T &= 4\frac{1-\nu^2}{\pi E}p_0\left[\sqrt{c^2-a^2}\left(\sqrt{\frac{r^2}{a^2}-1} - \cos^{-1}\frac{a}{r}\right) - c^2\int_a^{\min(r,c)}\frac{\sqrt{r^2-t^2}}{t^2\sqrt{c^2-t^2}}dt\right] \\ &+ \frac{1-\nu^2}{\pi E}K_m\sqrt{\pi a}\cos^{-1}\frac{a}{r}, \end{aligned} \tag{A108}$$

which is the same as the result of Equation (3.150) obtained in [81].

Case (b): superposing the solutions of a rigid conducting circular punch

The solutions to the Boussinesq problem under the action of a rigid conducting circular punch are given by Equations (A14)–(A18). For a rigid conducting circular punch with zero electric potential (i.e., $\phi_0 = 0$), substituting $-P^{'}$ into Equations (A14)–(A18) yields

$$\sigma_{zz}^B(r,0) = \frac{P^{'}}{2\pi a\sqrt{a^2-r^2}}, \tag{A109}$$

$$D_z^B(r,0) = \frac{B_5}{B_4}\frac{P^{'}}{2\pi a\sqrt{a^2-r^2}}, \tag{A110}$$

$$h^B = -\frac{P^{'}}{4aB_4}, \tag{A111}$$

$$u_z^B(r,0) = \begin{cases} -\frac{P^{'}}{4aB_4}, & 0 \le r \le a, \\ -\frac{P^{'}}{2\pi aB_4}sin^{-1}\left(\frac{a}{r}\right), & r > a, \end{cases} \tag{A112}$$

$$\phi^B(r,0) = 0, \quad r \ge 0. \tag{A113}$$

By adding the stress distribution given by Equations (A87)–(A109) and combining the result of Equation (A91), one can obtain

$$\sigma_{zz}(r,0) = \begin{cases} \frac{K_m}{\sqrt{\pi a}}\frac{a}{\sqrt{a^2-r^2}} - \frac{2p_0}{\pi}\tan^{-1}\sqrt{\frac{c^2-a^2}{a^2-r^2}}, & r < a, \\ -p_0, & a < r < c, \\ 0, & r > c, \end{cases} \tag{A114}$$

which are the same as the results given by Equation (A98).

Inserting Equation (A91) into Equation (A110) yields

$$D_z(r,0) = \frac{B_5}{B_4}\frac{K_m\sqrt{\pi a} - 2p_0\sqrt{c^2-a^2}}{\pi\sqrt{a^2-r^2}},\ r < a, \tag{A115}$$

where K_m is defined by Equation (A97).

By adopting the same solution procedures as those of Equations (A101)–(A107), the crack opening displacement and the discontinuity of the electric potential under the action of $-P^{'}$ can be defined as

$$\begin{aligned} u_T = {} & \tfrac{2p_0}{B_1\pi a}\left[\sqrt{(c^2-a^2)(r^2-a^2)} - ac^2\textstyle\int_a^{\min(r,c)} \frac{\sqrt{r^2-t^2}}{t^2\sqrt{c^2-t^2}}dt\right] \\ & + \tfrac{K_m\sqrt{\pi a}-2p_0\sqrt{c^2-a^2}}{B_4\pi}\cos^{-1}\tfrac{a}{r},\ r > a. \end{aligned} \tag{A116}$$

$$\phi_T = \frac{B_2}{B_1}\frac{2p_0}{\pi a}\left[\sqrt{(c^2-a^2)(r^2-a^2)} - ac^2\int_a^{\min(r,c)} \frac{\sqrt{r^2-t^2}}{t^2\sqrt{c^2-t^2}}dt\right],\ r > a. \tag{A117}$$

Appendix F. Verification of the Results in Section 4.2

In this section, the correctness of the results obtained in Section 4.2 will be verified, which was achieved by checking whether the corresponding JKR solutions presented in Section 3.2 can be degenerated as the limiting cases of the M-D solutions obtained in Section 4.2.

First, Equations (62) and (63) can be rewritten in the following forms:

$$\sigma_{zz}^{\mathrm{M-D}}(\rho,0) = \begin{cases} -B_4\cot\alpha\cosh^{-1}\frac{1}{\rho} + \frac{2\sigma_0}{\pi}\tan^{-1}\sqrt{\frac{m^2-1}{1-\rho^2}}, & \rho < 1, \\ \sigma_0, & 1 < \rho < m, \end{cases} \tag{A118}$$

$$D_z^{\mathrm{M-D}}(\rho,0) = \frac{2B_5(B_6+B_3)\phi_0}{\pi a\sqrt{1-\rho^2}} - B_5\cot\alpha\cosh^{-1}\frac{1}{\rho} + \frac{B_5}{B_4}\frac{2\sigma_0}{\pi}\sqrt{\frac{m^2-1}{1-\rho^2}},\ \rho < 1, \tag{A119}$$

where $\rho = r/a, m = c/a$.

From Equation (60), one can obtain

$$K_I = \frac{\sigma_0 a}{\sqrt{\pi a}}\left(\sqrt{m^2-1} + m^2\cos^{-1}\frac{1}{m}\right). \tag{A120}$$

Using the following relation from [81]:

$$\cos^{-1}\left(\frac{1}{m}\right) = \tan^{-1}\sqrt{m^2-1},\ m > 0, \tag{A121}$$

Equation (A120) can be expressed as

$$\frac{K_I\sqrt{\pi a}}{\sigma_0 a} = \sqrt{m^2-1} + m^2\tan^{-1}\sqrt{m^2-1}. \tag{A122}$$

When $m \to 1$, considering the relation $\tan^{-1}\sqrt{m^2-1} \sim \sqrt{m^2-1}$, one can determine that

$$\frac{K_I\sqrt{\pi a}}{\sigma_0 a} \approx 2\sqrt{m^2-1}. \tag{A123}$$

Substituting Equation (A123) into Equations (A118) and (A119) yields

$$\begin{cases} \sigma_{zz}(\rho,0) = -B_4 \cot\alpha \cosh^{-1}\frac{1}{\rho} + \frac{K_I}{\sqrt{\pi a}}\frac{1}{\sqrt{1-\rho^2}}, & \rho < 1, \\ D_z(\rho,0) = \frac{2B_5(B_6+B_3)\phi_0}{\pi a\sqrt{1-\rho^2}} - B_5 \cot\alpha \cosh^{-1}\frac{1}{\rho} + \frac{B_5}{B_4}\frac{K_I}{\sqrt{\pi a}}\frac{1}{\sqrt{1-\rho^2}}, & \rho < 1, \end{cases} \tag{A124}$$

which are consistent with the JKR solutions obtained in Equations (47) and (48).

When $m \to \infty$, from Equation (A122), one can determine that $\sigma_0 \to 0$. In this case, Equations (62) and (63) can be simplified as

$$\begin{cases} \sigma_{zz}(\rho,0) = -B_4 \cot\alpha \cosh^{-1}\frac{1}{\rho}, & \rho < 1, \\ D_z(\rho,0) = \frac{2B_5(B_6+B_3)\phi_0}{\pi a\sqrt{1-\rho^2}} - B_5 \cot\alpha \cosh^{-1}\frac{1}{\rho}, & \rho < 1, \end{cases} \tag{A125}$$

which are the same as the corresponding Hertz solutions presented in Equations (A2) and (A3).

For the discontinuity displacement outside the contact region, $\sigma_0 \to 0$ as $m \to \infty$, and Equation (65) degenerates into the following form:

$$[u_z(r,0)] = \left(\frac{2B_3\phi_0}{\pi} - a\cot\alpha\right)\cos^{-1}\frac{a}{r} + \sqrt{r^2-a^2}\cot\alpha,\ r > a, \tag{A126}$$

which is consistent with the Hertz solution presented in Equation (A7).

When $m \to 1$, using the relation in Equation (A123), Equation (65) can be simplified as follows:

$$\begin{aligned} [u_z(r,0)] &= \left(\tfrac{2B_3\phi_0}{\pi} - a\cot\alpha\right)\cos^{-1}\tfrac{a}{r} + \sqrt{r^2-a^2}\cot\alpha + \tfrac{K_I\sqrt{\pi a}}{B_4\pi}\cos^{-1}\tfrac{a}{r} \\ &- \tfrac{2\sigma_0 a}{B_1\pi}\left[\sqrt{(m^2-1)(\rho^2-1)} - m^2\textstyle\int_1^{\min(\rho,m)}\frac{\sqrt{\rho^2-t^2}}{t^2\sqrt{m^2-t^2}}dt\right],\ r > a. \end{aligned} \tag{A127}$$

Considering the following integral result [81]:

$$\begin{aligned} &\lim_{m\to 1}\left(m^2\textstyle\int_1^m \frac{\sqrt{\rho^2-t^2}}{t^2\sqrt{m^2-t^2}}dt\right) = \lim_{m\to 1}\left(m^2\sqrt{\rho^2-\xi^2}\textstyle\int_1^m \frac{dt}{t^2\sqrt{m^2-t^2}}\right) \\ &= \lim_{m\to 1}\sqrt{\rho^2-\xi^2}\sqrt{m^2-1} = \sqrt{(m^2-1)(\rho^2-1)}. \end{aligned} \tag{A128}$$

By inserting Equation (A128) into Equation (A127), one can obtain

$$\begin{aligned} [u_z(r,0)] &= \left(\tfrac{2B_3\phi_0}{\pi} - a\cot\alpha\right)\cos^{-1}\tfrac{a}{r} + \sqrt{r^2-a^2}\cot\alpha \\ &+ \tfrac{K_I\sqrt{\pi a}}{B_4\pi}\cos^{-1}\tfrac{a}{r},\ r > a, \end{aligned} \tag{A129}$$

which is the same as the corresponding JKR solution presented in Equation (50).

From the results given by Equations (A126) and (A128), one can determine that for both $m \to \infty$ and $m \to 1$, Equation (67) can be simplified as follows:

$$[\phi(r,0)] = -\frac{2\phi_0}{\pi}\cos^{-1}\frac{a}{r},\ r > a, \tag{A130}$$

which is consistent with the Hertz solution and the JKR solution obtained in Equations (A8) and (51), respectively.

For the indentation depth, superposing Equations (14) and (56) yields

$$h^{\mathrm{M-D}} = \frac{\pi a}{4}\cot\alpha + \frac{P}{4B_4 a} - B_3\phi_0 + \frac{\sigma_0 a}{2B_4}\left(m^2\tan^{-1}\sqrt{m^2-1} - \sqrt{m^2-1}\right). \tag{A131}$$

Using Equations (45) and (A122), one can determine that

$$\sigma_0 a = \frac{B_4 \pi a^2 \cot\alpha - P}{2a\left(\sqrt{m^2-1} + m^2 \tan^{-1}\sqrt{m^2-1}\right)}. \tag{A132}$$

Substituting Equation (A132) into Equation (A131) yields

$$\begin{aligned} h^{\mathrm{M-D}} &= \tfrac{\pi a}{4}\cot\alpha + \tfrac{P}{4B_4 a} - B_3\phi_0 \\ &+ \tfrac{m^2\tan^{-1}\sqrt{m^2-1}-\sqrt{m^2-1}}{m^2\tan^{-1}\sqrt{m^2-1}+\sqrt{m^2-1}}\,\tfrac{B_4\pi a^2\cot\alpha - P}{4B_4 a}. \end{aligned} \tag{A133}$$

As $m \to 1$,

$$\frac{m^2\tan^{-1}\sqrt{m^2-1}-\sqrt{m^2-1}}{m^2\tan^{-1}\sqrt{m^2-1}+\sqrt{m^2-1}} \approx \frac{\sqrt{m^2-1}-\sqrt{m^2-1}}{2\sqrt{m^2-1}} = 0, \tag{A134}$$

and as such, Equation (A133) can be simplified as

$$h = \frac{\pi a}{4}\cot\alpha + \frac{P}{4B_4 a} - B_3\phi_0, \tag{A135}$$

which is consistent with the corresponding JKR solution obtained in Equation (14).

When $m \to \infty$, it can be determined that

$$\frac{m^2\tan^{-1}\sqrt{m^2-1}-\sqrt{m^2-1}}{m^2\tan^{-1}\sqrt{m^2-1}+\sqrt{m^2-1}} \approx \frac{\pi m^2/2-\sqrt{m^2-1}}{\pi m^2/2+\sqrt{m^2-1}} \approx 1, \tag{A136}$$

then one can determine that

$$h = \frac{\pi a}{2}\cot\alpha - B_3\phi_0, \tag{A137}$$

which is the same as the Hertz solution presented in Equation (A4).

Using the relation given by Equation (A121), the energy release rate obtained in Equation (79) can be expressed in the following form:

$$\begin{aligned} G &= \left(\sqrt{m^2-1} - \tan^{-1}\sqrt{m^2-1}\right)\sigma_0 a\cot\alpha + \tfrac{2B_3\phi_0\sigma_0}{\pi}\tan^{-1}\sqrt{m^2-1} \\ &+ \tfrac{2\sigma_0^2 a}{\pi B_4}\left[\sqrt{m^2-1}\tan^{-1}\sqrt{m^2-1} - \tfrac{B_4}{B_1}(m-1)\right] - \tfrac{B_5(B_3+B_6)\phi_0^2}{\pi a} \\ &- \tfrac{1}{\pi}\left[\tfrac{B_5}{B_4} + \tfrac{B_2B_5(B_3+B_6)}{B_1}\right]\phi_0\sigma_0\sqrt{m^2-1} - \tfrac{B_2B_5}{B_1B_4}\tfrac{\sigma_0^2 a}{\pi}(m^2-1). \end{aligned} \tag{A138}$$

Substitution of Equation (A132) into Equation (A138) yields

$$\begin{aligned} G &= \tfrac{\cot\alpha(P^H-P)\left(\sqrt{m^2-1}-\tan^{-1}\sqrt{m^2-1}\right)}{2a\left(\sqrt{m^2-1}+m^2\tan^{-1}\sqrt{m^2-1}\right)} \\ &+ \left\{B_3\tan^{-1}\sqrt{m^2-1} - \tfrac{1}{2}\left[\tfrac{B_5}{B_4} + \tfrac{B_2B_5(B_3+B_6)}{B_1}\right]\sqrt{m^2-1}\right\}\times \\ &\tfrac{(P^H-P)\phi_0}{\pi a^2\left(\sqrt{m^2-1}+m^2\tan^{-1}\sqrt{m^2-1}\right)} - \tfrac{B_2B_5}{4\pi B_1B_4a^3}\tfrac{(P^H-P)^2(m^2-1)}{\sqrt{m^2-1}+m^2\tan^{-1}\sqrt{m^2-1}} \\ &+ \tfrac{(P^H-P)^2}{2\pi B_4a^3}\tfrac{\sqrt{m^2-1}\tan^{-1}\sqrt{m^2-1}-\frac{B_4}{B_1}(m-1)}{\left(\sqrt{m^2-1}+m^2\tan^{-1}\sqrt{m^2-1}\right)^2} - \tfrac{B_5(B_3+B_6)\phi_0^2}{\pi a}. \end{aligned} \tag{A139}$$

When $m \to 1$, using the relation $\tan^{-1}\sqrt{m^2-1} \sim \sqrt{m^2-1}$, Equation (A139) can be simplified as

$$\begin{aligned} G = &\left\{B_3 - \tfrac{1}{2}\left[\tfrac{B_5}{B_4} + \tfrac{B_2B_5(B_3+B_6)}{B_1}\right]\right\}\tfrac{(P^H-P)\phi_0}{2\pi a^2} \\ &+\tfrac{(P^H-P)^2}{2\pi B_4 a^3}\tfrac{\sqrt{m^2-1}\tan^{-1}\sqrt{m^2-1}-\frac{B_4}{B_1}(m-1)}{\left(\sqrt{m^2-1}+m^2\tan^{-1}\sqrt{m^2-1}\right)^2} - \tfrac{B_5(B_3+B_6)\phi_0^2}{\pi a}. \end{aligned} \tag{A140}$$

For several common piezoelectric materials (e.g., PZT-4, PZT-5A, $BaTiO_3$ and $Ba_aCa_bTiO_3$), the numerical results indicate that

$$B_3 \approx \frac{1}{2}\left[\frac{B_5}{B_4} + \frac{B_2B_5(B_3+B_6)}{B_1}\right],\ \frac{B_4}{B_1} \approx 1. \tag{A141}$$

Using the above results, Equation (A140) can be further simplified as

$$G = \frac{(P^H-P)^2}{2\pi B_4 a^3}\frac{\sqrt{m^2-1}\tan^{-1}\sqrt{m^2-1}-m+1}{\left(\sqrt{m^2-1}+m^2\tan^{-1}\sqrt{m^2-1}\right)^2} - \frac{B_5(B_3+B_6)\phi_0^2}{\pi a}. \tag{A142}$$

As $m \to 1$, letting $m = 1+\varepsilon$, one can obtain [81]:

$$\tan^{-1}\sqrt{m^2-1} \approx \sqrt{2\varepsilon}\left(1-\frac{5\varepsilon}{12}\right), \tag{A143}$$

and as such,

$$\sqrt{m^2-1}\tan^{-1}\sqrt{m^2-1}-m+1 \approx 2\varepsilon,\ \sqrt{m^2-1}+m^2\tan^{-1}\sqrt{m^2-1} \approx 2\sqrt{2\varepsilon}. \tag{A144}$$

Inserting Equation (A144) into Equation (A142) yields

$$G = \frac{(P^H-P)^2}{16\pi B_4 a^3} - \frac{B_5(B_3+B_6)\phi_0^2}{\pi a}. \tag{A145}$$

Using the energy balance relation as presented in Equation (80), one can determine that

$$P = P^H \pm 4a\sqrt{\pi B_4 a\Delta\gamma + B_4B_5(B_3+B_6)\phi_0^2}. \tag{A146}$$

Combining the stable equilibrium condition of the contact system, we can determine that

$$P = P^H - 4a\sqrt{\pi B_4 a\Delta\gamma + B_4B_5(B_3+B_6)\phi_0^2}. \tag{A147}$$

Substituting Equation $(A4)_2$ into Equation (A147) yields

$$P = \pi B_4 a^2\cot\alpha - 4a\sqrt{\pi B_4 a\Delta\gamma + B_4B_5(B_3+B_6)\phi_0^2}, \tag{A148}$$

which is the same as the corresponding JKR solution obtained in Equation (27).

Therefore, the above results indicate that the JKR solutions of a piezoelectric solid under the action of a rigid conducting conical punch can be regarded as the limiting case, which can be degenerated from the corresponding M-D solutions. The correctness of the corresponding solutions is verified.

References

1. Zhao, C.; Knisely, K.E.; Colesa, D.J.; Pfingst, B.E.; Raphael, Y.; Grosh, K. Voltage readout from a piezoelectric intracochlear acoustic transducer implanted in a living guinea pig. *Sci. Rep.* **2019**, *9*, 3711. [CrossRef] [PubMed]
2. Ejeian, F.; Azadi, S.; Razmjou, A.; Orooji, Y.; Kottapalli, A.; Warkiani, M.E.; Asadnia, M. Design and applications of MEMS flow sensors: A review. *Sens. Actuators A Phys.* **2019**, *295*, 483–502. [CrossRef]
3. Murray, C.; McCoul, D.; Sollier, E.; Ruggiero, T.; Niu, X.; Pei, Q.; Di Carlo, D. Electro-adaptive microfluidics for active tuning of channel geometry using polymer actuators. *Microfluid. Nanofluidics* **2012**, *14*, 345–358. [CrossRef]
4. Deng, W.; Zhou, Y.; Libanori, A.; Chen, G.; Yang, W.; Chen, J. Piezoelectric nanogenerators for personalized healthcare. *Chem. Soc. Rev.* **2022**, *51*, 3380–3435. [CrossRef] [PubMed]
5. Kim, S.-G.; Priya, S.; Kanno, I. Piezoelectric MEMS for energy harvesting. *MRS Bull.* **2012**, *37*, 1039–1050. [CrossRef]
6. Awada, A.; Younes, R.; Ilinca, A. Optimized Active Control of a Smart Cantilever Beam Using Genetic Algorithm. *Designs* **2022**, *6*, 36. [CrossRef]
7. Wang, Z.; Qin, X.; Zhang, S.; Bai, J.; Li, J.; Yu, G. Optimal Shape Control of Piezoelectric Intelligent Structure Based on Genetic Algorithm. *Adv. Mater. Sci. Eng.* **2017**, *2017*, 6702183. [CrossRef]
8. Mangaiyarkarasi, P.; Lakshmi, P. Numerical and experimental analysis of piezoelectric vibration energy harvester in IoT based F-SEPS application using optimization techniques. *Microsyst. Technol.* **2021**, *27*, 2955–2979. [CrossRef]
9. Fountas, N.A.; Vaxevanidis, N.M. Optimization of abrasive flow nano-finishing processes by adopting artificial viral intelligence. *J. Manuf. Mater. Process.* **2021**, *5*, 22. [CrossRef]
10. Nabavi, S.; Zhang, L. Frequency Tuning and Efficiency Improvement of Piezoelectric MEMS Vibration Energy Harvesters. *J. Microelectromech. Syst.* **2018**, *28*, 77–87. [CrossRef]
11. Abdeljaber, O.; Avci, O.; Inman, D.J. Active vibration control of flexible cantilever plates using piezoelectric materials and artificial neural networks. *J. Sound Vib.* **2016**, *363*, 33–53. [CrossRef]
12. Abolhasani, M.M.; Shirvanimoghaddam, K.; Khayyam, H.; Moosavi, S.M.; Zohdi, N.; Naebe, M. Towards predicting the piezoelectricity and physiochemical properties of the electrospun P(VDF-TrFE) nanogenrators using an artificial neural network. *Polym. Test.* **2018**, *66*, 178–188. [CrossRef]
13. Kachanov, M.; Kalinin, S. Nanoelectromechanics of piezoelectric indentation and applications to scanning probe microscopies of ferroelectric materials. *Philos. Mag.* **2005**, *85*, 1017–1051.
14. Carrillo, F.; Gupta, S.; Balooch, M.; Marshall, S.J.; Marshall, G.W.; Pruitt, L.; Puttlitz, C.M. Nanoindentation of polydimethylsiloxane elastomers: Effect of crosslinking, work of adhesion, and fluid environment on elastic modulus. *J. Mater. Res.* **2011**, *20*, 2820–2830. [CrossRef]
15. Lin, Z.; Yu, Z.; Wei, Y. Measurement of nanoindentation properties of polymers considering adhesion effects between AFM sharp indenter and material. *J. Adhes. Sci. Technol.* **2020**, *34*, 1591–1608. [CrossRef]
16. Kohn, J.C.; Ebenstein, D. Eliminating adhesion errors in nanoindentation of compliant polymers and hydrogels. *J. Mech. Behav. Biomed. Mater.* **2013**, *20*, 316–326. [CrossRef]
17. Zhao, Y.P.; Wang, L.S.; Yu, T.X. Mechanics of adhesion in MEMS—A review. *J. Adhes. Sci. Technol.* **2003**, *17*, 519–546. [CrossRef]
18. Zhou, S.A. On forces in microelectromechanical systems. *Int. J. Eng. Sci.* **2003**, *41*, 313–335. [CrossRef]
19. Lim, A.E.; Lam, Y.C. Vertical Squeezing Route Taylor Flow with Angled Microchannel Junctions. *Ind. Eng. Chem. Res.* **2021**, *60*, 14307–14317. [CrossRef]
20. Yang, F.Q. Effect of adhesion energy on the contact stiffness in nanoindentation. *J. Mater. Res.* **2006**, *21*, 2683–2688. [CrossRef]
21. Chen, W.-Q.; Shioya, T.; Ding, H.-J. The Elasto-Electric Field for a Rigid Conical Punch on a Transversely Isotropic Piezoelectric Half-Space. *J. Appl. Mech.* **1999**, *66*, 764–771. [CrossRef]
22. Giannakopoulos, A.; Suresh, S. Theory of indentation of piezoelectric materials. *Acta Mater.* **1999**, *47*, 2153–2164. [CrossRef]
23. Sridhar, S.; Giannakopoulos, A.E.; Suresh, S. Mechanical and electrical responses of piezoelectric solids to conical indentation. *J. Appl. Phys.* **2000**, *87*, 8451–8456. [CrossRef]
24. Makagon, A.; Kachanov, M.; Kalinin, S.V.; Karapetian, E. Indentation of spherical and conical punches into piezoelectric half-space with frictional sliding: Applications to scanning probe microscopy. *Phys. Rev. B* **2007**, *76*, 064115. [CrossRef]
25. Wang, J.H.; Chen, C.Q.; Lu, T.J. Indentation responses of piezoelectric films. *J. Mech. Phys. Solids* **2008**, *56*, 3331–3351. [CrossRef]
26. Yang, F. Analysis of the axisymmetric indentation of a semi-infinite piezoelectric material: The evaluation of the contact stiffness and the effective piezoelectric constant. *J. Appl. Phys.* **2008**, *103*, 074115. [CrossRef]
27. Kamble, S.N.; Kubair, D.V.; Ramamurty, U. Indentation strength of a piezoelectric ceramic: Experiments and simulations. *J. Mater. Res.* **2009**, *24*, 926–935. [CrossRef]
28. Liu, M.; Yang, F.Q. Orientation effect on the Boussinesq indentation of a transversely isotropic piezoelectric material. *Int. J. Solids Struct.* **2013**, *50*, 2542–2547. [CrossRef]
29. Berndt, E.A.; Sevostianov, I. Action of a smooth flat charged punch on the piezoelectric half-space possessing symmetry of class 6. *Int. J. Eng. Sci.* **2016**, *103*, 77–96. [CrossRef]
30. Rodríguez-Tembleque, L.; Sáez, A.; Aliabadi, M. Indentation response of piezoelectric films under frictional contact. *Int. J. Eng. Sci.* **2016**, *107*, 36–53. [CrossRef]
31. Hou, P.F.; Zhang, W.H. 3D Axisymmetric exact solutions of the piezo-coating sensors for coating/substrate system under charged conical contact. *Int. J. Solids Struct.* **2019**, *185–186*, 342–364. [CrossRef]

32. Guillermo, R.; Paul, H. Frictionless contact in a layered piezoelectric half-space. *Smart Mater. Struct.* **2003**, *12*, 612–625.
33. Hao, T.H. Exact solution of a flat smooth punch on a piezoelectric half plane. *Mech. Res. Commun.* **2003**, *30*, 455–461.
34. Guillermo, R. Frictionless contact in a layered piezoelectric medium characterized by complex eigenvalues. *Smart Mater. Struct.* **2006**, *15*, 1287–1295.
35. Wang, B.L.; Han, J.C.; Du, S.Y.; Zhang, H.Y.; Sun, Y.G. Electromechanical behaviour of a finite piezoelectric layer under a flat punch. *Int. J. Solids Struct.* **2008**, *45*, 6384–6398. [CrossRef]
36. Zhou, Y.T.; Lee, K.Y. New, real fundamental solutions to the transient thermal contact problem in a piezoelectric strip under the coupling actions of a rigid punch and a convective heat supply. *Int. J. Solids Struct.* **2011**, *48*, 2706–2717. [CrossRef]
37. Zhou, Y.-T.; Lee, K.Y. Theory of moving contact of anisotropic piezoelectric materials via real fundamental solutions approach. *Eur. J. Mech. A Solids* **2012**, *35*, 22–36. [CrossRef]
38. Zhou, Y.-T.; Zhong, Z. Application of dual series equations to wavy contact between piezoelectric materials and an elastic solid. *Int. J. Appl. Mech.* **2014**, *6*, 1450046. [CrossRef]
39. Zhou, Y.-T.; Zhong, Z. The interaction of two rigid semi-cylinders over anisotropic piezoelectric materials by the generalized Almansi theorem. *Smart Mater. Struct.* **2015**, *24*, 085011. [CrossRef]
40. Çömez, İ.; Güler, M.A.; El-Borgi, S. Continuous and discontinuous contact problems of a homogeneous piezoelectric layer pressed by a conducting rigid flat punch. *Acta Mech.* **2019**, *231*, 957–976. [CrossRef]
41. Su, J.; Ke, L.-L.; Wang, Y.-S. Elastohydrodynamic lubrication line contact of piezoelectric materials. *Int. J. Mech. Sci.* **2019**, *163*, 105145. [CrossRef]
42. Fan, H.; Sze, K.-Y.; Yang, W. Two-dimensional contact on a piezoelectric half-space. *Int. J. Solids Struct.* **1996**, *33*, 1305–1315. [CrossRef]
43. Zhou, Y.T.; Lee, K.Y. Thermo-electro-mechanical contact behavior of a finite piezoelectric layer under a sliding punch with frictional heat generation. *J. Mech. Phys. Solids* **2011**, *59*, 1037–1061. [CrossRef]
44. Zhou, Y.T.; Lee, K.Y. Exact solutions of the 2-D frictional sliding contact problem of electrically insulated triangular and cylindrical punches on piezoelectric materials. *Zamm-Z. Angew. Math. Phys.* **2013**, *93*, 217–232. [CrossRef]
45. Li, X.; Zhou, Y.-T.; Zhong, Z. On the analytical solution for sliding contact of piezoelectric materials subjected to a flat or parabolic indenter. *Z. Angew. Math. Phys.* **2014**, *66*, 473–495. [CrossRef]
46. Ma, J.; Ke, L.-L.; Wang, Y.-S. Electro-mechanical sliding frictional contact of a piezoelectric half-plane under a rigid conducting punch. *Appl. Math. Model.* **2014**, *38*, 5471–5489. [CrossRef]
47. Zhou, Y.-T.; Lee, K.Y. Investigation of frictional sliding contact problems of triangular and cylindrical punches on monoclinic piezoelectric materials. *Mech. Mater.* **2014**, *69*, 237–250. [CrossRef]
48. Su, J.; Ke, L.-L.; Wang, Y.-S. Two-dimensional fretting contact analysis of piezoelectric materials. *Int. J. Solids Struct.* **2015**, *73-74*, 41–54. [CrossRef]
49. Su, J.; Ke, L.-L.; Wang, Y.-S. Two-dimensional fretting contact of piezoelectric materials under a rigid conducting cylindrical punch. *J. Mech. Mater. Struct.* **2016**, *11*, 535–558. [CrossRef]
50. Shu, Y.-J.; Ke, L.-L.; Su, J.; Wang, Y.-S. Experimental Investigation on Fretting Wear Behavior of Piezoceramics under Sphere-on-Flat Contact. *Tribol. Trans.* **2020**, *63*, 971–985. [CrossRef]
51. Lv, X.; Ke, L.-L.; Su, J.; Tian, J.-Y. Axisymmetric contact vibration analysis of a rigid spherical punch on a piezoelectric half-space. *Int. J. Solids Struct.* **2020**, *210–211*, 224–236. [CrossRef]
52. Lv, X.; Su, J.; Tian, J.-Y.; Ke, L.-L. Dynamic contact response of an elastic sphere on a piezoelectric half-space. *Appl. Math. Model.* **2021**, *100*, 16–32. [CrossRef]
53. Ding, H.-J.; Hou, P.-F.; Guo, F.-L. The elastic and electric fields for three-dimensional contact for transversely isotropic piezoelectric materials. *Int. J. Solids Struct.* **2000**, *37*, 3201–3229. [CrossRef]
54. Wu, Y.F.; Yu, H.Y.; Chen, W.Q. Mechanics of indentation for piezoelectric thin films on elastic substrate. *Int. J. Solids Struct.* **2012**, *49*, 95–110. [CrossRef]
55. Chen, Z.-R.; Yu, S.-W. Micro-scale adhesive contact of a spherical rigid punch on a piezoelectric half-space. *Compos. Sci. Technol.* **2005**, *65*, 1372–1381. [CrossRef]
56. Johnson, K.L.; Kendall, K.; Roberts, A.D. Surface energy and the contact of elastic solids. *Proc. R. Soc. A Math. Phys. Eng. Sci.* **1971**, *324*, 301–313.
57. Maugis, D. Adhesion of spheres: The JKR-DMT transition using a Dugdale model. *J. Colloid Interface Sci.* **1992**, *150*, 243–269. [CrossRef]
58. Rogowski, B.; Kaliński, W. The adhesive contact problem for a piezoelectric half-space. *Int. J. Press. Vessel. Pip.* **2007**, *84*, 502–511. [CrossRef]
59. Guo, X.; Jin, F. A generalized JKR-model for two-dimensional adhesive contact of transversely isotropic piezoelectric half-space. *Int. J. Solids Struct.* **2009**, *46*, 3607–3619. [CrossRef]
60. Jin, F.; Yan, S.P.; Guo, X.; Wang, X.Y. On the contact and adhesion of a piezoelectric half-space under a rigid punch with an axisymmetric power-law profile. *Mech. Mater.* **2018**, *129*, 189–197. [CrossRef]
61. Kanda, K.; Hirai, S.; Fujita, T.; Maenaka, K. Piezoelectric MEMS with multilayered Pb(Zr,Ti)O_3 thin films for energy harvesting. *Sens. Actuators A Phys.* **2018**, *281*, 229–235. [CrossRef]

62. Zhou, Y.-T.; Luo, Q.-H. Asymmetric non-slipping adhesion behavior of layered piezoelectric structures. *Int. J. Mech. Sci.* **2022**, *224*, 107330. [CrossRef]
63. Luo, Q.-H.; Zhou, Y.-T. Adhesive contact behavior between piezoelectric and elastic materials with a mismatch strain. *Acta Mech.* **2022**, *233*, 617–639. [CrossRef]
64. Luo, Q.-H.; Zhou, Y.-T. Adhesive behavior of transversely isotropic piezoelectric bimaterials. *Int. J. Solids Struct.* **2021**, *236–237*, 111360. [CrossRef]
65. Shirbani, M.M.; Shishesaz, M.; Hajnayeb, A.; Sedighi, H.M. Coupled magneto-electro-mechanical lumped parameter model for a novel vibration-based magneto-electro-elastic energy harvesting systems. *Phys. E Low-Dimens. Syst. Nanostruct.* **2017**, *90*, 158–169. [CrossRef]
66. Shishesaz, M.; Shirbani, M.M.; Sedighi, H.M.; Hajnayeb, A. Design and analytical modeling of magneto-electro-mechanical characteristics of a novel magneto-electro-elastic vibration-based energy harvesting system. *J. Sound Vib.* **2018**, *425*, 149–169. [CrossRef]
67. Skrzypacz, P.; Ellis, G.; He, J.H.; He, C.H. Dynamic pull-in and oscillations of current-carrying filaments in magnetic micro-electro-mechanical system. *Commun. Nonlinear Sci. Numer. Simul.* **2022**, *109*, 106350. [CrossRef]
68. Wu, F.; Li, X.-Y.; Zheng, R.-F.; Kang, G.-Z. Theory of adhesive contact on multi-ferroic composite materials: Spherical indenter. *Int. J. Eng. Sci.* **2018**, *134*, 77–116. [CrossRef]
69. Wu, F.; Li, C. Theory of adhesive contact on multi-ferroic composite materials: Conical indenter. *Int. J. Solids Struct.* **2021**, *233*, 111217. [CrossRef]
70. Rar, A.; Pharr, G.M.; Oliver, W.C.; Karapetian, E.; Kalinin, S.V. Piezoelectric nanoindentation. *J. Mater. Res.* **2006**, *21*, 552–556. [CrossRef]
71. Pan, K.; Liu, Y.Y.; Xie, S.H.; Liu, Y.M.; Li, J.Y. The electromechanics of piezoresponse force microscopy for a transversely isotropic piezoelectric medium. *Acta Mater.* **2013**, *61*, 7020–7033. [CrossRef]
72. Broitman, E.; Soomro, M.Y.; Lu, J.; Willander, M.; Hultman, L. Nanoscale piezoelectric response of ZnO nanowires measured using a nanoindentation technique. *Phys. Chem. Chem. Phys.* **2013**, *15*, 11113–11118. [CrossRef]
73. Derjaguin, B.; Muller, V.; Toporov, Y. Effect of contact deformations on the adhesion of particles. *J. Colloid Interface Sci.* **1975**, *53*, 314–326. [CrossRef]
74. Greenwood, J.A.; Johnson, K.L. An alternative to the Maugis model of adhesion between elastic spheres. *J. Phys. D Appl. Phys.* **1998**, *31*, 3279–3290. [CrossRef]
75. Tabor, D. Surface forces and surface interactions. *J. Colloid Interface Sci.* **1977**, *58*, 3–14. [CrossRef]
76. Ganser, C.; Czibula, C.; Tscharnuter, D.; Schoberl, T.; Teichert, C.; Hirn, U. Combining adhesive contact mechanics with a viscoelastic material model to probe local material properties by AFM. *Soft Matter* **2017**, *14*, 140–150. [CrossRef]
77. Argatov, I.; Mishuris, G. Cylindrical lateral depth-sensing indentation of anisotropic elastic tissues: Effects of adhesion and incompressibility. *J. Adhes.* **2017**, *94*, 583–596. [CrossRef]
78. Vallet, D.; Barquins, M. Adhesive contact and kinetics of adherence of a rigid conical punch on an elastic half-space (natural rubber). *Int. J. Adhes. Adhes.* **2002**, *22*, 41–46. [CrossRef]
79. Dugdale, D.S. Yielding of stress sheets containing slits. *J. Mech. Phys. Solids* **1960**, *8*, 100–104. [CrossRef]
80. Suo, Z.G.; Kuo, C.M.; Barnett, D.M.; Willis, J.R. Fracture mechanics for piezoelectric ceramics. *J. Mech. Phys. Solids* **1992**, *40*, 739–765. [CrossRef]
81. Maugis, D. *Contact, Adhesion and Rupture of Elastic Solids*; Springer: Berlin/Heidelberg, Germany, 2000.
82. Cacucciolo, V.; Shea, H.; Carbone, G. Peeling in electroadhesion soft grippers. *Extreme Mech. Lett.* **2021**, *50*, 101529. [CrossRef]
83. Lowengrub, M.; Sneddon, I.N. The distribution of stress in the vicinity of an external crack in an infinite elastic solid. *Int. J. Eng. Sci.* **1965**, *3*, 451–460. [CrossRef]
84. Sneddon, I.N. The elementary solution of dual integral equation. *Glasg. Math. J.* **1960**, *4*, 108–110. [CrossRef]